SYNTHESIS OF LANTHANIDE NANOPARTICLES: ITS' CHARACTERIZATION THROUGH CRYSTALLOGRAPHY AND SPECTRAL TECHNIQUES ALONG WITH APPLICATIONS

A THESIS SUBMITTED IN PARTIAL FULFILMENT OF THE REQUIREMENTS FOR THE DEGREE OF DOCTOR OF PHILOSOPHY

PUNAZUNGBA IMSONG

Ph. D. REGN NO. Ph.D./CHE/00057

DEPARTMENT OF CHEMISTRY

SCHOOL OF SCIENCES

AUGUST 2024

SYNTHESIS OF LANTHANIDE NANOPARTICLES: ITS' CHARACTERIZATION THROUGH CRYSTALLOGRAPHY AND SPECTRAL TECHNIQUES ALONG WITH APPLICATIONS

BY

Punazungba Imsong

Department of Chemistry

Prof. M. Indira Devi

Submitted

In partial fulfilment of the requirement of the Degree of Doctor of Philosophy in Chemistry of Nagaland University

नागालैण्ड विश्वविद्यालय
NAGALAND UNIVERSITY
(संसद द्वारा पारित अधिनियम 1989, क्रमांक 35 के अंतर्गत स्थापित केंद्रीय विश्वविद्यालय)
(A Central University established by an Act of Parliament No.35 of 1989)
मुख्यालय : लुमामी, जिला : जुन्हेबोटो (नागालैण्ड), पिनकोड – 798627
Hqrs : Lumami, Dist. Zunheboto (Nagaland), Pin Code – 798627
वेबसाइट / Website : www.nagalanduniversity.ac.in

Prof. M. Indira Devi
cam_indira@yahoo.co.in
Senior Professor

Department of Chemistry

CERTIFICATE

This is to certify that the thesis entitled "***Synthesis of Lanthanide Nanoparticles: Its' Characterization through Crystallography and Spectral Techniques along with their applications.***" is a record of original research work carried out by **Mr. Punazungba Imsong** under my supervision. He is a registered research scholar, bearing the registration no. **Ph.D./CHE/00057** dated **28/08/2017** of the Department of Chemistry.

The candidate has fulfilled all the requirements of Ph.D. regulations of Nagaland University for the submission of thesis. The work is original and neither the thesis nor any part of it has been submitted elsewhere for the award of any degree or diploma. The thesis, therefore, forwarded for adjudication and consideration for the award of degree of Doctorate of Philosophy in Chemistry under Nagaland University.

I am highly impressed with his keen interest and hard work in completing the thesis and with best wishes for grand success in his future endeavor.

(**Prof. M. Indira Devi**)
Supervisor

NORTH-EAST INSTITUTE OF SCIENCE & TECHNOLOGY
(FORMERLY REGIONAL RESEARCH LABORATORY)
(A national R&D Institute of CSIR)
JORHAT 785006, ASSAM, INDIA
Phone:(0376)2370121/9435713687(M)
Fax: 0376 2370011, Gram: RESEARCH
E-mail: swapnali@neist.res.in
shrrljt@yahoo.com
www.neist.res.in

उत्तर-पूर्व विज्ञान तथा प्रौद्योगिकी संस्थान
(सीएसआईआर का अंगीभूत प्रतिष्ठान)
जोरहाट 785006, असम, भारत
फोन 0376-2370121/9435713687 (म)
फक्स 0376 2370011 ग्राम : रिसर्च
ई मेल : swapnali@neist.res.in
www.neist.res.in

Dr Swapnali Hazarika, FRSC
Senior Principal Scientist

Date:

Certificate

This is to certify that the original works described in this accompanying thesis "***Synthesis of Lanthanide Nanoparticles: Its' Characterization through Crystallography and Spectral Techniques along with their applications''*** *has been carried out by* ***Mr. Punazungba Imsong*** under my co-guidance and consultation. I am highly impressed with his keen interest and hard work in completing the thesis.

I hereby forward this thesis as the partial fulfilment for the award of the Degree of Doctor of Philosophy of Nagaland University.

Dr. Swapnali Hazarika
Senior Principal Scientist & Professor (AcSIR)
Head, Centre for Petroleum Research
Group Leader, Chemical Engineering Group
Engineering Sciences and Technology Division
CSIR-North East institute of Science & Technology
Jorhat-785006, Assam, INDIA

नागालैण्ड विश्वविद्यालय
NAGALAND UNIVERSITY
(संसद द्वारा पारित अधिनियम 1989, क्रमांक 35 के अंतर्गत स्थापित केंद्रीय विश्वविद्यालय)
(A Central University established by an Act of Parliament No.35 of 1989)
मुख्यालय : लुमामी, जिला : जुन्हेबोटो (नागालैण्ड), पिनकोड – 798627
Hqrs : Lumami, Dist. Zunheboto (Nagaland), Pin Code – 798627
वेबसाइट / Website : www.nagalanduniversity.ac.in

DECLARATION

I, Mr. **Punazungba Imsong**, bearing registration No. **Ph.D./CHE/00057** dated **28/08/2017** hereby declare that the subject matter of the thesis entitled "***Synthesis of Lanthanide Nanoparticles: Its' Characterization through Crystallography and Spectral Techniques along with their applications.***" is the pure record of work done by me, that the contents of this thesis did not form basis of the award of any previous degree to me or to the best of my knowledge to anybody else, and the thesis has not been submitted for any research degree in any other university/institute. This is being submitted to the Nagaland University for the degree of Doctor of Philosophy in Chemistry.

(**Prof. M. Indira Devi**)
Supervisor

(**Punazungba Imsong**)

Head
Department of Chemistry
Nagaland University

नागालैण्ड विश्वविद्यालय
NAGALAND UNIVERSITY
(संसद द्वारा पारित अधिनियम 1989, क्रमांक 35 के अंतर्गत स्थापित केंद्रीय विश्वविद्यालय)
(A Central University established by an Act of Parliament No.35 of 1989)
मुख्यालय : लुमामी, जिला : जुन्हेबोटो (नागालैण्ड), पिनकोड – 798627
Hqrs : Lumami, Dist. Zunheboto (Nagaland), Pin Code – 798627
वेबसाइट / Website : www.nagalanduniversity.ac.in

CERTIFICATE

This is to Certify that Mr. **Punazungba Imsong**, a registered Research Scholar for Ph.D. degree in Chemistry under Nagaland University, bearing Ph.D. Registration No. Ph.D./CHE/00057, has satisfactorily completed all the courses offered in the Pre-Ph.D. Course Work Programme in the Department of Chemistry, Nagaland University, *Hqrs*. Lumami.

The Course Includes:

CHEM-601 Research Methodology
CHEM-602 Advance in Chemistry
CHEM-603 Literature Review, Report Writing and Presentation

Head
Department of Chemistry
Nagaland University

Sl. No. : 16- 59050

NAGALAND UNIVERSITY

STATEMENT OF MARKS

Ph. D COURSE WORK EXAMINATION, 2017

DEPARTMENT OF CHEMISTRY

The following are the marks secured by **Punazunba**
Roll No. **3/17** *of Ph.D Course Work Examination held in* **2018**

Subject(s)/Paper(s)	Max. Marks	Minimun Qualifying Marks	Marks Secured
Paper No. Chem-601 Research Methodology	100	35	**68**
Paper No. Chem-602 (D) Advance in Chemistry	100	35	**63**
Paper No. Chem-603 Literature Review, Report Writing and Presentation	100	35	**65**
Total Aggregate Marks			**196**
Average Pass Mark – 55 %			

Result	Division	Percentage
Passed	**I Division**	**65.33 %**

Marks compared by

NAGALAND UNIVERSITY H.Q. LUMAMI

COE/Dy. Reg./AR (Exams)

NAGALAND UNIVERSITY

HEAD QUARTERS : LUMAMI

Ph. D COURSE WORK EXAMINATION

This is to certify that Mr/Ms. PUNAZUNGBA

of Nagaland University bearing Roll No. 3/17 is qualified in the Ph.D Course Work Examination

in the Department of CHEMISTRY, Nagaland University held in the Year 20 18

17/5/18

Head of Department
Head
Department of Chemistry
Nagaland University

17/05/18

Dean
Dean
School of Sciences
School of Sciences
Nagaland University
Hqs. Lumami Nagaland

ACKNOWLEDGEMENTS

Thanks to the Almighty God for giving me the strength and ability to understand, learn and complete this work.I have many people to thank for their help but words will probably fall short.

I would like to thank my supervisor, ***Prof. M. Indira Devi****, Department of Chemistry, Nagaland University, Headquarters – Lumami, for her valuable guidance, knowledge, advice and involvement in helping me complete my work successfully.*

I would like to extend my heartfelt appreciation to my co-supervisor Dr. Swanali Hazarika, CSIR- Northeast Institute of Science & Technology, Jorhat, Assam, India. Your unwavering support, expert guidance, and thoughtful insights have been invaluable throughout this journey. Your commitment to excellence and your encouragement have greatly contributed to the success of this research. I am truly grateful for your mentorship and the time you have dedicated to helping me achieve my goals.

I am thankful to the Department of Chemistry, Nagaland, University, Lumami, for providing laboratory facilities to carry out my Ph.D. thesis work. I would like to respectfully thank all the teaching and non-teaching staff in the Department of Chemistry for their assistance and cooperation. I also express my gratitude to my lab mates and all my fellow research scholars for their constant support, love and help.

I thank the UGC Non-NET, India, for financial support.

Thank you to my family and friends for all your support throughout my studies at Nagaland University.

I stay grateful!

Date…….

(Punazungba Imsong)

Department of Chemistry
Nagaland University

DEDICATIONS

This Ph.D. thesis is dedicated to my family. To my parents and sisters, for supporting me and believing that I could accomplish anything I put to my mind. Thank you for all of your support along the way. Thank you for being so patient with me and bringing out the best in me, even when research took turns for the worse. I couldn't have done this without you.

CONTENTS

List of Figures i-ii

List of Tables iii

CHAPTER 1 (1-13)

Introduction

CHAPTER 2 (14-40)

Quantitative analysis of the co-ordination nature of the synthesized Praseodymium (III) Isonicotinic acid nanomaterial: characterization and study of antimicrobial properties

Abstract

2.1. Introduction

2.2. Materials and Method

2.3. Results and Discussion

2.4. Applications

2.5. Conclusion

Acknowledgements

Declaration of Interest

References

CHAPTER 3 (41-56)

Facile synthesis of multifunctional $GdF_3:Eu^{3+}$ nanoparticles and it's characterization

Abstract

3.1. Introduction

3.2. Experimental

3.3. Characterization

3.4. Results and Discussion

3.5. Conclusion

Acknowledgements

Declaration of Interest

References

CHAPTER 4 **(57-75)**

Lanthanum Fluoride nano Crystals doped with Europium: Synthesis and Characterizations

Abstract

4.1. Introduction

4.2. Experimental

4.3. Results and Discussion

4.4. Conclusion

Acknowledgements

Declaration of Interest

References

CHAPTER 5 **(76-91)**

Synthesis and Characterization of Pr(III)F_3:GSH Nanoparticles: Study of Antimicrobial and Antioxidant properties including mammalian blood haemolysis test

Abstract

5.1. Introduction

5.2. Experimental

5.3. Results and Discussion

5.4. Conclusion

Acknowledgements

Declaration of Interest

References

CHAPTER 6 (92-93)

Summary and Conclusion

APPENDIX

List of Figures

Figure No.	Figure Caption	Page No.
Figure 1.1.	Probable chemical reaction for the synthesized Praseodymium(III):Isonicotinic acid nanocrystal.	**17**
Figure 1.2.	FT-IR spectra of (a) Isonicotinic acid and (b) Pr(III):Isonicotinic acid nanomaterial.	**20**
Figure 1.3.	Emission spectra of Pr(III) and Pr(III):Isonicotinic acid nanocomplex.	**22**
Figure 1.4.	Excitation spectra of Pr(III) and Pr(III):Isonicotinic acid nanocrystal.	**22**
Figure 1.5.	XRD spectrum of Praseodymium(III):Isonicotinic acid nanocrystal.	**25**
Figure 1.6.	TGA of the synthesized Praseodymium(III): Isonicotinic acid nanocrystal.	**25**
Figure 1.7.	Absorption spectra of Pr(III) and Pr(III):Isonicotinic acid nanocrystal in aquated DMF (50%v/v).	**29**
Figure 2.1	FT-IR Spectra of GdF_3: Eu^{3+}	**45**
Figure 2.2.	Fluorescent Emission spectra of GdF_3: Eu^{3+} (Europium doped)	**46**
Figure 2.3.	Luminescence Decay curve of GdF_3: Eu^{3+}	**46**
Figure 2.4.	*XRD pattern of* GdF_3:Eu^{3+}	**47**
Figure 2.5.	SEM image of GdF3:$Eu3^{+}$ at (a) 300nm and (b) 100nm	**48**
Figure 2.6.	EDX image Showing the presence of Eu^{3+}, Gd^{3+} & Fluoride compound	**49**
Figure 2.7.	TEM image of GdF_3:Eu^{3+} observed at (a) 20nm and (b) 50nm	**50**
Figure 2.8.	HRTEM and SAED images of of GdF_3:Eu^{3+}	**50**
Figure 3.1.	FT-IR Spectra of GdF_3: Eu^{3+}	**62**
Figure 3.2.	Fluorescence spectra of Lanthanum Fluoride doped with Europium compound	**63**
Figure 3.3.	*XRD pattern of* LaF_3:Eu^{3+} obtained by Solvothermal method	**64**
Figure 3.4.	XPS Survey of LaF_3 doped with Eu^{3+}	**65**

Figure 3.5.	Independent Variable of different elements present in $LaF_3:Eu^{3+}$ Compound	**66**
Figure 3.6.	*SEM image of $LaF_3:Eu^{3+}$ at (a) 200nm and (b) 10 micro meter*	**67**
Figure 3.7.	SAED pattern of *$LaF_3:Eu^{3+}$* with different hkl values	**68**
Figure 3.8.	HR-TEM images of Lanthanum Fluoride doped with Europium	**69**
Figure 3.9.	TEM image of $LaF_3:Eu^{3+}$ observed at (a) 10nm and (b) 50nm	**69**
Figure 4.1.	Spectra from FTIR for PrF3 doped Glutathione	**81**
Figure 4.2.	XRD pattern of PrF_3 doped Glutathione	**82**
Figure 4.2. a.	Assessment of DPPH free-radical scavenging activity in the presence of various concentrations of Trolox.	**84**
Figure 4.2 b.	Assessment of DPPH free-radical scavenging activity in the presence of various concentrations of sample.	**85**
Figure 4.2 c.	Antioxidant activity of standard (Trolox) and the sample using FRAP assay.	**86**
Figure 4.3.	Blood Hemolysis of PrF_3:GSH	**87**

List of Tables

Table No.	**Table Caption**	**Page No.**
Table 1.1.	Analytical data of Praseodymium (III):Isonicotinic acid nanocrystal; calculated values are given in brackets().	**19**
Table 1.2.	FT-IR wavenumbers with functional groups assigned to the Pr(III):Isonicotinic acid nanomaterial.	**21**
Table 1.3.	Antibacterial activity of Pr(III):Isonicotinic acid nanocrystal, metal ion as negative control, commercial drug as positive control.	**26**
Table 1.4.	Minimum Inhibitory Concentration of Pr(III):Isonicotinic acid complex against bacterial pathogens.	**27**
Table 1.5.	Antifungal Activity of Pr(III):Isonicotinic acid nanocrystal.	**27**
Table 1.6.	Computed value of energy interaction parameters Slater-Condon F_k (cm^{-1}), Spin Orbit Interaction ξ_{4f} (cm^{-1}), Nephelauxetic ratio (β), bonding ($b_{1/2}$), and covalency (δ) parameters of Pr(III) and Pr(III)	**29**

	with Isonicotinic acid in aquated (N,N Dimethylformamide) solvent.	
Table 1.7.	Observed and calculated *P* and T_λ (T_λ, λ= 2, 4, 6) intensity parameter of Pr(III) with Isonicotinic acid in aquated Dimethylformamide solvent.	**30**
Table 3.1.	SAED calculations of d-spacing to compare with hkl values	**68**
Table 4.1.	DPPH radical scavenging activity and IC 50 values of the standard Trolox and Sample.	**85**

CHAPTER 1

Introduction

In the realm of nanotechnology, lanthanide nanoparticles stand out as a captivating class of materials, showcasing exceptional properties stemming from the unique characteristics of lanthanide elements. The lanthanide series, which includes 15 elements ranging from atomic number 57 (Lanthanum) to 71 (Lutetium), displays fascinating electronic structures and magnetic properties, making them valuable for numerous applications. Lanthanide nanoparticles, derived from these rare earth elements, offer a plethora of opportunities in fields such as biomedicine, photonics, catalysis, and environmental remediation. This thorough introduction seeks to examine the production, characteristics, and uses of lanthanide nanoparticles.

The unique electronic configuration of lanthanide ions, which is defined by partially occupied 4f orbitals protected by fully occupied 5s and 5p orbitals, results in extraordinary optical and magnetic characteristics. One of the most intriguing features of lanthanide ions is their ability to emit light in response to external stimuli, making them valuable candidates for luminescent materials. Lanthanide-doped nanoparticles, especially Upconversion nanoparticles (UCNPs), have become highly regarded in bioimaging and sensing because of their distinctive capability to transform low-energy near-infrared light into higher-energy visible or ultraviolet light. [1, 2].

Nanostructured materials are characterized by having at least one dimension within the "nanoscale" range, which spans 1-100 nm (with "nano" deriving from the Greek word for dwarf, where 1 nm equals 10^{-9} meters). Based on their dimensional properties, these materials can be categorized into several types: nanoparticles, which are zero-dimensional (such as nanoscale powders and quantum dots); one-dimensional structures (like layered or thin films); two-dimensional forms (including nanowires and nanorods); and three-dimensional configurations (such as bulk nanostructured materials, including crystallites, and certain forms of quasicrystals or amorphous substances).

The production of lanthanide nanoparticles is vital for adjusting their size, shape, composition, and surface features to meet specific application requirements. Various

synthetic methods, including co-precipitation, thermal decomposition, hydrothermal synthesis, and Solvothermal Techniques, have been developed to achieve precise control over the morphology and crystallinity of lanthanide-based nanomaterials. Surface modification strategies such as ligand exchange, encapsulation, and functionalization with biomolecules enable the stabilization of nanoparticles in biological environments, facilitating their use in biomedical applications [3, 4].

Additionally, the magnetic properties of Gadolinium nanoparticles provide potential for use in magnetic resonance imaging (MRI), magnetic hyperthermia therapy, and magnetic separation methods. Lanthanide-doped magnetic nanoparticles possess high magnetic moments and increased relaxivity, making them appealing as contrast agents for MRI, offering enhanced sensitivity and resolution. Moreover, the integration of magnetic and luminous characteristics in bifunctional nanomaterials based on lanthanides shows significant potential for applications in multimodal imaging and theranostics [5, 6].

In recent years, lanthanide nanoparticles have emerged as versatile platforms for environmental monitoring, catalysis, and energy conversion applications. Lanthanide-doped nanomaterials have been investigated as efficient catalysts for various chemical transformations, including organic synthesis, hydrogenation, and pollutant degradation. The unique catalytic properties of lanthanide ions, such as their Lewis acid-base behaviour and redox activity, make them valuable components in heterogeneous catalysis systems [7, 8].

Moreover, the optical characteristics of lanthanide nanoparticles, such as distinct emission bands, significant Stokes shifts, and durability against photobleaching, render them very suitable for optical encoding and information storing purposes. Lanthanide-doped nanocrystals have been employed as luminescent probes for high-throughput screening, multiplexed detection, and anti-counterfeiting technologies. The development of lanthanide-based nanomaterials with tailored optical signatures holds great potential for advancing optical data storage and encryption systems [9, 10].

Furthermore, lanthanide nanoparticles represent a fascinating class of nanomaterials with diverse properties and applications spanning across multiple disciplines [11].

Continued research efforts aimed at understanding the fundamental properties, optimizing synthesis techniques, and exploring novel applications; such findings are expected to drive further advancements in lanthanide-based nanotechnology[12]. Through interdisciplinary collaboration and innovation, lanthanide nanoparticles hold promise for addressing complex challenges revolutionizing various technological fields [13].

Nanomaterials, often referred to as nanostructured materials, exhibit structural features that are intermediate between those of single atoms or molecules and bulk materials [14]. These materials have at least one dimension ranging from 1 to 100 nm (where 1 nm equals 10^{-9} meters) [15]. The swift growth in the use of nanomaterials is driven by their unique physical and chemical properties, which often differ significantly from those of their larger-scale counterparts [16]. It has been recognised in the past twenty years that the dimensions and configuration of materials significantly influence their characteristics. The unique properties of nanomaterials offer significant potential in various advanced technological areas, including nanoelectronics, nanophotonics, biomedicine, information storage, communication, energy conversion, catalysis, environmental protection, and space exploration [17]. The optical properties of nanomaterials, such as linear and nonlinear absorption, photoluminescence, electroluminescence, and light scattering, are both intriguing and useful [18]. The optical or luminescence characteristics of nanomaterials might originate from either their intrinsic features or the introduction of luminous species such as lanthanide ions through doping [19]. In the present study, nanomaterials with both types of luminescent properties have been investigated. The 4f electrons in lanthanide ions are effectively shielded by the filled outer shell orbitals. This shielding, provided by the 5d and 6s electrons, accounts for the sharp emission lines and prolonged excited state lifetimes observed in lanthanide ions [20]. Lanthanide-based materials have a broad range of applications, such as phosphors for fluorescent lighting, amplifiers for fiber-optic communications, display monitor components, X-ray imaging, scintillators, and lasers. These luminescent materials are typically prepared by either complexing Ln^{3+} ions with suitable organic ligands or doping Ln^{3+} into an appropriate inorganic lattice with varying dimensions [21]. Nanometer-sized

particles exhibit reduced optical scattering, making them ideal for use in polymer or glass-based lasers and amplifiers [22]. During synthesis, these nanoparticles can be stabilized with appropriate ligands and incorporated into various matrices [23]. Composites made of luminescent nanoparticles dispersed within a polymer matrix offer notable benefits, as the polymer provides excellent processability and desirable mechanical properties, while the inorganic luminescent material ensures high luminescence efficiency and long-term chemical stability [24]. It contains brief introduction about the history of nanomaterials, different types of nanomaterials, their properties and applications [25]. Emphasis is given to luminescent properties of different types of nanomaterials. Various methods used for the synthesis of nanomaterials are discussed briefly [26]. As the present study mainly deals with the lanthanide ions doped nanomaterials, an overview of lanthanide ions luminescence in solids and its dependence on concentration in the host, particle size of the host, etc. has been given.

Rare-earth fluorides find broad utility in lasers, up- and down-conversion materials, optical communication technology, biological labelling, owing to their high ionicity, coordination numbers, resultant low vibrational energies and wide bandgaps, making them promising candidates for forefront materials [27]. Lanthanide fluoride nanomaterials have demonstrated exceptional optical properties; however, challenges persist in achieving precise control over nanocrystal size, enhancing up-conversion luminescence efficiency, optimizing energy transfer processes, and addressing key scientific issues. It is widely acknowledged that meticulous control over the morphology, dimensionality, and size of fluorides leads to enhancements in the luminous characteristics of the crystals [28].

By modifying factors like temperature, pressure, time, and precursor concentration during reactions, scientists can customize the size and morphology of lanthanide nanoparticles to suit different needs in multiple applications. The solvothermal method enables the synthesis of lanthanide nanoparticles with high purity and crystallinity. The use of organic solvents as reaction media helps to minimize impurities and promote the formation of crystalline nanoparticles with well-defined crystal structures. By choosing suitable lanthanide starting materials and solvents, the solvothermal

technique makes it possible to create lanthanide nanoparticles with desired characteristics in terms of phases and compositions [29]. This flexibility makes it possible to produce various lanthanide-centered materials customized for specific uses in fields like optoelectronics, catalysis, and biomedical imaging [30]. Scaling up solvothermal synthesis allows for the production of lanthanide nanoparticles in large quantities, making it ideal for industrial use. Additionally, the process offers reliable reproducibility, ensuring consistent quality and performance of the nanoparticles in various batches [31]. In summary, the solvothermal method offers precise control over the size, morphology, purity, crystallinity, phase, and composition of lanthanide nanoparticles, making it a versatile and powerful technique for their synthesis with tailored properties for various applications [32].

The application of absorption spectrophotometry has proved to be a valuable and innovative approach for investigating lanthanide chemistry, especially in solution. This method offers a window into the complexities of f-electron transitions within various complexes, shedding light on their conformation and coordination environment [33]. As a result, it has emerged as a robust tool for delving into the intricate chemistry of lanthanides. The power of the metal-ligand bond, coordination geometry, structure of the resulting complex, and interaction of chelate-solvent can be determined by the analysis of various transition states of 4f-4f spectra of lanthanide ions [34].

Lanthanide nanoparticles can be added to medication delivery systems to improve the durability and effectiveness of antioxidant medicines [35]. By encapsulating antioxidant compounds within lanthanide-doped nanoparticles or conjugating them onto the nanoparticle surface, controlled release and targeted delivery of antioxidants can be achieved. This approach allows for localized delivery of antioxidants to specific tissues or organs affected by oxidative stress-related diseases [36].

Lanthanide nanoparticles are being considered as potential antibacterial agents because of their distinctive physicochemical features and ability to specifically target and combat microorganisms [37]. Lanthanide-doped nanoparticles, such as lanthanide-doped upconversion nanoparticles (UCNPs) or lanthanide-doped quantum

dots (QDs), can be engineered to generate reactive oxygen species (ROS) under light irradiation [38]. When lanthanide ions in nanoparticles are exposed to specific wavelengths of light, they engage in energy transfer processes that generate reactive oxygen species (ROS), such as singlet oxygen and hydroxyl radicals. These ROS possess potent antibacterial properties and can induce oxidative damage to various microbial cells, including bacteria, viruses, and fungi. As a result, they can be used as photosensitizers in photodynamic therapy (PDT) for the inactivation of microorganisms [39]. By conjugating antimicrobial agents or photosensitizing molecules onto the surface of lanthanide nanoparticles, targeted delivery of ROS-generating species to microbial cells can be achieved. Upon exposure to light of the appropriate wavelength, lanthanide nanoparticles can produce ROS that selectively kill or inhibit the growth of pathogens, while minimizing damage to surrounding healthy tissues. Lanthanide nanoparticles can be functionalized with antimicrobial agents or peptides to enhance their antimicrobial properties [40]. Surface modification of lanthanide nanoparticles with cationic antimicrobial peptides or antibiotics can facilitate interactions with microbial membranes, leading to membrane disruption, cell lysis, and eventual microbial death [41]. Moreover, the lanthanide nanoparticles possess a favourable ratio of surface area to volume, which enables effective loading and precise release of antimicrobial agents. This, in turn, enhances their effectiveness in combating microbial infections. Lanthanide nanoparticles can be incorporated into antimicrobial nanocomposites or coatings to impart antimicrobial properties to various surfaces and materials [40]. By embedding lanthanide nanoparticles within polymeric matrices or coatings, surfaces can be rendered antimicrobial, preventing the growth and colonization of pathogens [42]. Lanthanide nanoparticle-based nanocomposites have been explored for applications in medical devices, textiles, food packaging, and water purification, offering effective and long-lasting antimicrobial protection [43]. Lanthanide nanoparticles can be combined with other antimicrobial strategies, such as antibiotics, photo thermal therapy, or immunomodulatory agents, to achieve synergistic antimicrobial effects. By integrating multiple antimicrobial mechanisms, lanthanide nanoparticle-based therapies can overcome microbial resistance and improve treatment outcomes for infectious diseases [44].

References:

[1] Wang, Y., Song, S., Zhang, S., & Zhang, H. (2019). Stimuli-responsive nanotheranostics based on lanthanide-doped upconversion nanoparticles for cancer imaging and therapy: current advances and future challenges. *Nano Today*, *25*, 38-67.

[2] Bünzli, J. C. G., & Eliseeva, S. V. (2010). Lanthanide NIR luminescence for telecommunications, bioanalyses and solar energy conversion. *Journal of Rare Earths*, *28*(6), 824-842.

[3] Boyer, J. C., Cuccia, L. A., & Capobianco, J. A. (2007). Synthesis of colloidal upconverting NaYF4: Er3+/Yb3+ and Tm3+/Yb3+ monodisperse nanocrystals. *Nano letters*, *7*(3), 847-852.

[4] Shan, J., Qin, X., Yao, N., & Ju, Y. (2007). Synthesis of monodisperse hexagonal NaYF4: Yb, Ln (Ln= Er, Ho and Tm) upconversion nanocrystals in TOPO. *Nanotechnology*, *18*(44), 445607.

[5] Shen, J., Sun, L. D., & Yan, C. H. (2008). Luminescent rare earth nanomaterials for bioprobe applications. *Dalton Transactions*, (42), 5687-5697.

[6] Cheignon, C., Kassir, A. A., Soro, L. K., & Charbonnière, L. J. (2022). Dye-sensitized lanthanide containing nanoparticles for luminescence based applications. *Nanoscale*, *14*(38), 13915-13949.

[7] Pier, T., & Jüstel, T. (2024). Application of Eu3+ Doped Tungstates for Solid State Lighting.

[8] Wang, F., & Liu, X. (2009). Recent advances in the chemistry of lanthanide-doped upconversion nanocrystals. *Chemical Society Reviews*, *38*(4), 976-989.

[9] Gnach, A., & Bednarkiewicz, A. (2012). Lanthanide-doped up-converting nanoparticles: Merits and challenges. *Nano Today*, *7*(6), 532-563.

[10] Li, Y., Chen, C., Liu, F., & Liu, J. (2022). Engineered lanthanide-doped upconversion nanoparticles for biosensing and bioimaging application. *Microchimica Acta*, *189*(3), 109.

[11] Dong, H., Du, S. R., Zheng, X. Y., Lyu, G. M., Sun, L. D., Li, L. D., Zhang, P. Z., Zhang, C., & Yan, C. H. (2015a). Lanthanide Nanoparticles: From Design toward Bioimaging and Therapy. *Chemical Reviews*, *115*(19), 10725–10815. https://doi.org/10.1021/acs.chemrev.5b00091

[12] Zhang, X., Wang, Y., Cheng, F., Zheng, Z., & Du, Y. (2016). Ultrathin lanthanide oxides nanomaterials: synthesis, properties and applications. *Science Bulletin*, *61*(18), 1422–1434. https://doi.org/10.1007/s11434-016-1155-2

[13] Y ang, D., Ma, P., Hou, Z., Cheng, Z., Li, C., & Lin, J. (2015). Current advances in lanthanide ion (Ln3+)-based upconversion nanomaterials for drug delivery. *Chemical Society Reviews*, *44*(6), 1416–1448. https://doi.org/10.1039/c4cs00155a

[14] Koch, C. C., Langdon, T. G., & Lavernia, E. J. (2017). Bulk Nanostructured Materials. *Metallurgical and Materials Transactions A*, *48*(11), 5181–5199. https://doi.org/10.1007/s11661-017-4298-0

[15] Xia, Y., Yang, P., Sun, Y., Wu, Y., Mayers, B., Gates, B., Yin, Y., Kim, F., & Yan, H. (2003). One-Dimensional Nanostructures: Synthesis, Characterization, and Applications. *Advanced Materials*, *15*(5), 353–389. https://doi.org/10.1002/adma.200390087

[16] Nasilowski, M., Mahler, B., Lhuillier, E., Ithurria, S., & Dubertret, B. (2016). Two-Dimensional Colloidal Nanocrystals. *Chemical Reviews*, *116*(18), 10934–10982. https://doi.org/10.1021/acs.chemrev.6b00164

[17] Behera, A. (2022). Advanced Materials. In *Springer eBooks*. https://doi.org/10.1007/978-3-030-80359-9

[18] Flory, F., Escoubas, L., & Berginc, G. (2011). Optical properties of nanostructured materials: a review. *Journal of Nanophotonics*, *5*(1), 052502. https://doi.org/10.1117/1.3609266

[19] Marin, R., & Jaque, D. (2020). Doping Lanthanide Ions in Colloidal Semiconductor Nanocrystals for Brighter Photoluminescence. *Chemical Reviews*, *121*(3), 1425–1462. https://doi.org/10.1021/acs.chemrev.0c00692

[20] Qin, X., Liu, X., Huang, W., Bettinelli, M., & Liu, X. (2017). Lanthanide-Activated Phosphors Based on 4f-5d Optical Transitions: Theoretical and Experimental Aspects. *Chemical Reviews*, *117*(5), 4488–4527. https://doi.org/10.1021/acs.chemrev.6b00691

[21] Tessitore, G., Mandl, G. A., Maurizio, S. L., Kaur, M., & Capobianco, J. A. (2023). The role of lanthanide luminescence in advancing technology. *RSC Advances*, *13*(26), 17787–17811. https://doi.org/10.1039/d3ra00991b

[22] Ghosh, B., & Chakraborty, P. (2011). Optical Nonlinearities of Colloidal Metal Quantum Dot - Glass Composites for Nanophotonics. In *InTech eBooks*. https://doi.org/10.5772/17109

[23] Heuer-Jungemann, A., Feliu, N., Bakaimi, I., Hamaly, M., Alkilany, A., Chakraborty, I., Masood, A., Casula, M. F., Kostopoulou, A., Oh, E., Susumu, K., Stewart, M. H., Medintz, I. L., Stratakis, E., Parak, W. J., & Kanaras, A. G. (2019). The Role of Ligands in the Chemical Synthesis and Applications of Inorganic Nanoparticles. *Chemical Reviews*, *119*(8), 4819–4880. https://doi.org/10.1021/acs.chemrev.8b00733

[24] Escribano, P., Julián-López, B., Planelles-Aragó, J., Cordoncillo, E., Viana, B., & Sanchez, C. (2008). Photonic and nanobiophotonic properties of

luminescent lanthanide-doped hybrid organic–inorganic materials. *Journal of Materials Chemistry*, *18*(1), 23–40. https://doi.org/10.1039/b710800a

[25] *Introduction to Nanomaterials and Nanotechnology*. (2007). http://books.google.ie/books?id=fVayPgAACAAJ&dq=Pokropivny+V,+Lohmus+R,+Hussainova+I,+Pokropivny+A,+Vlassov+S.+Introduction+to+nanomaterials+and+nanotechnology.+Tartu:+Tartu+University+Press%3B+2007.&hl=&cd=1&source=gbs_api

[26] Baig, N., Kammakakam, I., & Falath, W. (2021). Nanomaterials: a review of synthesis methods, properties, recent progress, and challenges. *Materials Advances*, *2*(6), 1821–1871. https://doi.org/10.1039/d0ma00807a

[27] Zheng, B., Fan, J., Chen, B., Qin, X., Wang, J., Wang, F., Deng, R., & Liu, X. (2022). Rare-Earth Doping in Nanostructured Inorganic Materials. *Chemical Reviews*, *122*(6), 5519–5603. https://doi.org/10.1021/acs.chemrev.1c00644

[28] Zhang, L., Kang, W., Ma, Q., Xie, Y., Jia, Y., Deng, N., Zhang, Y., Ju, J., & Cheng, B. (2019). Two-dimensional Acetate-based Light Lanthanide Fluoride Nanomaterials (F–Ln, Ln = La, Ce, Pr, and Nd): Morphology, Structure, Growth Mechanism, and Stability. *Journal of the American Chemical Society*, *141*(33), 13134–13142. https://doi.org/10.1021/jacs.9b05355

[29] Sun, C., Schäferling, M., Resch-Genger, U., & Gradzielski, M. (2020). Solvothermal Synthesis of Lanthanide-doped NaYF4 Upconversion Crystals with Size and Shape Control: Particle Properties and Growth Mechanism. *ChemNanoMat*, *7*(2), 174–183. https://doi.org/10.1002/cnma.202000564

[30] Cui, Y., Zhang, J., Chen, B., & Qian, G. (2016). Lanthanide Metal-Organic Frameworks for Luminescent Applications. In *Deleted Journal* (pp. 243–268). https://doi.org/10.1016/bs.hpcre.2016.04.001

[31] Saldanha, P. L., Lesnyak, V., & Manna, L. (2017). Large scale syntheses of colloidal nanomaterials. *Nano Today*, *12*, 46–63. https://doi.org/10.1016/j.nantod.2016.12.001

[32] Gai, S., Li, C., Yang, P., & Lin, J. (2013). Recent Progress in Rare Earth Micro/Nanocrystals: Soft Chemical Synthesis, Luminescent Properties, and Biomedical Applications. *Chemical Reviews*, *114*(4), 2343–2389. https://doi.org/10.1021/cr4001594

[33] Choppin, G. R., & Peterman, D. R. (1998). Applications of lanthanide luminescence spectroscopy to solution studies of coordination chemistry. *Coordination Chemistry Reviews*, *174*(1), 283–299. https://doi.org/10.1016/s0010-8545(98)00125-8

[34] Parker, D., Suturina, E. A., Kuprov, I., & Chilton, N. F. (2020). How the Ligand Field in Lanthanide Coordination Complexes Determines Magnetic Susceptibility Anisotropy, Paramagnetic NMR Shift, and Relaxation Behavior. *Accounts of Chemical Research*, *53*(8), 1520–1534. https://doi.org/10.1021/acs.accounts.0c00275

[35] Zhang, Y., Wei, W., Das, G. K., & Tan, T. T. Y. (2014). Engineering lanthanide-based materials for nanomedicine. *Journal of Photochemistry and Photobiology C Photochemistry Reviews*, *20*, 71–96. https://doi.org/10.1016/j.jphotochemrev.2014.06.001

[36] Banavar, S., Deshpande, A., Sur, S., & Andreescu, S. (2021). Ceria nanoparticle theranostics: harnessing antioxidant properties in biomedicine and beyond. *Journal of Physics Materials*, *4*(4), 042003. https://doi.org/10.1088/2515-7639/ac0594

[37] Nethi, S. K., Bollu, V. S., P, N. a. A., & Patra, C. R. (2020). Rare Earth-Based Nanoparticles: Biomedical Applications, Pharmacological and Toxicological Significance. In *Springer eBooks* (pp. 1–43). https://doi.org/10.1007/978-981-15-0391-7_1

[38] Wang, Y., Song, S., Zhang, S., & Zhang, H. (2019). Stimuli-responsive nanotheranostics based on lanthanide-doped upconversion nanoparticles for cancer imaging and therapy: current advances and future challenges. *Nano Today*, *25*, 38–67. https://doi.org/10.1016/j.nantod.2019.02.007

[39] Zhou, Z., Song, J., Nie, L., & Chen, X. (2016). Reactive oxygen species generating systems meeting challenges of photodynamic cancer therapy. *Chemical Society Reviews*, *45*(23), 6597–6626. https://doi.org/10.1039/c6cs00271d

[40] Kandoth, N., Barman, S., Chatterjee, A., Sarkar, S., Dey, A. K., Pramanik, S. K., & Das, A. (2021a). Photoactive Lanthanide-Based Upconverting Nanoclusters for Antimicrobial Applications. *Advanced Functional Materials*, *31*(43). https://doi.org/10.1002/adfm.202104480

[41] Li, Z., Lu, S., Li, X., Chen, Z., & Chen, X. (2023a). Lanthanide Upconversion Nanoplatforms for Advanced Bacteria-Targeted Detection and Therapy. *Advanced Optical Materials*, *11*(11). https://doi.org/10.1002/adom.202202386

[42] Jia, B., Du, X., Wang, W., Qu, Y., Liu, X., Zhao, M., Li, W., & Li, Y. (2022). Nanophysical Antimicrobial Strategies: A Rational Deployment of Nanomaterials and Physical Stimulations in Combating Bacterial Infections. *Advanced Science*, *9*(10). https://doi.org/10.1002/advs.202105252

[43] De Pasquale, I., Lo Porto, C., Dell'Edera, M., Petronella, F., Agostiano, A., Curri, M. L., & Comparelli, R. (2020). Photocatalytic TiO2-Based Nanostructured Materials for Microbial Inactivation. *Catalysts*, *10*(12), 1382. https://doi.org/10.3390/catal10121382

[44] Bueno, J. (2019). Nanotheranostics approaches in antimicrobial drug resistance. *Nanotheranostics: Applications and Limitations*, 41-61. https://doi.org/10.1007/978-3-030-29768-8_3

CHAPTER 2

Quantitative analysis of the co-ordination nature of the synthesized Praseodymium(III)Isonicotinic acid nanomaterial: characterization and study of antimicrobial properties

Abstract:

Praseodymium(III):Isonicotinic acid nano crystal was successfully synthesized through a simple technique and characterised by elemental analysis, molar conductance, FT-IR, X-ray powder diffraction, fluorescence, UV-vis spectroscopy and thermogravimetric studies. The evaluated Energy interaction and Judd Ofelt Intensity parameters from the UV- vis spectra of the synthesised nano crystal could suggest the mode of co-ordination of Pr(III) with isonicotinic acid. Further, there *in vitro* antimicrobial properties were also studied. The isonicotinic acid ligand is composed of carbonyl oxygen atom and nitrogen atom of the pyridine ring as potential donor sites. Deprotonation of the ligand sites enabled metal-ligand coordination, and as a result, isonicotinic acid behaves as a bidentate ligand. A coordination number of nine was assigned to the praseodymium(III) ion in this nano crystal with monoclinic structure. The nanomaterial was found to be thermally stable and shows good photochemical and antimicrobial properties.

2.1 Introduction

Over the last few decades, the domain of lanthanide chemistry has gained increasing prominence in the realm of modern science. These efforts focus largely on the creation of complexes with novel structural features for the production of advanced materials as well as the use of their unique spectroscopic properties in the development of biological probes and sensors in the fields of molecular biology and clinical chemistry. The wide range of applications for lanthanide compounds in biology and medicine has made lanthanide coordination chemistry an increasingly significant part of contemporary chemistry. The low toxicity and exceptional magnetic and luminous properties of lanthanide compounds make them particularly attractive for prospective uses [1] in medicine and diagnosis. There is a lot of interest in the interactions of rare earths with enzymes and proteins and their application as luminous probes in physiologically significant systems. Lanthanide ions have been commonly utilised as spectroscopic Ca^{2+} probes and as diagnostic tools in clinical research [2]. This is particularly notable due to the contrasting magnetic behaviours of calcium (diamagnetic) and praseodymium (paramagnetic). The bonding mechanism between the lanthanide and their ligands is extremely interesting and significant since their bio-applications involve the interaction of the biological ligands with the lanthanide [3].

Pyridine, an essential heterocyclic compound prevalent in many natural products, holds notable biological significance. The pyridine ring system serves as a vital component in numerous pharmaceuticals available in the market. Isonicotinic acid is a derivative of pyridine which has various applications in the synthesis of pharmaceuticals, agrochemicals, and coordination complexes due to its ability to form stable complexes with metal ions. It is often used as a ligand in coordination chemistry studies involving transition metals and lanthanides. As reported, lanthanides have demonstrated the capacity to create stable complexes with Schiff bases and many other newly synthesized compounds or its derivatives [4]. A significant percentage of these described nanomaterial have been utilised pharmaceutically. Lanthanide complexes have been reported to possess anticancer, antibacterial, antifungal, and several other diverse therapeutic characteristics [5]. Regarding biological efficacy, research

indicates that lanthanide complexes exhibit enhanced antimicrobial activity contrast to the lanthanide ion and ligand [6].

The application of absorption spectrophotometry has proved to be a valuable and innovative approach for investigating lanthanide chemistry, especially in solution. This method offers a window into the complexities of f-electron transitions within various complexes, shedding light on their conformation and coordination environment. As a result, it has emerged as a robust tool for delving into the intricate chemistry of lanthanides.[7–9]. The power of the metal-ligand bond, coordination geometry, structure of the resulting complex, and interaction of chelate-solvent can be determined by the analysis of various transition states of *4f-4f spectra* of lanthanide ions [10].

In this study we have successfully synthesized Praseodymium(III):Isonicotinic acid nano crystal through a facile method. The synthesized nanomaterial was characterized using the following techniques: elemental analysis, IR, powdered XRD, fluorescence studies, UV-Vis spectroscopy and TGA. UV-Vis absorption data was employed for computing the energy interaction and intensity parameters of Pr(III) and Pr(III):isonicotinic. This approach facilitated a theoretical exploration of the mode of binding of Pr(III) with isonicotinic acid. Molar conductance was measured, solubility and *in vitro* antimicrobial properties of the synthesized Pr(III): Isonicotinic acid complex was also further studied.

2.2. Materials and methods

Praseodymium(III) nitrate hexahydrate [$Pr(NO)_3.6H_2O$] of 99.9% purity was purchaed from Sigma Aesar and Isonicotinic acid ($C_6H_5NO_2$) was purchased from HIMEDIA. Various Agar were procured from HIMEDIA. Nutrient Broth and Sabouraud dextrose agar were purchased from HIMEDIA. The percentage contents of C, H, O and N were estimated employing CHNS-O analyzer EuroVector. The metal content was determined by the oxalate-oxide method. Molar conductance with 10^{-3} M solutions of the sample is measured in a suitable solvent at room temperatures with Systronic direct reading conductometer. The IR spectra of the sample was run with KBr pellets through spectrophotometer (Spectrum two) over the IR range. Luminescence analysis of the sample was done with SHIMADZU RF – 6000 spectrofluorometer. Powder X-Ray

diffraction study was conducted with Rigaku Ultima IV diffractometer using $Cu_{k\alpha}$ radiation of wavelength λ = 1.5406 Å from 10° to 80° (2θ) at room temperature. Thermal analysis was done using the SDT Q600V20.9 Build.

Synthesis of Pr(III):Isonicotinic acid complex

Praseodymium(III):Isonicotinic acid nanomaterial was synthesized using the general method outlined below. 20 ml of 0.01 mol aqueous solution of the ligand was added to 20 ml of hot alcoholic solution of praseodymium(III) nitrate hexahydrate and refluxed for 24-36 hours at its isoelectric point with a definite pH of the solution. The solution was then concentrated by keeping it in a water bath until its volume was reduced to half. After cooling, the solution underwent filtration; the residue got retained at normal temperature. Later on, the developed crystallite at the bottom of the beaker were collected and washed it with distilled water, alcohol and followed with ether. Collected crystals were then dried in a desiccator.

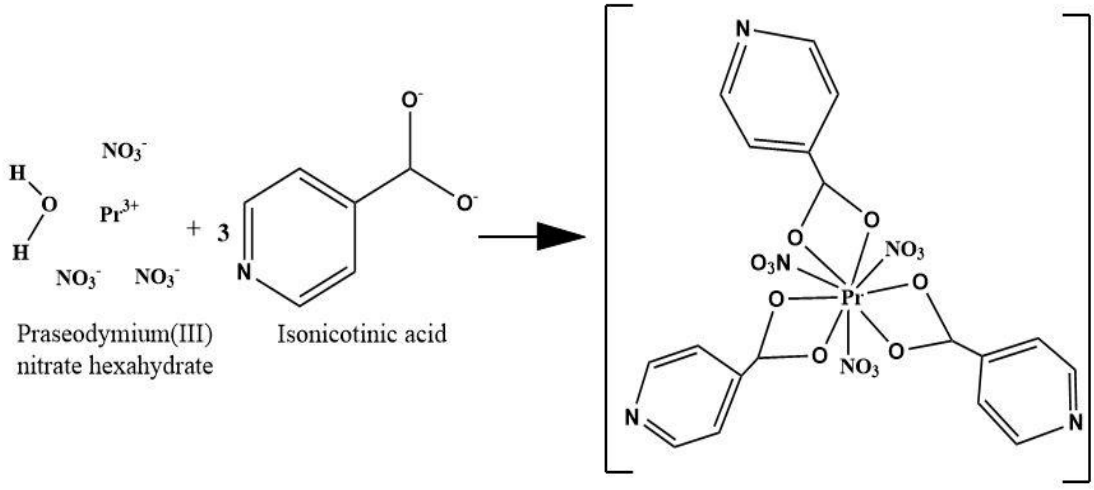

Figure 1.1. Probable chemical reaction for the synthesized Praseodymium(III):Isonicotinic acid nanocrystal.

Biological Activity

Source of Microorganism: For evaluating the antimicrobial effects, various isolates including Gram-positive bacteria like *Staphylococcus aureus* and *Bacillus subtilis*, as well as Gram-negative bacteria *Escherichia coli* and *Klebsiella pneumonia* were used.

Additionally, fungal cultures like *Fusarium oxysposum, Penicillium italicum, Aspergillus niger* and *Candida albicans* were also involved in the study.

Antibacterial Assay: The antibacterial property of the synthesised nano crystal was evaluated focusing the zone of inhibition applying the well-diffusion method. Ampicillin was used as the standard drug for the antibacterial activity tests. The bacterial strains were cultured on 20ml of sterile nutrient broth and incubated overnight at 37 ˚C. The standard cultures were employed in a loop for the antibacterial test. Agar media was poured into the petri plates and left to solidify. The agar plate surface is used as the basal-medium for growth of the cultured bacteria. With the use of sterile borers, wells are made on the solidified agar media. The bacterial broth was spread uniformly on top of solid nutrient agar medium in petri plates. After air drying the inoculated agar medium, 50 µL of the sample with a 1 mg/mL concentration were loaded on to the bored wells and incubated for 24 hrs at 37 ˚C. Reference antimicrobial drug is added to additional wells [10]. Following incubation, the clear zone of inhibition diameter (mm), formed around the centre of the well was measured and compared with the inhibition diameter of positive control ampicillin.

Following the same procedure of the antibacterial assessment, other antifungal tests were followed. Antifungal activity of the praseodymium complex was studied against four fungal strains, *Aspergillus niger, Penicillium italicum, Candida albicans* and *Fusarium oxysposum.* In contrast to the previous assay, Sabouraud dextrose agar was used instead of nutrient agar for media preparation. 50 µl of the specimen has been put in the wells. The samples have been incubated at 30°C for 72 hours. The resulting outcome have been recorded for the area of hinderance in mm [13].

Minimum Inhibitory Concentration (MIC): MIC has been found out employing the method of tube dilution with various dilution of sample (i.e., 300 µg/ml, 500 µg/ml, 600 µg/ml, 800 µg/ml and 1 mg/ml) [11]. These different concentrations of the sample were added into individual test tubes adjusting to 2 ml using nutrient broth. 2ml of prepared solution taken in a test tube got autoclaved at 121°C with 15 lbs pressure for 15 minutes followed by sterilization. After cooling 0.2ml of 24 hours cultures for every bacterial strain were passed out into the antiseptic intermediate and the further

incubated for overnight. These action is observed with examining the cloudiness in the stock [12].

2.3. Results and discussion

Analytical data indicates that praseodymium(III):Isonicotinic acid nanomaterial was formed with a metal-ligand stoichiometry of 1:3 and it possess good keeping qualities. The nano crystal is low water solubility solid and is soluble in methanol, ethanol, MeCN, DMF etc. Analytical values of the complex were found to be in conformation with their formation; elemental analysis and metal composition data which are given in Table 1.1. The molar conductance value of the complex (**Table 1.1**) was in the range of 11.9 Ω cm^{-2} mol^{-1} in DMF solution at room temperature. This value implies that the nanocrystal doesn't form ions easily in nature [14].

Table 1.1. Analytical data of Praseodymium (III):Isonicotinic acid nanocrystal; calculated values are given in brackets().

Sl. No.	Complex	%Yield	Colour	M	C	H	N	O	Molar conductance (DMF) Ω cm^{-2} mol^{-1}
1	$Pr(INA)_3(NO_3)_3$	91	Greenish	19.06 (19.01)	34.11 (34.16)	3.01 (2.96)	11.37 (11.46)	32.45 (32.40)	11.9

IR Spectra

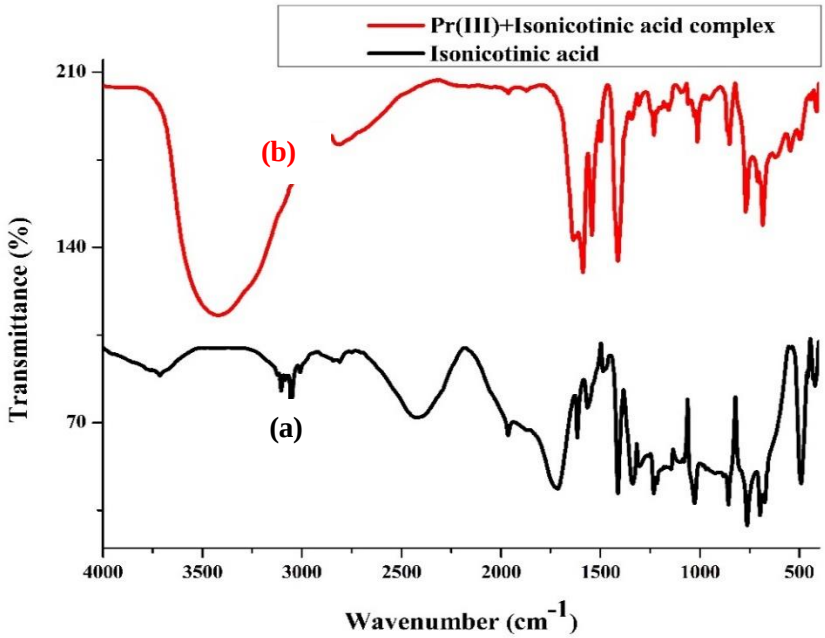

Figure 1.2. FT-IR spectra of (a) Isonicotinic acid and (b) Pr(III):Isonicotinic acid nanomaterial.

The infrared spectra of Pr(III):Isonicotinic acid complex and pure ligand is shown in **Fig. 1.2.** The nature of infrared absorption frequencies of the synthesized nano complex in solid state are tabulated in **Table 1.2**. On analysing the characteristic infrared absorption frequencies for the synthesize nano complex, we could observe intense peaks at 1644.98 cm^{-1} corresponding to the asymmetric stretching vibrations of the carboxyl group as observed for the coordinated carboxylate ligands [15]. When a carboxylic acid is protonated, the stretching frequency shifts to 1700 cm^{-1} and when it is deprotonated the frequency shifts towards 1600 cm^{-1}. The -(C=O) vibration found in the IR spectrum for the complex at 1644.98 cm^{-1} got disappear in the spectrum of the ligand suggesting the deprotonation of the carboxyl group [6]. Electronic transition bands at 3414.92, 1231.62, 1021.06 and 690.70 cm^{-1} corresponded to -(C=N) and -(C=C) modes of the pyridine ring. C-H bending vibration becomes visible at 1409.47 cm^{-1}. The peaks in around 491.99 cm^{-1} and 419.62 cm^{-1} may correlate with metal coordination with oxygen and nitrogen sites; M-O and M-N, respectively [16,17].

Presence of asymmetric stretching vibration of -N-O was seen in 1539.49 which was absent in the ligand spectra.

Table 1.2. FT-IR wavenumbers with functional groups assigned to the Pr(III):Isonicotinic acid nanomaterial

Sl. No.	Assignments (Functional groups)	Wavenumber (cm^{-1})
		Pr(III):Isonicotinic acid complex
1	-HC=CH stretching (aromatic compound)	3414.92
2	-O-H (carboxylic acid)	2889.95(s), 2797.96(b)
3	-C=O (Carboxylic acid)	1644.98
4	-COO stretching	1589.78,
5	-N-O asymmetric stretching (nitro compound)	1539.49
6	-C-H bending (aromatic compound)	1409.47
7	-C-N stretching (aromatic compound)	1231.62
8	-CH=CH bending (aromatic compound)	1021.06, 690.70
9	Ring	851.38, 766.75

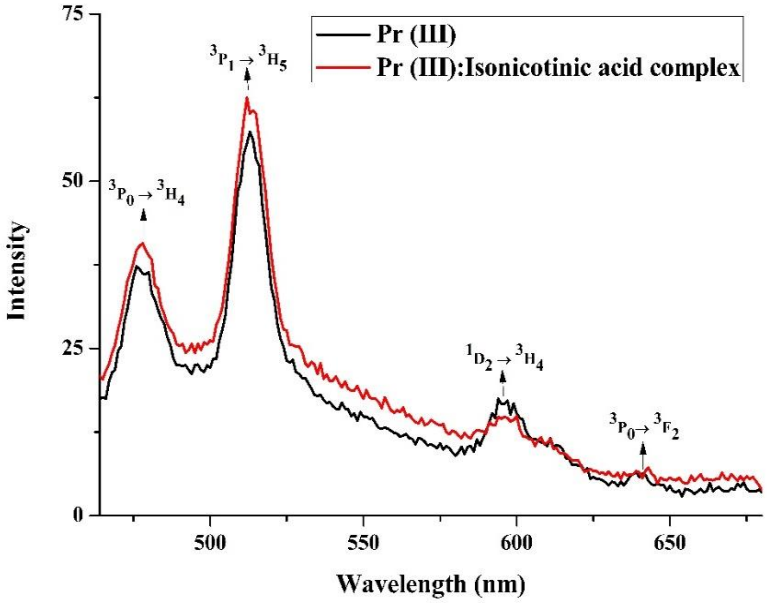

Figure 1.3. Emission spectra of Pr(III) and Pr(III):Isonicotinic acid nanocomplex.

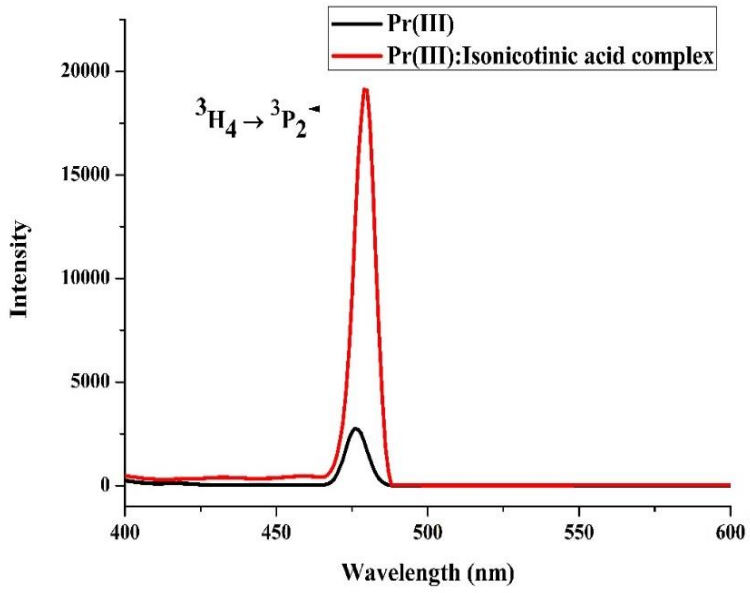

Figure 1.4. Excitation spectra of Pr(III) and Pr(III):Isonicotinic acid nanocrystal.

Fig. 1.3. shows the optical emission spectra of Pr^{3+} ion and Pr(III):Isonicotinic acid complex in the spectral region of 430–680 nm obtained by excitation at 444 nm

corresponding to the $^3H_4 \rightarrow {}^3P_2$ transition of Pr(III). The emission bands centred at 477, 512, 595 and 640 nm are assigned to $^3P_0 \rightarrow {}^3H_4$, $^3P_1 \rightarrow {}^3H_5$, $^1D_2 \rightarrow {}^3H_4$ and $^3P_0 \rightarrow {}^3F_2$ transitions, respectively. Upon 444 nm excitation, the excited Pr^{3+} ion decays non-radiatively from the ^3P_J and $^1D_2$ excited state to the lower lying $^3H_4$, $^3H_5$ and $^3F_4$ energy states[18,19]. The luminescence intensity of the emission transitions depends on the population of the complexes and Pr^{3+} ion in the excited levels. However, the intensity of the $^3P_0 \rightarrow {}^3H_4$ transition is high due to the fast non-radiative decay from the higher lying $^3P_{2,1,0}$ levels. The inset of **Fig. 1.3.** describes the emission channels of Pr^{3+} ions in Pr(III):isonicotinic nanocomplex. From the emission spectra it is clear that the emission intensity of the $^3P_0 \rightarrow {}^3H_4$ transition is almost constant for the Pr(III):Isonicotinic acid complex due to the increase in the energy transfer among the excited Pr(III) ions. Moreover, the free metal ion and praseodymium(III) complex of the emission bands $^3P_0 \rightarrow {}^3F_4$ and $^1D_2 \rightarrow {}^3H_4$ transition overlap each other, whereas for $^3P_0 \rightarrow {}^3H_4$, $^3P_1 \rightarrow {}^3H_5$ are well resolved. Significant red shift has been observed for all the emission spectra; $^3P_0 \rightarrow {}^3H_4$, $^3P_1 \rightarrow {}^3H_5$, $^1D_2 \rightarrow {}^3H_4$ and $^3P_0 \rightarrow {}^3F_4$. The red shift associated could be due to the dispersion of excited ions in the sorrundings of ligand fields during complexation [20]. The intensities of all the observed emission bands increase on complexation to form nanocrystal. This may be mainly due to the phenomenon of quenching through drive between the excited states of Pr(III) ion. The discharge dominates from the $^3P_0$ state which is populated by fast multiphonon non-radiative relaxation from the higher lying $^3P_{2,1,0}$ levels. As the interraction between Pr(III) ion and isonicotonic acid takes place, energy transfer process becomes more predominant and fast quenching in emission intensity takes place [21]. For Ln(III):Ligand complexes, red emission quenches significantly. The lanthanide nanocomplexes show distinct increase in the emission intensity compared to that of the free ionic form of the metal. Enhancement with the emission intensity associated with the complex shows clear evidence of metal-ligand complexation. The quantum yield for Pr(III):Isonicotinic acid nanocomplex was found to be 0.0575. Compared to the Pr(III) ion, which served as their precursor, the Pr(III) complex displayed significant fluorescence intensities. Binding of Pr(III) with ligand in the formation of the complex could have made the ligand more rigid in its conformation, which would have raised the fluorescence intensities of the complexes. These findings along with

the value of quantum yield could indicate that the complex could be useful in photochemical applications [22–24].

X-Ray Diffraction

X-ray emission model of Praseodymium(III):Isonicotinic acid nanocrystal is given in **Fig. 1.5.** Unit cell data and Miller indices were used to connect the Bragg angles and the set of inter planar spacing to these values, which were then applied to the individual reflections using the formula of sin 2θ [25]. The reflections between 2θ in the diffractogram of the complexes ranged from 10 to 80°, with a maxima at 2θ = 16.69. The lattice parameters calculated for the unit cell value of Pr(III):Isonicotinic acid nanocrystal are; a = 7.2391 (Å), b = 7.4661 (Å), c = 6.3910 (Å) and cell volume of cell : 275.03 $(Å)^3$. The observed diffraction pattern corresponds to Anorthic crystal system which match with the JCPDS PDF No. 00-038-1885. The presence of possible phase such as PrO_3 is not observed. This confirms the possible lattice substitution of Pr^{3+} in $(C_6H_5NO)_3^-$ site. The crystallite size was estimated using the Scherrer formula:

$$d_{XRD} = \frac{\kappa\lambda}{\beta \cos\theta}$$

where k is the shape factor (≈0.9), β is the full width at half maximum of the reflection peak, θ is Bragg's angle, and λ is the wavelength of Cu k_α radiation. The average crystallite size (d_{XRD}) is found to be 27.32 nm.

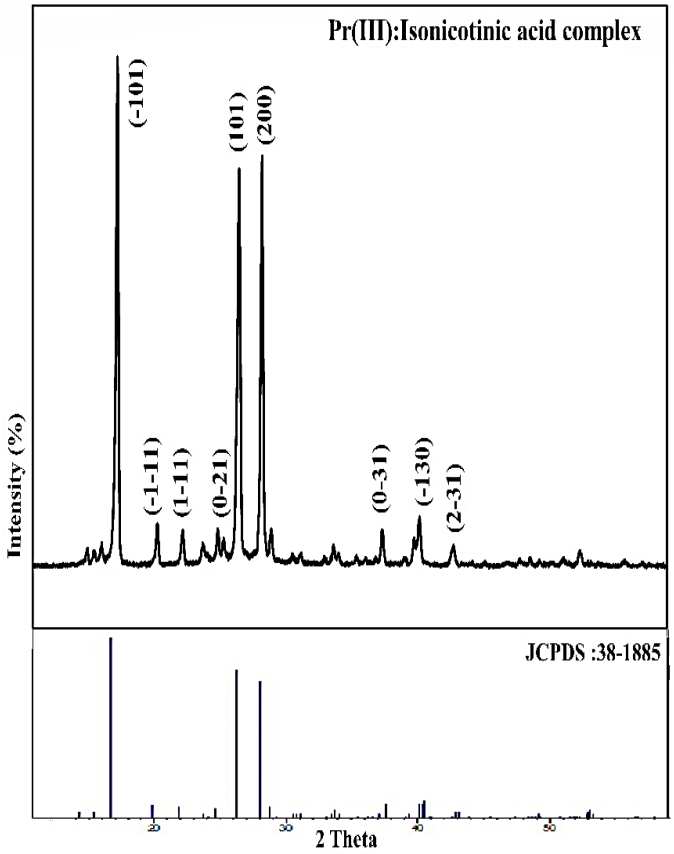

Figure 1.5. XRD spectrum of Praseodymium(III):Isonicotinic acid nanocrystal.

Thermal analysis

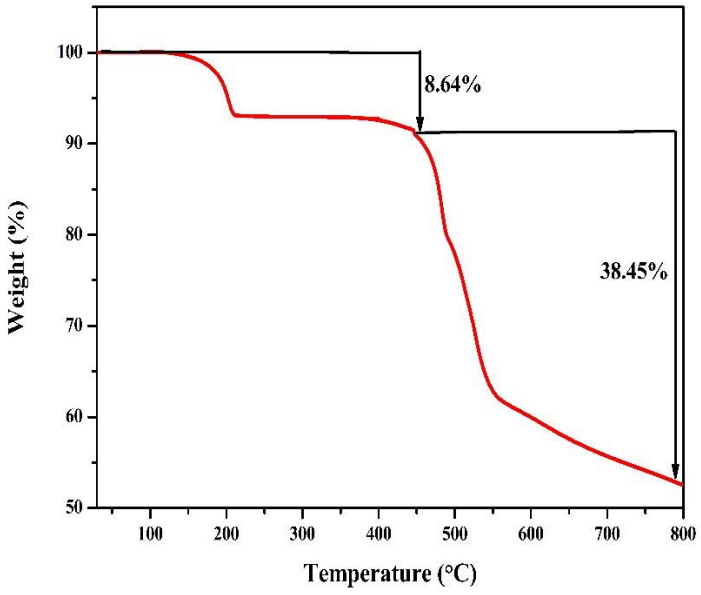

Figure 1.6. TGA of the synthesized Praseodymium(III): Isonicotinic acid nanocrystal.

The TGA measurements for Pr(III):Isonicotinic acid complex was done in dynamic air while being heated at a rate of 20°C/min. **Fig. 1.6** shows TGA curve associated with the complex from which it can be revealed that Praseodymium(III):Isonicotinic acid complex decomposes thermally in two stages; in the first stage a single molecule of pyridine decomposes and in the second stage two molecules of the Isonicotinic acid and methanoic acid was decomposed thus leaving $Pr(NO_3)_3$ as the final residue. The stages of decomposition were in good agreement when compared with the elemental analysis result. The praseodymium (III): Isonicotinic acid complex starts decomposition at a temperature higher than 470^oC which shows that the crystal is thermally stable at room temperature.

Antimicrobial activity

Table 1.3. Antibacterial activity of Pr(III):Isonicotinic acid nanocrystal, metal ion as negative control, commercial drug as positive control.

Sl. No.	Name of bacterial pathogens	Zone of inhibition(mm)		
		Pr(III):Isonicotinic acid complex	Negative control	Positive control (Ampicillin)
1	*Escherichia coli*	28	No zone	25
2	*Klebsiella pneumonia*	21	No zone	28
3	*Staphylococcus aureus*	22	No zone	26
4	*Bacillus subtilis*	23	No zone	19

Table 1.4. Minimum Inhibitory Concentration of Pr(III):Isonicotinic acid complex against bacterial pathogens.

Sl. No.	Name of the bacterial pathogens	Observation of Growth				
		300 µg/ml	500 µg/ml	600 µg/ml	800 µg/ml	1 mg/ml
[Pr(Aspartic acid)$_3$(NO$_3$)$_3$]						
1	***Escherichia coli***	+	-	-	-	-
2	***Bacillus subtilis***	+	+	-	-	-
[Pr(Histidine)$_3$(NO$_3$)$_3$]						
1	***Escherichia coli***	+	+	-	-	-
2	***Bacillus subtilis***	+	-	-	-	-
[Pr(Valine)$_3$(NO$_3$)$_3$]						
1	***Escherichia coli***	+	+	-	-	-
2	***Bacillus subtilis***	+	-	-	-	-

Note: + = Growth of bacteria, - = No growth of bacteria

Table 1.5. Antifungal Activity of Pr(III):Isonicotinic acid nanocrystal.

Sl. No.	Name of Fungal Pathogens	Zone of inhibition (mm)
1	***Candida albicans***	38
2	***Aspergillus niger***	29
3	***Penicillium italicum***	17
4	***Fusarium oxysposum***	14

Antimicrobial Activity of Praseodymium(III) Complex: The antibacterial activity of Pr(III):Isonicotinic acid along with positive control commercial drug (Ampicillin) and negative control metal ion [15] were studied *in vitro* against four microbes organisms such as *Escherichia coli, Klebsiella pneumonia, Staphylococcus aureus* and *Bacillus subtilis. A*ntimicrobial accent of manufactured complex is show in **Table 1.3.** Interestingly, the antimicrobial activity of Pr(III):Isonicotonic acid complex was found to be better than that of the reference drug ampicillin, as observed in the case of *Escherichia coli* and *Bacillus subtilis* while in the case of *Staphylococcus aureus* and *Klebsiella pneumonia* the activities were moderate in comparison to the reference drug. The zone of inhibition (mm) of Pr(III):Isonicotinic acid was 28 mm against

Escherichia coli and 23 mm against *Bacillus subtilis* respectively. Negative control (metal ion) showed no zone of inhibition (**Table 1.3**).

With reference to **Table 1.4.** For the minimum inhibitory concentration of Pr(III)Isonicotinic acid, it is vividly seen that in the case of $Pr(Aspartic\ acid)_3(NO_3)_3$, the pathogen Escherichia coli growth is observed at 300 µg/ml and no growth in 500,600,800 µg/ml and 1mg/ml. whereas in the case of $Pr(Histidine)_3(NO_3)_3$ and $Pr(Histidine)_3(NO_3)_3$, pathogen Escherichia coli growth is found at both 300 µg/ml and 500 µg/ml and no growth for the rest. Considering for the Bacillus subtilis, bacteria growth is found for 300 and 500 µg/ml in the case of $Pr(Aspartic\ acid)_3(NO_3)_3$, whereas for the case of $Pr(Histidine)_3(NO_3)_3$ and $Pr(Histidine)_3(NO_3)_3$ bacterial growth is at 300 µg/ml and no growth for the rest.

The inhibitory activity of Pr(III):Isonicotinic acid nanomaterial was tested against four fungal pathogens; *Candida albicans*, *Aspergillus niger*, *Penicillium italicum* and *Fusarium oxysposum*. Among the fungal germs *Candida albicans* was highly venerable (38 mm) followed by *Aspergillus niger* (29 mm), *Penicillium italicum* (17 mm) and *Fusarium oxysposum* (14 mm). Antifungal outcomes are shown in **Table 1.5**. The antimicrobial studies of confirm that the synthesized complex is biologically active. Overall, the complex exhibited very good antimicrobial activity against all of the tested pathogens.

Minimum Inhibitory Concentration Assay: *Escherichia coli* and *Bacillus subtilis* have been examined to see the lowest level hampering obsession of microbe organisms and it has been found out *Bacillus subtilis at* 300 µg/ml and *Escherichia coli* at 500 µg/ml (**Table 1.4**). This finding are in confirmation with that of Chohan *et al* [26].

UV-Vis spectroscopy studies

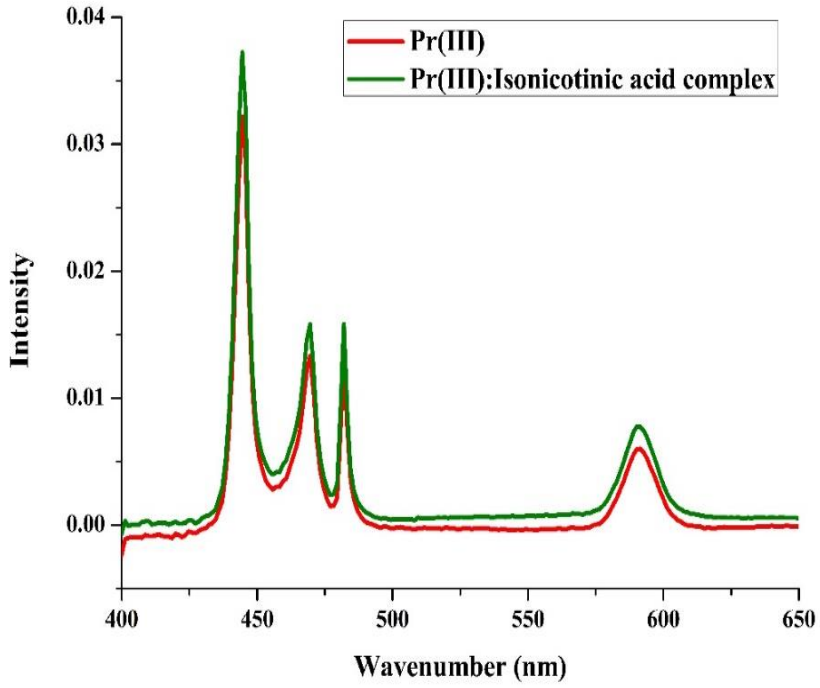

Figure 1.7. Absorption spectra of Pr(III) and Pr(III):Isonicotinic acid nanocrystal in aquated DMF (50%v/v).

Table 1.6. Computed value of energy interaction parameters Slater-Condon F_k (cm^{-1}), Spin Orbit Interaction ξ_{4f}(cm^{-1}), Nephelauxetic ratio (β), bonding ($b_{1/2}$), and covalency (δ) parameters of Pr(III) and Pr(III) with Isonicotinic acid in aquated (N,N Dimethylformamide) solvent.

System	F_2	F_4	F_6	ξ_{4f}	E_1	E_2	E_3	β	$b^{1/2}$	δ	RMS
DMF:Water											
Pr(III)	308.895	42.643	4.664	719.965	3507.395	23.735	614.104	0.944	0.166	5.856	122.50

Pr(III):Isonicotinic acid	**308.592**	**42.601**	**4.649**	**719.767**	**3503.955**	**23.712**	**613.502**	**0.943**	**0.167**	**5.921**	**121.20**

Table 1.7. Observed and calculated *P* and T_λ (T_λ, λ= 2, 4, 6) intensity parameter of Pr(III) with Isonicotinic acid in aquated Dimethylformamide solvent.

System	**$^3H_4 \rightarrow {}^3P_2$**		**$^3H_4 \rightarrow {}^3P_1$**		**$^3H_4 \rightarrow {}^3P_0$**		**$^3H_4 \rightarrow {}^1D_2$**		**T_2**	**T_4**	**T_6**
	Pobs	**Pcal**	**Pobs**	**Pcal**	**Pobs**	**Pcal**	**Pobs**	**Pcal**			
DMF:Water											
Pr(III)	**5.355**	**5.355**	**1.826**	**1.288**	**0.739**	**1.270**	**0.915**	**0.915**	**-147.4**	**3.544**	**16.62**
Pr(III):Isonicotinic acid	**7.838**	**7.838**	**2.991**	**2.038**	**1.071**	**2.010**	**1.125**	**1.125**	**-265.5**	**5.614**	**24.24**

The associated extensively comprehensive available internal f-electron along with susceptibility of Lanthanides to collaboration background and the shape of composite produced with different ligating molecules in simply available spectral regions, have created a technique to an extensive means for employing absorption spectrophotometry as an important technique for analysing chemistry of lanthanides with solutions both in water and non-hygroscopic medium [27,28]. 4*f*-4*f* transitions spectra due to absorption by the Ln^{3+} ions are employed to evaluate the capability of coordination of Ln(III) incorporating suitable ligands, their resulting geometry,

possible configuration of metal-ligand complex formed along with the mode of interaction as well as solvent-chelate [29–31].

Due to the presence of 4f electrons of lanthanide inside the deep core shell, they are naturally not vulnerable to the interaction background and their transitions are known as non-hypersensitive. Contrary to it, hypersensitive transitions obey the selection rule, $\Delta S = 0$, $\Delta L \leq 2$ and $\Delta J = \leq 2$ and are immensely susceptible to the variations of interaction background and consequently the strength of their band intensities becomes stronger when a lanthanide ions make complexation with suitable ligands [32].

These have been observed: transitions associated with Pr^{3+}, ($^3H_4 \rightarrow {}^3P_2$, $^3H_4 \rightarrow {}^3P_1$, $^3H_4 \rightarrow {}^3P_0$ and $^3H_4 \rightarrow {}^1D_2$) defy selection rules. But in some cases, their sensitivity associated with small variation in their coordination surroundings they could able to show uncommon sensitive nature. In fact, these transitions are pseudoquadrupole in nature and also named as Ligand Mediated Pseudohypersensitive transitions which is because of the prompted outcome of their coordination surroundings. These Pseudo hypersensitive transitions have been employed considerably for the analysis of absorption spectrophotometry to comprehend the mode of binding, structural configurations of Pr(III) with various ligands in solution. The bindings of Pr(III) with various ligands and their susceptibility for making of complexes are displayed clearly by the associated increased intensity of the pseudo hypersensitive transitions [33]. In order to study the binding between Pr(III) ion and the Isonicotonic acid ligand, we have performed UV-vis analysis on the free Pr^{3+} ion with the complex system in solution. Additionally, spectral parameters like the energy interaction and intensity parameters have been evaluated using UV-vis data to analyse theoretically the Pr(III) systems in solution.

Table 1.6. shows the computed values of the various parameters: Slator-Condon F_k *(k=2,4,6),* Lande parameter ξ_{4f}, Racah parameter E^k (k=1,2,3), Nephelauxetic ratio β, bonding parameter $b^{1/2}$, covalency δ and RMS values. Getting through the variations of these data of Pr^{3+} and Pr(III):Isonicotinic acid complex in hydrated Dimethylformamide solutions, nature of bonding between Pr(III) and isonicotinic acid ligand could be studied. It could be revealed that the evaluated values of the inter-

electronic repulsion parameters β, ξ_{4f} and F_k for the formation of Pr(III):Isonicotinic acid complex is less compared to that of the Pr(III) metal ion leading to the apparent making of complexes. The increase in inter-electronic binding parameters of percent covalency (δ) and the bonding parameter ($b^{1/2}$) followed by the nephelauxetic ratio (β) values, (that was revealed below unity), could provide the probability of making covalent bond in the formation of complex of Pr^{3+} with isonicotinic acid. Reduced value of (β) could explain the extension of the central metal ion orbital there by shortening the Pr^{3+} ligand bond distance known as nephelauxetic effect. The reduced values of β *could revealed* its association to the increase intensity of different electronic transition bands of Pr(III) ($^3P_2$, $^3P_1$, $^3P_0$, and $^1D_2$) as shown in **Table 1.6**. RMS values could convey how far the evaluated values of energy interaction parameters are valid.

The intensity parameters: Judd-Ofelt parameters (T_λ) and Oscillator strength (P) for the ligand-mediated pseudohypersensitive transitions ($^3H_4 \rightarrow {}^3P_2$, $^3H_4 \rightarrow {}^3P_1$, $^3H_4 \rightarrow {}^3P_0$, and $^3H_4 \rightarrow {}^1D_2$) for Pr^{3+} ion and Pr^{3+}:isonicotinic acid complex was evaluated (Table 1.7). The distinct variations of P (oscillator strength) values corresponding to *4f-4f* bands given in **Table 1.7**. implies the propability of inner sphere coordination linking Pr(III) with isonicotinic acid. When Pr(III) interconnect with the ligand in solution, the magnitude of Judd-Ofelt parameter, T_λ ($\lambda = 2, 4, 6$) varies significantly; this validates the possible inner sphere binding of isonicotinic acid to Pr(III). The evaluated T_4 and T_6 parameters have been observed to be affected significantly on complexation and their values are found to be non-negative; hence, it may be employed in Judd-Ofelt theory for *4f-4f* transitions. T_4 and T_6 parameters are connected to variations in symmetry properties of the complex species hence, the distinct variation in the evaluated values of intensity parameters, T_4 and T_6 could covey the propable variations in its nearest coordination environment thereby produces to the variations in the formation of complex Pr(III) with Isonicotinic acid. On other hand, $^3H_4 \rightarrow {}^3F_3$ transformation found on the other side of UV-Visible region hence, the evaluation of T_2 are non-positive accordingly, T_2 is neglected [31,34]. Evaluation of Oscillator Strength P and its correlated T_λ have distinct changes; it could reveal the probability of inner-sphere complexation whereas minor variations of Oscillator Strength P and

T_λ parameters could convey the possibility of outer-sphere complexation of Pr(III) with isonicotinic acid [35]. The distinct variations of evaluated *P* and T_λ values could convey possible proof of the association of isonicotinic acid with nona-inner-sphere coordination of Pr(III).

2.4. Application

The application for the synthesized Praseodymium(III): Isonicotinic acid nano crystal lies in its potential utilization in various fields including:

Catalysis: Due to its specific coordination structure and thermal stability, the nano crystal could serve as an effective catalyst in organic synthesis or industrial processes, where its unique properties could enhance reaction efficiency.

Photoluminescent Materials: The fluorescence properties of the nano crystal, as evaluated through fluorescence and UV-vis spectroscopy, suggest potential applications in optoelectronic devices, such as LEDs or sensors, where its photochemical properties can be exploited.

Antimicrobial Agents: The in vitro antimicrobial properties indicate that this nano crystal could be explored as an antimicrobial agent in pharmaceuticals or biomedicine, offering a novel approach to combating microbial infections.

Drug Delivery Systems: The thermally stable nature of the nano crystal makes it a promising candidate for drug delivery systems, where controlled release of therapeutic agents can be achieved with minimal degradation or loss of activity.

Material Science: The characterization techniques employed, including elemental analysis, molar conductance, FT-IR, X-ray powder diffraction, provide valuable insights into the structural and chemical properties of the nano crystal, which can be leveraged in the development of advanced materials for various applications.

2.5. Conclusion

Pr(III): Isonicotinic acid nanocrystal was fruitfully manufactured and the it was further analyzed with different scientific methods. These complexes were found to be non-hygroscopic solid and soluble in water and most of the organic solvents. The molar conductance was found to be 11.9 $\Omega^{-1}cm^2mol^{-1}$ with DMF solution at normal temperature indicating the nanomaterial to be normal insulator. Praseodymium (III)

was found to coordinate with Isonicotinic acid ligand via its oxygen anion of deprotonated carboxyl group and the nitrogen atom of the pyridine ring. The metal to oxygen and metal to nitrogen coordination have been justified by our IR data. The synthesized nanomaterial was crystalline in nature and they match the JCPDS PDF No. 00-038-1885 and average crystallite size (d_{XRD}) was calculated to be nano size of 27.32 nm. The lattice constants for the unit cell value of Pr (III): Isonicotinic acid complex are; a = 7.2391 (Å), b = 7.4661 (Å), c = 6.3910 (Å) and cell volume of cell: 275.03 $(Å)^3$. The synthesized complexes possess high thermal stability in air at normal temperature. Metal ion and the complex both are excited at 444 nm and the excited metal ion and complex decayed non-radiatively from the ^3P_J and $^1D_2$ excited state to the lower lying $^3H_4$, $^3H_5$ and $^3F_4$ energy states. The quantum yield was found to was 0.0575. The synthesized nanocrystal was found to exhibit good photochemical properties. The variation in the evaluated values of binding energy parameters (Slator-Condon F_k *(k=2,4,6),* Lande parameter ξ_{4f}, Racah parameter E^k (k=1,2,3), Nephelauxetic ratio β, bonding parameter $b^{1/2}$, covalency δ) could reveal formation of complex between Pr(III) and isonicotinic acid. This fact is again substantiated with variations of values of oscillator strength (P) and Judd-Ofelt intensity parameters with the possible conclusion of formation of inner-sphere coordination between metal Pr(III) and ligand (Isonicotinic acid) with nona-coordinated structure. Based on the *in vitro* antimicrobial study, the synthesized complex was found to be biologically active and possess remarkable antimicrobial properties. Thus, such finding indicate that the synthesized nanocrystal could have potential photochemical and therapeutic applications.

Acknowledgement

The authors would like to acknowledge the department of Chemistry, Nagaland University; Lumami for providing the laboratory facilities. The authors are also grateful UGC NON-NET fellowship for the financial support.

Declaration of Interest

The authors declare no conflicts of interest regarding the publication of this paper.

References:

[1] L.R. Lin, H.H. Tang, Y.G. Wang, X. Wang, X.M. Fang, L.H. Ma, Functionalized Lanthanide(III) Complexes Constructed from Azobenzene Derivative and β-Diketone Ligands: Luminescent, Magnetic, and Reversible Trans-to-Cis Photoisomerization Properties, Inorg. Chem. 56 (2017) 3889–3900. https://doi.org/10.1021/ACS.INORGCHEM.6B02819/SUPPL_FILE/IC6B02819_SI_002.CIF.

[2] C.H. Evans, Biochemistry of the Lanthanides, 1st ed., Springer, New York, 1990. https://doi.org/10.1007/978-1-4684-8748-0.

[3] C.H. Evans, The Interaction of Lanthanides with Amino Acids and Proteins, Biochem. Lanthanides. (1990) 85–172. https://doi.org/10.1007/978-1-4684-8748-0_4.

[4] E. Balogh, M. Mato-Iglesias, C. Platas-Iglesias, É. Tóth, K. Djanashvili, J.A. Peters, A. De Blas, T. Rodríguez-Blas, Pyridine- and phosphonate-containing ligands for stable Ln complexation. Extremely fast water exchange on the GdIII chelates, Inorg. Chem. 45 (2006) 8719–8728. https://doi.org/10.1021/ic0604157.

[5] A. Ali Altaf, A. Shahzad, Z. Gul, N. Rasool, A. Badshah, B. Lal, E. Khan, E.A. Khan, A Review on the Medicinal Importance of Pyridine Derivatives, Http://Www.Sciencepublishinggroup.Com. 1 (2015) 1. https://doi.org/10.11648/J.JDDMC.20150101.11.

[6] M. Nazir, I.I. Naqvi, M. Nazir, I.I. Naqvi, Synthesis, Spectral and Electrochemical Studies of Complex of Uranium(IV) with Pyridine-3-Carboxylic Acid, Am. J. Anal. Chem. 4 (2013) 134–140. https://doi.org/10.4236/AJAC.2013.43018.

[7] Z. Ahmed, K. Iftikhar, Synthesis and visible light luminescence of mononuclear nine-coordinate lanthanide complexes with 2,4,6-tris(2-pyridyl)-1,3,5-triazine,

Inorg. Chem. Commun. 11 (2010) 1253–1258. https://doi.org/10.1016/J.INOCHE.2010.07.009.

[8] Y.F. Zhao, H. Bin Chu, F. Bai, D.Q. Gao, H.X. Zhang, Y.S. Zhou, X.Y. Wei, M.N. Shan, H.Y. Li, Y.L. Zhao, Synthesis, crystal structure, luminescent property and antibacterial activity of lanthanide ternary complexes with 2,4,6-tri(2-pyridyl)-s-triazine, J. Organomet. Chem. 716 (2012) 167–174. https://doi.org/10.1016/J.JORGANCHEM.2012.06.031.

[9] L. Sorace, C. Benelli, D. Gatteschi, Lanthanides in molecular magnetism: old tools in a new field, Chem. Soc. Rev. 40 (2011) 3092–3104. https://doi.org/10.1039/C0CS00185F.

[10] C. Sumitra, T.D. Singh, M.I. Devi, N.R. Singh, Absorption spectral studies of 4f-4f transitions for the complexation of Pr(III) and Nd(III) with glutathione reduced (GSH) in presence of Zn(II) in different aquated organic solvents and kinetics for the complexation of Pr(III):GSH with Zn(II), J. Alloys Compd. 451 (2008) 365–371.

[11] T. Balasankar, M. Gopalakrishnan, S. Nagarajan, Synthesis and antibacterial activity of some 5-(4-biphenylyl)-7-Aryl[3,4-d]-1,2,3-benzoselenadiazoles, Http://Dx.Doi.Org/10.1080/14756360601051365. 22 (2008) 171–175. https://doi.org/10.1080/14756360601051365.

[12] K. Mohanan, R. Aswathy, L.P. Nitha, N.E. Mathews, B.S. Kumari, Synthesis, spectroscopic characterization, DNA cleavage and antibacterial studies of a novel tridentate Schiff base and some lanthanide(III) complexes, J. Rare Earths. 32 (2014) 379–388. https://doi.org/10.1016/S1002-0721(14)60081-8.

[13] M.S. Kadam, S.A. Khiste, S.A. Dake, B.C. Khade, Studies on X-Ray Diffraction, Thermogravimetric Stability, Antibacterial- Antifungal Activity of Fe(II), Ni(II), Cu(II) Metal Chloroquine Complexes Against Bacterial Strains and Fungal Spore, Anti-Infective Agents. 18 (2019) 339–351. https://doi.org/10.2174/2211352517666191021090630.

[14] W.J. Geary, The use of conductivity measurements in organic solvents for the

characterisation of coordination compounds, Coord. Chem. Rev. 7 (1971) 81–122. https://doi.org/10.1016/S0010-8545(00)80009-0.

[15] M.M. Omar, H.F. Abd El-Halim, E.A.M. Khalil, Synthesis, characterization, and biological and anticancer studies of mixed ligand complexes with Schiff base and 2,2′-bipyridine, Appl. Organomet. Chem. 31 (2017) e3724. https://doi.org/10.1002/AOC.3724.

[16] P.P. Devi, F.A.S. Chipem, C.B. Singh, R.K. Lonibala, Complexation of 2-amino-3-(4-hydroxyphenyl)-N′-[(2-hydroxyphenyl) methylene] propane hydrazide with Mn(II), Co(II), Ni(II), Cu(II) and Zn(II) ions: Structural characterization, DFT, DNA binding and antimicrobial studies, J. Mol. Struct. 1176 (2019) 7–18. https://doi.org/10.1016/J.MOLSTRUC.2018.08.070.

[17] M. Nazir, I.I. Naqvi, Synthesis and characterization of uranium (IV) complexes with various amino acids, J. Saudi Chem. Soc. 14 (2010) 101–104. https://doi.org/10.1016/J.JSCS.2009.12.016.

[18] A. Herrera, N.M. Balzaretti, Effect of High Pressure in the Luminescence of Pr 3+ -Doped Ge 2 O-PbO Glass Containing Au Nanoparticles, J. Phys. Chem. C. 122 (2018) 27829–27835. https://doi.org/10.1021/ACS.JPCC.8B08325/ASSET/IMAGES/MEDIUM/JP-2018-08325Q_0010.GIF.

[19] C. Liu, F. Pan, Q. Peng, W. Zhou, R. Shi, L. Zhou, J. Zhang, J. Chen, H. Liang, Excitation wavelength dependent luminescence of LuNbO4:Pr3+-Influences of intervalence charge transfer and host sensitization, J. Phys. Chem. C. 120 (2016) 26044–26053. https://doi.org/10.1021/ACS.JPCC.6B09806/SUPPL_FILE/JP6B09806_SI_001.PDF.

[20] D. Rajesh, A. Balakrishna, M. Seshadri, Y.C. Ratnakaram, Spectroscopic investigations on Pr3+ and Nd3+ doped strontium–lithium–bismuth borate glasses, Spectrochim. Acta Part A Mol. Biomol. Spectrosc. 97 (2012) 963–974. https://doi.org/10.1016/J.SAA.2012.07.100.

[21] B.C. Jamalaiah, J. Suresh Kumar, A. Mohan Babu, L. Rama Moorthy, K. Jang, H.S. Lee, M. Jayasimhadri, J.H. Jeong, H. Choi, Optical absorption, fluorescence and decay properties of Pr3+-doped PbO–H3BO3–TiO2–AlF3 glasses, J. Lumin. 129 (2009) 1023–1028. https://doi.org/10.1016/J.JLUMIN.2009.04.018.

[22] C. Liu, W. Zhou, R. Shi, L. Lin, R. Zhou, J. Chen, Z. Li, H. Liang, Host-sensitized luminescence of Dy3+ in LuNbO4 under ultraviolet light and low-voltage electron beam excitation: energy transfer and white emission, J. Mater. Chem. C. 5 (2017) 9012–9020. https://doi.org/10.1039/C7TC03260A.

[23] R. Kamal, H. Hafez, Novel Down-converting single-phased white light Pr3+ doped BaWO4 Nanophosphors material for DSSC applications, Opt. Mater. (Amst). 121 (2021) 111646. https://doi.org/10.1016/J.OPTMAT.2021.111646.

[24] M. V Sasi Kumar, B.R. Reddy, S. Babu, A. Balakrishna, Y.C. Ratnakaram, B. Rajeswara Reddy, Thermal, structural and spectroscopic properties of Pr3+-doped lead zinc borate glasses modified by alkali metal ions, Https://Doi.Org/10.1016/j.Jtusci.2016.04.004. 11 (2018) 593–604. https://doi.org/10.1016/J.JTUSCI.2016.04.004.

[25] S. Mathews, B.S. Kumari, G. Rijulal, K. Mohanan, Synthesis, Characterization and Antibacterial Activity of Some Transition Metal Complexes of 2-N-(isatinamino)-3-carboxyethyl-4,5,6,7-tetrahydrobenzo[b]thiophene, Http://Dx.Doi.Org/10.1080/00387010802007981. 41 (2008) 154–161. https://doi.org/10.1080/00387010802007981.

[26] Z.H. Chohan, C.T. Supuran, T. Ben Hadda, F.U.H. Nasim, K.M. Khan, Metal based isatin-derived sulfonamides: Their synthesis, characterization, coordination behavior and biological activity, Http://Dx.Doi.Org/10.1080/14756360802447636. 24 (2009) 859–870. https://doi.org/10.1080/14756360802447636.

[27] W.T. Carnall, P.R. Eieids, K. Rajnak, Electronic energy levels of the trivalent lanthanide aquo ions. II. Gd 3+, J. Chem. Phys. 49 (1968) 4407–4411.

https://doi.org/10.1063/1.1669894.

[28] J.B. Gruber, G.W. Burdick, S. Chandra, D.K. Sardar, Analyses of the ultraviolet spectra of Er3+ in Er 2O3 and Er3+ in Y2O3, J. Appl. Phys. (2010). https://doi.org/10.1063/1.3465615.

[29] J. Sanchu, C. Imsong, Z. Thakro, D.M. Indira, Absorption spectral study for the interaction of Pr(III) with L-Aspartic acid in various aquated organic solvents through 4f-4f transition spectra: Analysis of reaction pathways and thermodynamic parameters, J. Pharm. Negat. Results. 13 (2022). https://doi.org/10.47750/PNR.2022.13.S01.105.

[30] J. Sanchu, M. Ziekhrü, Z. Thakro, M.I. Devi, 4f-4f Transition Spectra of the Interaction of Pr(III) with L-Valine in Solution: Kinetics and Thermodynamic Studies, Asian J. Chem. 34 (2022) 2688–2696.

[31] N. Bendangsenla, T. Moainla, J. Sanchu, M.I. Devi, Computation of Energy, Intensity and Thermodynamic Parameters for the Interaction of Ln(III) with Nucleic Acid: Analysis of Structural Conformations, Chemical Kinetics and Thermodynamic Behaviour through 4f-4f Transition Spectra as Probe, J. Mater. Sci. Chem. Eng. (2018). https://doi.org/10.4236/msce.2018.67018.

[32] S.N. Misra, K. John, Difference and Comparative Absorption Spectra and Ligand Mediated Pseudohypersensitivity for 4f-4f Transitions of Pr (lll) and Nd (lll) Difference and Comparative Absorption Spectra and Ligand Mediated Pseudo hypersensi tivi ty for 4f-4f Transitions o, 4928 (2016). https://doi.org/10.1080/05704929308018115.

[33] C. Klixbüll Jørgensen, B.R. Judd, C. Klixbüll Jørgensen, B.R. Judd, Hypersensitive pseudoquadrupole transitions in lanthanides, MolPh. 8 (1964) 281–290. https://doi.org/10.1080/00268976400100321.

[34] T. Moaienla, T.D. Singh, N.R. Singh, M.I. Devi, Computation of energy interaction parameters as well as electric dipole intensity parameters for the absorption spectral study of the interaction of Pr(III) with l-phenylalanine, l-glycine, l-alanine and l-aspartic acid in the presence and absence of Ca2+,

Spectrochim. Acta - Part A Mol. Biomol. Spectrosc. 74 (2009) 434–440. https://doi.org/10.1016/j.saa.2009.06.039.

[35] T. Moaienla, N. Bendangsenla, T. David Singh, C. Sumitra, N. Rajmuhon Singh, M. Indira Devi, Comparative 4f–4f absorption spectral study for the interactions of Nd(III) with some amino acids: Preliminary thermodynamics and kinetic studies of interaction of Nd(III):glycine with Ca(II), Spectrochim. Acta Part A Mol. Biomol. Spectrosc. 87 (2012) 142–150. https://doi.org/10.1016/J.SAA.2011.11.028.

CHAPTER 3

Facile synthesis of multifunctional GdF3: Eu3+ nanoparticles and it's characterization

Abstract

The realm of lanthanide-doped nanomaterials is significantly influencing materials science, driven by their unique spectral characteristics. These versatile materials find applications in the development of advanced optical devices, solar cells, phosphors, lasers,biomedical technologies, marking a revolutionary period in material. In this work, $GdF_3:Eu^{3+}$ nanoparticles were synthesized through a facile Solvothermal process, employing citric acid as a capping agent. The resulting nano-compounds underwent comprehensive characterization utilizing Fourier-transform infrared spectroscopy (FT-IR), fluorescence spectroscopy for photoluminescence analysis, X-ray diffraction (XRD), scanning electron microscopy (SEM), transmission electron microscopy (TEM) to elucidate their dimensional properties, morphology and crystal structure. High-resolution transmission electron microscopy (HRTEM)and crystalline nature of nanoparticles was confirmed by SAED patterns. Additionally, energy-dispersive X-ray spectroscopy (EDX) was employed to ascertain the elemental composition of the synthesized nanocrystals. The determination of the average crystallite size was conducted utilizing the Scherrer equation, deduced from the full-width at half-maximum (FWHM) of the XRD peaks.

Keywords: Rare earths; Gadolinium fluoride; Europium; Solvothermal; Luminescence.

3.1. Introduction

In contemporary research trends, nanomaterials doped with lanthanide ions have emerged as a distinct domain within materials science. Owing to their unique spectral characteristics, they find widespread utility in the fabrication of efficient optical devices, solar cells, phosphors, lasers, and biomedical applications [1]. Leveraging the luminescent properties of Ln^{3+} ions, they are utilized in bioimaging (MRI contrast agents) and phototherapy [2]. The broad spectrum of applications owes much to the exceptional attributes of their dopants, particularly the pronounced f-f transitions responsible for the observed luminescence [3]. In contrast to conventional luminescent nanomaterials such as gold nanoparticles, organic dyes, and semiconductor quantum dots, rare-earth nanoparticles offer several advantages, including well-defined UV/Vis emission lines, sharp absorption spectra, high quantum efficiency, prolonged lifetimes, enhanced photostability, remarkable biocompatibility, and non-toxicity [4,5]. Consequently, the luminescence of lanthanide ions is commonly triggered via indirect refinement processes employing light-harvesting systems [6].

Relative to oxide or sulfide counterparts, fluoride crystals offer distinct advantages such as extended lifetimes, reduced photon energy, and heightened ionicity, resulting in diminished absolute fundamental absorption [7]. Lanthanide fluorides are favoured host materials due to their lower vibrational energies compared to oxides, thereby minimizing quenching of the lanthanide cations' excited states and enhancing the quantum efficiency of luminescence [8]. Employing fluoride sources as host matrices, numerous benefits for lanthanide ions including high transparency, diminished energy phonon interactions, reduced multi-phonon relaxation and a wide bandgap [9]. Rare-earth fluorides find broad utility in lasers, up- and down-conversion materials, optical communication technology, biological labelling, owing to their high ionicity, coordination numbers, resultant low vibrational energies and wide bandgaps, making them promising candidates for forefront materials [10]. Lanthanide fluoride nanomaterials have demonstrated exceptional optical properties; however, challenges persist in achieving precise control over nanocrystal size, enhancing up-conversion luminescence efficiency, optimizing energy transfer processes, and addressing key scientific issues [11]. It is widely acknowledged that meticulous control over the

morphology, dimensionality, and size of fluorides leads to enhancements in the luminous characteristics of the crystals [12].

Moreover, it is widely acknowledged that various external factors, including pH, chelating agents, reaction duration, and the inherent crystal structure, play pivotal roles in governing the crystal growth process [13]. In numerous studies, the addition of chelating or capping agents has emerged as a promising strategy for directing and controlling the morphology of resultant products [14]. When utilized as a capping agent, citrate ions (Cit^{3-}) exert significant influence as ligands and shape modulators, effectively modulating the growth of different crystal facets under hydrothermal and solvothermal conditions, thereby yielding a diverse array of final product geometries [15].

Researcher's endeavours concerning rare-earth fluoride nanocrystals predominantly focus on elucidating their luminescent properties, controlling morphology, optimizing synthesis parameters, and assessing biocompatibility. Among rare-earth ions, Eu^{3+} is frequently preferred for optically active materials due to its emission of narrow-band, nearly monochromatic light with extended average lifetimes in optically active states [16]. On a nanosecond scale, Gd^{3+} exhibits substantial magnetic moment and relaxation time, rendering it paramagnetic and thereby suitable for application as contrast agents in magnetic resonance imaging (MRI) [17]. To tailor crystal growth, chelating reagents are employed, offering the potential to alter crystal nature, yielding varied morphologies and expanding application possibilities [18]. Leveraging its size-selective management and excellent crystallinity, the solvothermal technique emerges as a promising synthetic approach [19]. In the hydrothermal method, numerous factors such as initial pH, reaction temperature, and duration exert significant influence on sample morphologies [20].

The predominant determinant of nanoparticle utility lies in the quantum size effect, contingent upon the abundance of free electrons within each particle. As the concentration of nanomaterials is intricately tied to production methodology, spectroscopic characterization offers insights into their size-related attributes [21]. Through modulation of reducing agents, we investigated the morphology, size, surface

area, and other characteristics of GdF_3: Eu^{3+} nanoparticles synthesized via a solvothermal route [22]. By altering the reducing agents, we were able to study the morphology, size, surface area, and other features of GdF_3: Eu^{3+} nanoparticles synthesised using a solvothermal approach [23].

3.2. Experimental

Materials

GdCl3(99.99%, Sigma Aldrich), Eu (NO3)3 (99.99%, Sigma Aldrich), NH4F (99.99%, HiMedia) Methanol (99.9%, Merck), Ethanol (99.9%, Merck) and Trisodium Citrate (HiMedia) were utilized as the starting material without additional purification.

Method

Synthesis of GdF_3: Eu^{3+}

A compound of GdF_3:Eu^{3+} nanoparticles were prepared by using Solvothermal synthesis. Taking Stoichiometric ratio, a solution of $GdCl_3$ (0.789 mol), Eu (NO3) (0.11 mol) and NH_4F (6.75 mol) were mixed and heat in DI (Deionized) water and methanol (1:1 ratio) using magnetic stirring. A calculated amount of Citric acid (3.952 mol) was added which acted as a chelating agent. After mixing the dissolved solution, it was dispensed inside a Teflon container which were confine in stainless steel autoclave, the solution is then secured and maintained at exact 180 °C for 18 hrs. The obtained compound at the bottom was segregated and cleaned by centrifugation process, followed with deionized water and ethanol solvent for time and again; finally, the remaining compound was dried in oven for about 12 hrs.

3.3. Characterization

The (PerkinElmer Spectrum Two FT-IR Spectrometer) spectrophotometer was used to record FTIR spectra using the KBr pellet technique. To analyse the nano-products, a Fluorescence spectrometer (Model: XRD pattern (Rigaku fitted with Ni filter Cu Ka (l = 1.54056) was employed to capture excitation and emission spectra. SEM was

utilized to examine the morphology and dimensions of the samples (SEM-EDX). TEM was employed to investigate the internal morphology of the nanocompound.

3.4. Results and Discussion

Crystal phases and morphology

FTIR (Fourier-transform infrared spectroscopy)

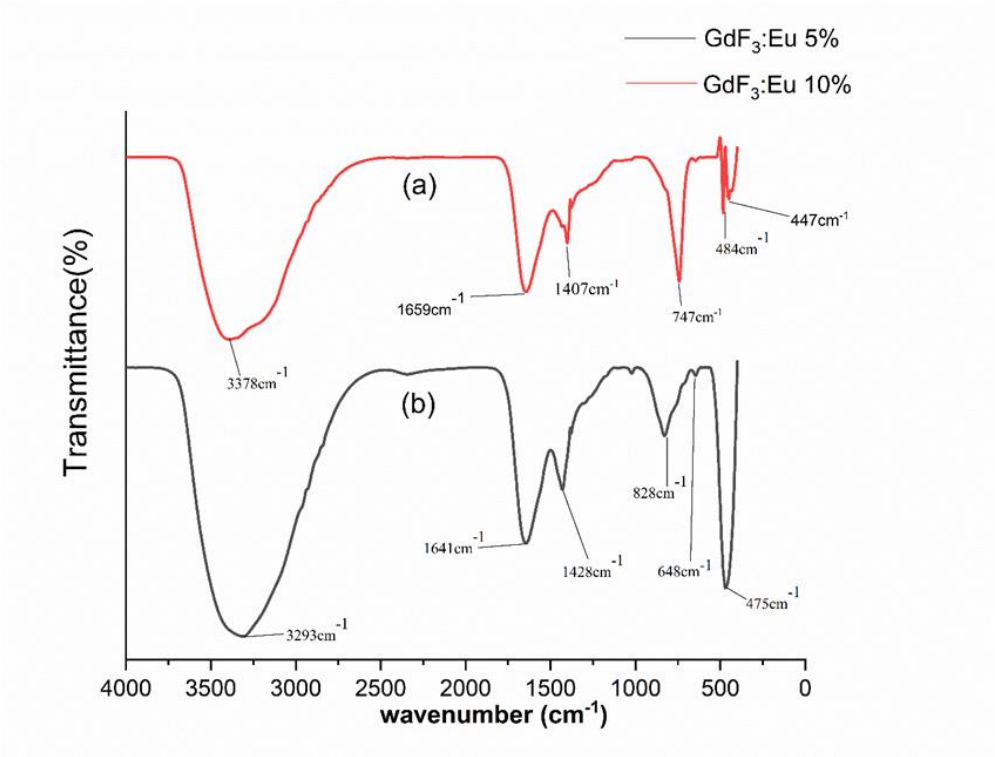

Figure 2.1. FT-IR Spectra of GdF_3: Eu^{3+}

Fig. 2.1. has shown FTIR spectra of the GdF_3:Eu^{3+} nanocrystals (5% & 10% concentration). The characteristic absorption peaks have been observed in the range from 4000cm^{-1} to 400 cm^{-1}.

The broad absorption band around 3378 cm^{-1} is likely due to O-H stretching and bending vibrations, indicative of water [24]. The peak observed at 1659 cm^{-1} can be associated with C=O stretching vibrations of a saturated amide group, as well as coated citric acid. The peak at 1407 cm^{-1} is likely due to the asymmetric and symmetric bending vibrations (Vas and Vs) of the O-H group from methanol. The distinct IR peak

at 1377.81 cm^{-1} can be attributed to C-F stretching, while the sharp peak at 747 cm^{-1} corresponds to C-Cl stretching [25].

Fluorescence Spectroscopy

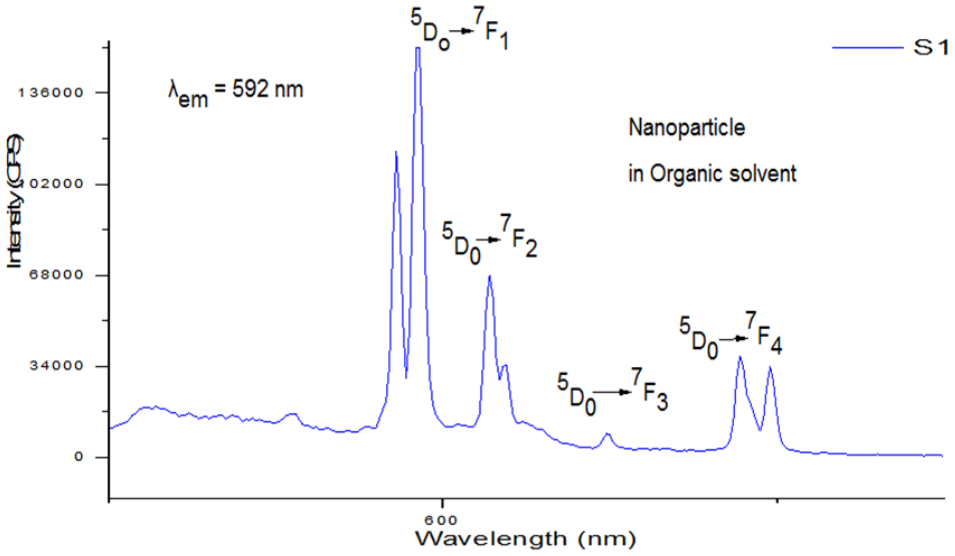

Figure. 2.2. Fluorescent Emission spectra of GdF_3: Eu^{3+} (Europium doped)

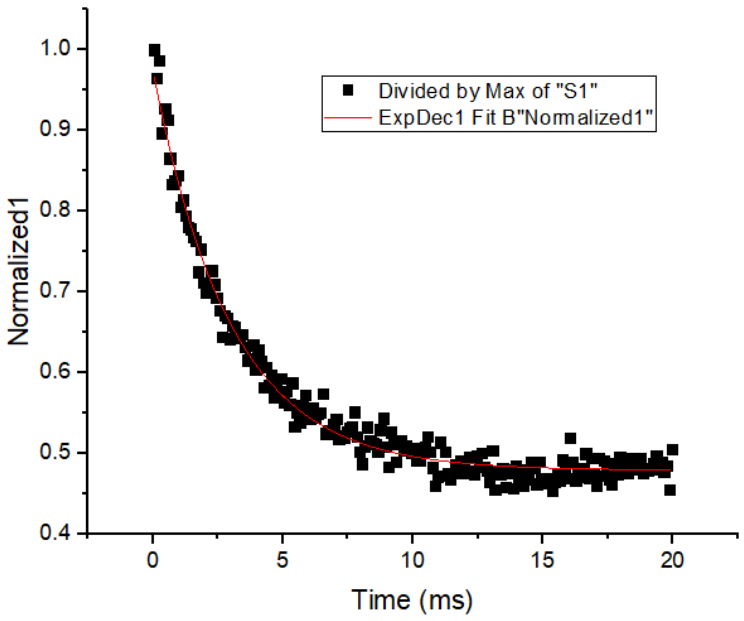

Figure 2.3. Luminescence Decay curve of GdF_3: Eu^{3+}

The decay times pertaining to the nanoparticles were ascertained at room temperature using various excitation energies. **Fig. 2.2.** Excitation spectra of Eu^{3+} emission in GdF_3: Eu^{3+} at ambient temperature measured at 592nm with the transition of $^5D_0 \rightarrow {}^7F_{15}$. The strength of the Gd^{3+} ions excitation peak at 272nm, as demonstrated by the transition $^5D_0 \rightarrow {}^7F_2$, is corresponding to that of the Eu^{3+} ions, indicating efficient energy transfer. **Fig. 2.3.** illustrates a biexponential luminous decay of 592 nm emission stimulated at 393 nm, indicating the appearance of two luminescent decay centres with differing non-radiative decay probabilities [26]. The value of average lifetime is found to be 12.2 ms using the average lifetime formula, indicating synchronized energy migration from Gd^{3+} to Eu^{3+} ions. This also suggests that the synthesized nanoparticles could be utilized for both Magnetic Resonance Imaging and optical applications.

X-ray Diffraction (XRD)

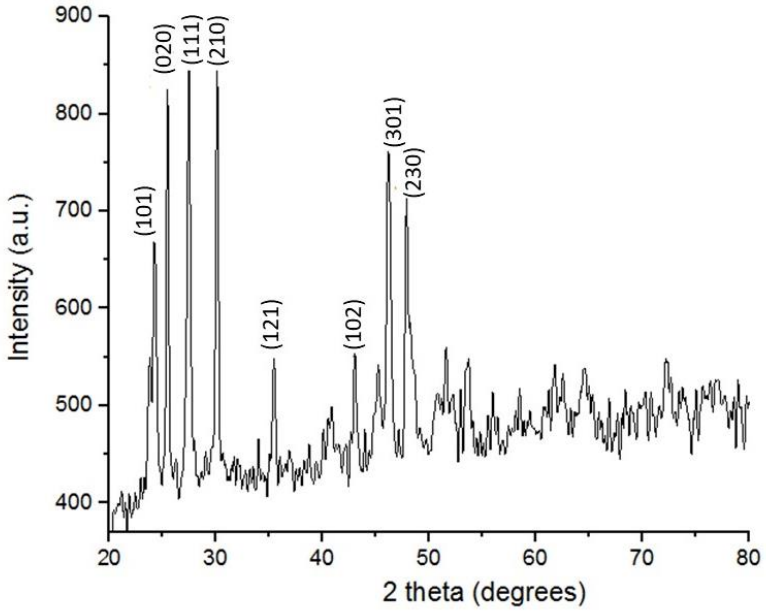

Figure 2.4. XRD pattern of GdF_3:Eu^{3+}

Fig. 2.4. represents the XRD pattern of $GdF_3:Eu^{3+}$ nanoparticles. From the figure, almost all reflection planes have pure crystalline orthorhombic GdF_3 structure (Space group number: 62, Space group: Pnma, with lattice constants a = 6.5710; b = 6.9850, c = 4.3930), which is consistent with standard data (Reference code: 00-012-0788).The orthorhombic phase of $GdF_3:Eu^{3+}$with high purity can be indexed for diffraction plane (101) (020) (111) (210) (121) (102) (301) (230).Since the amount of Eu^{3+} ion in the lattice sites of GdF_3 is too low, XRD could not identify the Eu^{3+} compound [27]. It was observed that the majority of nanoparticles were elongated, with only a few being spherical or nearly spherical. The elongated nanoparticles had average dimensions of approximately 100 nm in length and 50 nm in width. In contrast, the spherical or nearly spherical nanoparticles had typical diameters of about 25 nm, as determined using the Scherrer equation:

$$\text{“D (Å)} = \frac{K\lambda}{\beta \cos\theta}\text{”}$$

Scanning electron microscopy (SEM) and EDX

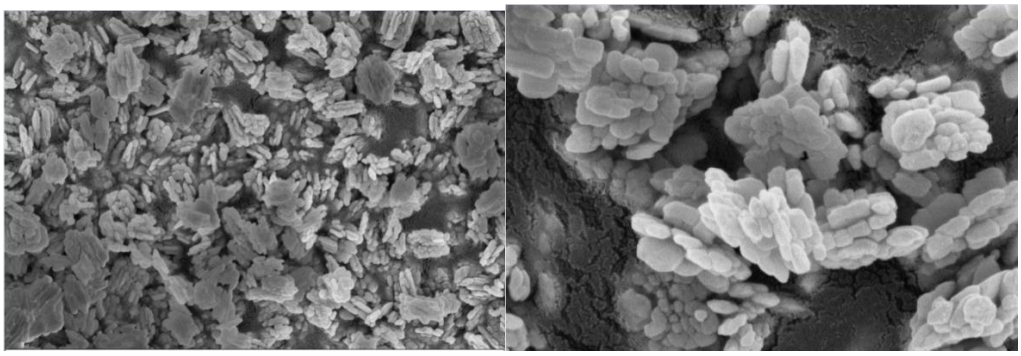

(a) 300nm (b) 100nm

Figure. 2.5. SEM image of $GdF_3:Eu^{3+}$ at (a) 300nm and (b) 100nm

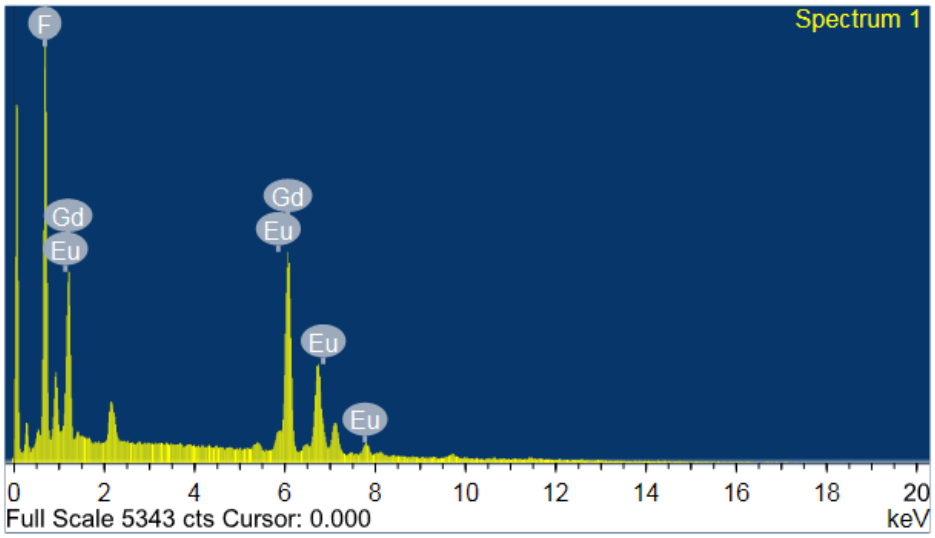

Figure 2.6. EDX image Showing the presence of Eu^{3+}, Gd^{3+} & Fluoride compound

Fig. 2.5. displays the SEM and TEM images that were utilised to evaluate the morphology and inner structure of the product. It is found that the GdF_3:Eu^{3+} sample has virtually sub-microsphere-like structures. The particle size distribution is quite narrow, with more than half of them being between 100 and 300 nanometres in size. **Fig. 2.6.** displays the outcomes of EDX, which was utilized to study the formation of elements in powder form. From the figure, it could be seen the presence of the elements: Europium, Fluoride, and Gadolinium which make up the product. The atomic percentages of the elements Europium and Fluorine are discovered to be in the stoichiometric ratio (1:3).

Transmission electron microscopy (TEM), HRTEM and SAED images

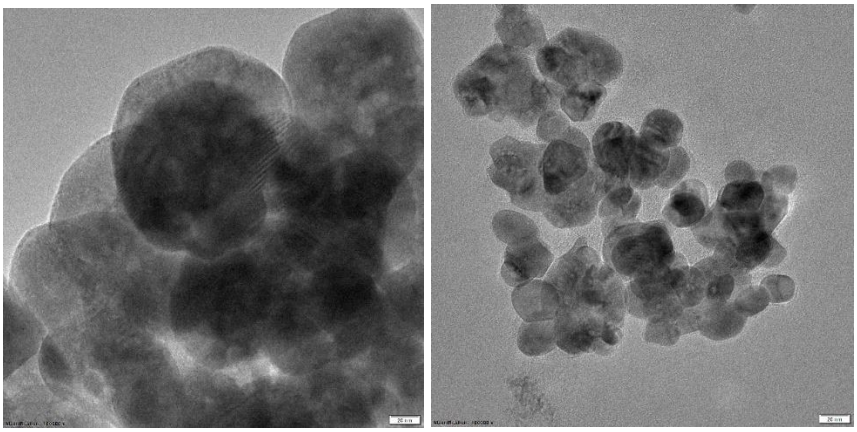

(a) 20nm (b) 50nm

Figure 2.7. TEM image of GdF3:Eu3+ observed at (a) 20nm and (b) 50nm

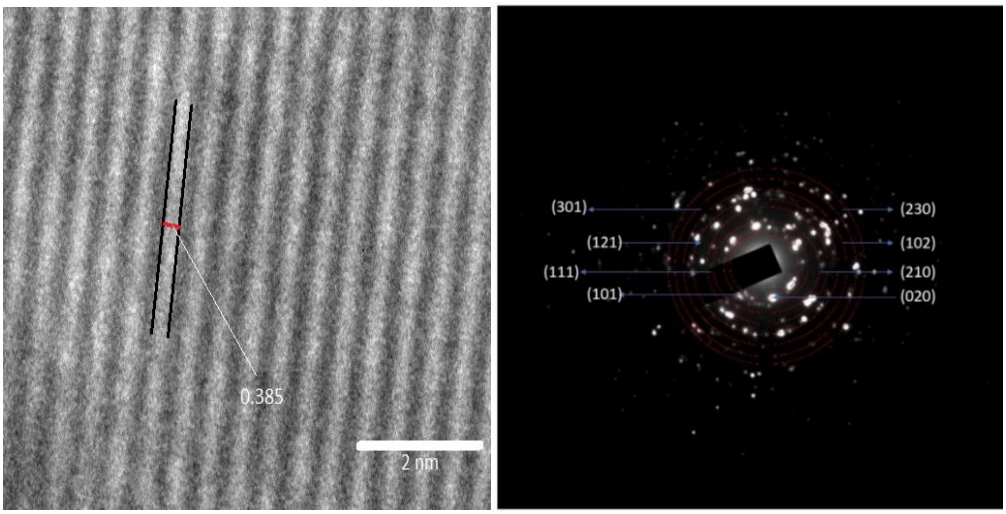

(a) (b)

Figure 2.8. HRTEM and SAED images of $GdF_3:Eu^{3+}$

The TEM images presented in **Fig. 2.7.** exhibits distinct shape, indicating nanoparticle aggregation. The measured diameters of the nano-crystal were found to be comparable to those calculated from the XRD pattern, which has sizes ranging from 20 to 50 nm.

The high-resolution TEM images clearly reveal well-defined lattice fringes **Fig. 2.8. (a)**. The distance between neighbouring lattice fringes is simply the interplanar distance of (111) planes for $LaF_3:Eu^{3+}$, which agrees well with the d-spacing values in the literature where it was found to be 0.385 nm [28]. The SAED patterns of $LaF_3:Eu^{3+}$in **Fig. 2.8. (b)** indicate that these nanoparticles possess a high degree of crystallinity. Nanoparticles of Gadolinium fluoride grow through a sequence of chemical transformations influenced by a surfactant Europium. The SAED image displays regular diffraction spots, indicating single crystallinity and facet dominance in the $GdF_3:Eu^{3+}$ Nano disks [29]. Amplification of the d-h k l reflection spots was revealed in the XRD patterns, correlating with the rise in the atomic number of the lanthanides.

3.5. Conclusion

The domain of lanthanide-doped nanomaterials stands as a pivotal force reshaping materials science, propelled by their distinctive spectral attributes. Their multifaceted utility spans across the fabrication of cutting-edge optical devices, solar cells, phosphors, lasers, and biomedical technologies, signifying a transformative epoch in material engineering. The present study represents a significant contribution to this field, where, via a facile solvothermal approach, uniform and well-crystallized $GdF_3:Eu^{3+}$ nanoparticles were successfully synthesized. Furthermore, the orthorhombic crystal structure and nanoparticle size were authenticated through a comprehensive suite of analytical techniques, including XRD, SEM, TEM and EDX. The well-resolved lattice fringes are clearly shown by HRTEM images and SAED image displays regular diffraction spots, indicating single crystallinity and facet dominance in the $GdF_3:Eu^{3+}$. This facilitated a thorough characterization of Eu^{3+} ion integration into the GdF_3 crystal lattice. The insights gleaned from this investigation serve to propel forward the realm of lanthanide fluoride chemistry, while concurrently bestowing invaluable comprehension regarding the development and formation

mechanisms of nanomaterial crystals. Investigating the intricate mechanisms governing the production of varied morphologies in LnF_3 nanocrystals, infrared spectroscopy delineated the formation of chemical bonds between lanthanide and fluoride moieties, while luminescence spectroscopy elucidated the dynamics of excitation and emission energy transfer with long emission lifetime of 12ms which could reveal that the synthesized nanoparticle can be used for Magnetic Resonance Imaging and other optic appliances.

Acknowledgement

The authors would like to acknowledge the department of Chemistry and Physics, Nagaland University; Lumami for providing the laboratory facilities. The authors are also grateful to Chemical Engineering Group, CSIR-NEIST; Jorhat for allowing us to do the characterizations. The authors are grateful to UGC NON-NET fellowship for the financial support.

Declaration of interests

The authors declare that they have no known competing financial interests or personal relationships that could have appeared to influence the work reported in this paper.

References:

[1] Gai, S., Li, C., Yang, P., & Lin, J. (2014). Recent progress in rare earth micro/nanocrystals: soft chemical synthesis, luminescent properties, and biomedical applications. *Chemical reviews*, *114*(4), 2343-2389.

[2] Li, Y., Chen, C., Liu, F., & Liu, J. (2022). Engineered lanthanide-doped upconversion nanoparticles for biosensing and bioimaging application. *Microchimica Acta*, *189*(3), 1-28.

[3] Zhang, D., Dong, Y., Li, D., Jia, H., & Qin, W. (2021). Growth regularity and phase diagrams of NaLu0. 795− xYxF4 upconversion nanocrystals synthesized by automatic nanomaterial synthesizer. *Nano Research*, *14*(12), 4760-4767.

[4] Zhang, Q., O'Brien, S., & Grimm, J. (2022). Biomedical applications of lanthanide nanomaterials, for imaging, sensing and therapy. *Nanotheranostics*, *6*(2), 184.

[5] T. Grzyb, & S.Lis, (2009). Photoluminescent properties of LaF_3: Eu^{3+} and GdF_3: Eu^{3+} nanoparticles prepared by co-precipitation method. *Journal of rare earths*, *27* (4), 588-592.

[6] Y.Shang, , T.Chen, , T. Ma, Hao, S., Lv, W., Jia, D., & Yang, C. (2021). Advanced lanthanide doped upconversion nanomaterials for lasing emission. *Journal of Rare Earths*.

[7] Zhong, H. X., Wang, M., Yang, H. L., Hong, J. M., Huang, Q. L., & Chen, X. T. (2009). Controlled synthesis and characterization of EuF_3 with ring-like morphology. *Materials Science and Engineering: B*, *156* (1-3), 62-67.

[8] Ha, H. M. (2016). Optical properties of Eu3+ ions in LaF3 nanocrystals. *Vietnam Journal of Science and Technology*, *54*(1A), 88-88.

[9] Huy, B. T., Kumar, A. P., Thuy, T. T., Nghia, N. N., & Lee, Y. I. (2022). Recent advances in fluorescent upconversion nanomaterials: novel strategies for enhancing optical and magnetic properties to biochemical sensing and imaging applications. *Applied Spectroscopy Reviews*, *57*(4), 265-299.

[10] Huang, Y., You, H., Jia, G., Zheng, Y., Song, Y., Yang, M., ... & Zhang, L. (2009). Hydrothermal synthesis and luminescence of Eu-doped Ba0. 92Y2. 15F8. 29 submicrospheres. *The Journal of Physical Chemistry C*, *113*(39), 16962-16968.

[11] Wong, H. T., Chan, H. L. W., & Hao, J. H. (2009). Magnetic and luminescent properties of multifunctional GdF_3: Eu^{3+} nanoparticles. *Applied physics letters*, *95*(2), 022512.

[12] Ansari, A. A., Aldalbahi, A. K., Labis, J. P., & Manthrammel, M. A. (2017). Impact of surface coating on physical properties of europium-doped gadolinium fluoride microspheres. *Journal of Fluorine Chemistry*, *199*, 7-13.

[13] Zhang, X., Hayakawa, T., Nogami, M., & Ishikawa, Y. (2010). Selective synthesis and luminescence properties of nanocrystalline GdF_3: Eu^{3+} with hexagonal and orthorhombic structures. *Journal of Nanomaterials*, *2010*.

[14] Li, Q., Zuo, W., & Li, F. (2013). Chelating ligand-mediated hydrothermal synthesis of samarium orthovanadate with decavanadate as vanadium source. *The Scientific World Journal*, *2013*.

[15] Li, F., Li, C., Liu, X., Chen, Y., Bai, T., Wang, L., ... & Feng, S. (2012). Hydrophilic, upconverting, multicolor, lanthanide-doped $NaGdF_4$ nanocrystals as potential multifunctional bioprobes. *Chemistry–A European Journal*, *18*(37), 11641-11646.

[16] He, F., Yang, P., Wang, D., Niu, N., Gai, S., & Li, X. (2011). Self-assembled β-$NaGdF_4$ microcrystals: hydrothermal synthesis, morphology evolution, and luminescence properties. *Inorganic chemistry*, *50*(9), 4116-4124.

[17] Fan, X., Pi, D., Wang, F., Qiu, J., & Wang, M. (2006). Hydrothermal synthesis and luminescence behavior of lanthanide-doped GdF/sub 3/nanoparticles. *IEEE transactions on nanotechnology*, *5*(2), 123-128.

[18] Lorbeer, C., Cybinska, J., & Mudring, A. V. (2010). Facile preparation of quantum cutting GdF_3: Eu^{3+} nanoparticles from ionic liquids. *Chemical communications*, *46*(4), 571-573.

[19] Hua, R., Niu, J., Chen, B., Li, M., Yu, T., & Li, W. (2006). Visible quantum cutting in GdF_3: Eu^{3+} nanocrystals via down conversion. *Nanotechnology*, *17*(6), 1642.

[20] Grzyb, T., Runowski, M., & Lis, S. (2014). Facile synthesis, structural and spectroscopic properties of GdF_3: Ce^{3+}, Ln^{3+} (Ln^{3+}= Sm^{3+}, Eu^{3+}, Tb^{3+}, Dy^{3+}) nanocrystals with bright multicolor luminescence. *Journal of luminescence*, *154*, 479-486.

[21] Lei, P., An, R., Li, C., Feng, J., & Zhang, H. (2020). Lanthanide-doped bismuth-based fluoride nanoparticles: controlled synthesis and ratiometric temperature sensing. *CrystEngComm*, *22*(20), 3432-3438.

[22] Li, C., Yang, J., Yang, P., Lian, H., & Lin, J. (2008). Hydrothermal synthesis of lanthanide fluorides LnF_3 (Ln= La to Lu) nano-/microcrystals with multiform structures and morphologies. *Chemistry of Materials*, *20*(13), 4317-4326.

[23] Bao, G., Wen, S., Lin, G., Yuan, J., Lin, J., Wong, K. L., ... & Jin, D. (2021). Learning from lanthanide complexes: The development of dye-lanthanide nanoparticles and their

[24] Guan, H., Sheng, Y., Xu, C., Dai, Y., Xie, X., & Zou, H. (2016). Energy transfer and tunable multicolor emission and paramagnetic properties of GdF 3: Dy 3+, Tb 3+, Eu 3+ phosphors. *Physical Chemistry Chemical Physics*, *18*(29), 19807-19819.

[25] Wen, H., & Wang, F. (2014). Lanthanide-Doped Nanoparticles: Synthesis, Property, and Application. In *Nanocrystalline Materials* (pp. 121-160). Elsevier.

[26] Liu, Y., Tu, D., Zhu, H., & Chen, X. (2013). Lanthanide-doped luminescent nanoprobes: controlled synthesis, optical spectroscopy, and bioapplications. *Chemical Society Reviews*, *42*(16), 6924-6958.

[27] Ladol, J., Khajuria, H., Khajuria, S., & Sheikh, H. N. (2016). Hydrothermal synthesis, characterization and luminescent properties of lanthanide-doped NaLaF 4 nanoparticles. *Bulletin of Materials Science*, *39*, 943-952.

[28] Yu, C., Yu, M., Li, C., Zhang, C., Yang, P., & Lin, J. (2009). Spindle-like lanthanide orthovanadate nanoparticles: facile synthesis by ultrasonic irradiation, characterization, and luminescent properties. *Crystal Growth and Design*, *9*(2), 783-791

[29] Sena, N. C., Castro, T. J., Garg, V. K., Oliveira, A. C., Morais, P. C., & da Silva, S. W. (2017). Gadolinium ferrite nanoparticles: Synthesis and morphological, structural and magnetic properties. *Ceramics International*, *43*(5), 4042-4047.

CHAPTER 4

Lanthanum Fluoride nano Crystals doped with Europium: Synthesis and Characterizations

Abstract

The domain of lanthanide-doped nanomaterials exerts a profound influence on materials science due to their distinct spectral properties. These versatile materials find applications in various fields such as the development of advanced optical devices, solar cells, phosphors, lasers etc. marking a transformative period in material science. In this study, $LaF_3:Eu^{3+}$nanoparticles were synthesized via a facile Solvothermal process, employing citric acid as a capping agent. The resulting nano compounds underwent comprehensive characterization using advanced analytical techniques including Fourier-transform infrared spectroscopy (FT-IR), fluorescence spectroscopy for photoluminescence analysis, X-ray diffraction (XRD), scanning electron microscopy (SEM), transmission electron microscopy (TEM) to elucidate their dimensional properties, morphology, HRTEM and crystalline nature of nanoparticles was confirmed by SAED patterns. Additionally, XPS was utilized to determine the elemental composition of the synthesized nanocrystals. The average crystallite size was determined using the Scherrer equation, calculated from the full-width at half-maximum (FWHM) of the XRD peaks. Ongoing research efforts continue to explore their potential applications and optimize their properties for various practical uses.

Keywords: Rare earths; Lanthanum fluoride; Europium; Solvothermal; Luminescence.

4.1. Introduction

The field of nanotechnology has experienced rapid expansion owing to the distinctive physical and chemical characteristics exhibited by nanostructures in contrast to those of bulk solids. Metallic nanostructured materials, especially gold nanoparticles, have been heavily researched for their importance and potential in various fields like optics and catalysis. Their applications are attributed to the quantum size effect, determined by the number of free electrons. Characterization of nanoparticles is based on size and synthesis method [1]. Lanthanide nanoparticles, stemming from the lanthanide series have gained significant attention for their unique properties. Their exceptional luminescence, magnetism, and catalytic activity make them versatile for various applications [2]. The luminescent behaviour of lanthanide nanoparticles is due to their unique electronic configurations with shielded 4f orbitals. Lanthanide-based catalysts have shown great promise in various chemical reactions, making them valuable in green chemistry. Despite their advantages, challenges in synthesis, characterization, and practical use remain. Interdisciplinary efforts are needed to overcome these challenges and further explore the potential of lanthanide nanoparticles in bioimaging, sensing, and display technologies [3]. Diverse shapes of rare-earth fluoride crystals have been made through various methods with uniform LaF_3 triangular nanoplates and EuF_3 nanocrystals with varied structures and shapes [4]. Rare-earth-doped nanocrystals are advantageous because they have a greater emission efficiency, have customisable solubility, and are easily functionalized on the particle's surface, especially when compared to typical rare earth chelates utilised in optical applications [5].

Among various RE ions, Eu^{3+} ion is a popular dopant in different compounds, resulting in red emission. With a large energy gap between luminescent and lower energy levels (~12000 cm^{-1}), Eu's red emission usually has a long photoluminescence duration of several milliseconds or more, making Eu^{3+}-doped rare-earth nanoparticles a great bio-probe for background-free bio-detection [6]. By using suitable doping methods, the energy levels of Eu ions can be controlled, enabling precise adjustment of luminescence features like emission wavelength, intensity, and longevity [7]. Europium-doped nanoparticles are used as effective tools in biological applications

like bioimaging, biosensing, and drug delivery due to their strong emission peaks, extended emission lifetimes, and resilience to photobleaching, making them perfect for multiplexed imaging and high-throughput screening tests [8]. These nanoparticles are used to identify pollutants, heavy metals, and biomolecules in environmental samples with strong sensitivity and selectivity [9]. Nanoparticles doped with Lanthanum usually show greater stability, conductivity, and catalytic activity when compared to those that are not doped [10]. Lanthanum-doped nanoparticles have a wide range of uses in various areas including environmental clean-up and as adsorbents for wastewater pollutant removal [11]. Although lanthanum-doped nanoparticles have many advantages, it's important to think about how they could affect the environment. If these nanoparticles are released, whether on purpose or by accident, they could harm ecosystems and people. Therefore, it's crucial to use proper waste disposal techniques to reduce negative effects [12]. Studies have shown that lanthanum-doped nanoparticles can exhibit biocompatible properties, making them suitable for biomedical applications. However, their potential toxicity, particularly upon long-term exposure or accumulation in living organisms, warrants further investigation to ensure their safe use [13]. It is essential to consider the environmental impact and potential toxicity of lanthanum-doped nanoparticles to ensure their safe and sustainable utilization.

With a high melting point, Lanthanum fluoride is thermally stable for operations requiring high temperatures. Its scintillation properties further enhance its usefulness in radiation detection and medical imaging, offering opportunities for advancements in these crucial fields [14]. By changing the doping concentration and excitation conditions, the emission wavelength of $LaF_3:Eu^{3+}$ can be modified to meet specific optical needs. This customization ability makes it useful for various industrial and scientific purposes, even in harsh environments [15]. The impact of nanostructure morphology on lanthanide doped fluorides' luminescence properties is still a topic of interest, with various methods utilized to control morphology. Changing the morphology can lead to a wide array of unique optical properties [16]. To achieve a more crystalline end product, the reagents are put into an autoclave (often Teflon-lined to protect against fluoride ion corrosion of glass), sealed, and heated [17]. Recent

research has focused on rare earth (RE) fluorides due to their unique properties such as chemical stability, low crystal lattice vibrations, and potential use in phosphors and luminescent markers. Coating REF_3 nanoparticles with modifiers improve water colloid stability for bio-related applications [18].

An important aspect of the solvothermal method for synthesizing lanthanide nanoparticles is its ability to control the size, shape, and crystallinity of the nanoparticles. Solvothermal synthesis involves the reaction of lanthanide precursors with a solvent at elevated temperatures and pressures, typically in a sealed autoclave. This method offers several advantages for the production of lanthanide nanoparticles. Under solvothermal conditions, researchers can carefully manage the growth of nanoparticles, achieving consistent size distribution and distinct shapes. By modifying factors like temperature, pressure, time, and precursor concentration during reactions, scientists can customize the size and morphology of lanthanide nanoparticles to suit different needs in multiple applications [19]. The solvothermal method enables the synthesis of lanthanide nanoparticles with high purity and crystallinity. The use of organic solvents as reaction media helps to minimize impurities and promote the formation of crystalline nanoparticles with well-defined crystal structures [20]. By choosing suitable lanthanide starting materials and solvents, the solvothermal technique makes it possible to create lanthanide nanoparticles with desired characteristics in terms of phases and compositions. This flexibility makes it possible to produce various lanthanide-centred materials customized for specific uses in fields like optoelectronics, catalysis, and biomedical imaging [21]. Scaling up solvothermal synthesis allows for the production of lanthanide nanoparticles in large quantities, making it ideal for industrial use. Additionally, the process offers reliable reproducibility, ensuring consistent quality and performance of the nanoparticles in various batches [22]. In summary, the solvothermal method offers precise control over the size, morphology, purity, crystallinity, phase, and composition of lanthanide nanoparticles, making it a versatile and powerful technique for their synthesis with tailored properties for various applications.

4.2. Experimental

Materials

Lanthanum Acetate Hydrate (99.99%, Sigma Aldrich), Europium Acetate Hydrate (99.99%, Sigma Aldrich), NH4F (99.99%, HiMedia) Methanol (99.9%, Merck), Ethanol (99.9%, Merck) and Trisodium Citrate (HiMedia) served as the base material without additional processing.

Method

Synthesis of LaF_3: Eu^{3+}

A compound of LaF_3:Eu^{3+} nanoparticles were prepared by using Solvothermal synthesis. Taking Stoichiometric ratio, a solution of Lanthanum acetate hydrate (675mg), Europium acetate hydrate (37mg) and NH4F (250mg) were mixed and heated in DI (Deionized) water and methanol (1:1 ratio) using magnetic stirring. A calculated amount of Citric acid (96.06mg) was incorporated, functioning as a chelator. Next Sonicator instrument "Probe Sonicator; Rivotek, Version 12.01 (5.3), CSIR-NEIST" was used to mix the solution thoroughly and thus to reduce the size of particles suspended in a liquid medium. This is particularly useful in nanoparticle synthesis, where precise control over particle size is essential for achieving desired properties and functionalities. After mixing the dissolved solution, it was transferred into a Teflon container which were confined within a stainless-steel autoclave, the solution is then secured and maintained at exact 180 °C for 18 hrs. The obtained compound at the bottom was segregated and cleaned by centrifugation process; after cleaning with DI water, it was followed with ethanol solvent for 3 times and then the compound was dried in oven for about 12 hrs.

Characterization

The (PerkinElmer Spectrum Two FT-IR Spectrometer) spectrophotometer was used to record FTIR spectra using the KBr pellet technique. To analyse the nano-products, a Fluorescence spectrometer (Model: XRD pattern (Rigaku fitted with Ni filter Cu Ka (l= 1.54056) was used to record excitation and emission spectra. SEM-XPS and HR-TEM were utilized to assess the structure and scale of the samples

4.3. Results and Discussion

FTIR

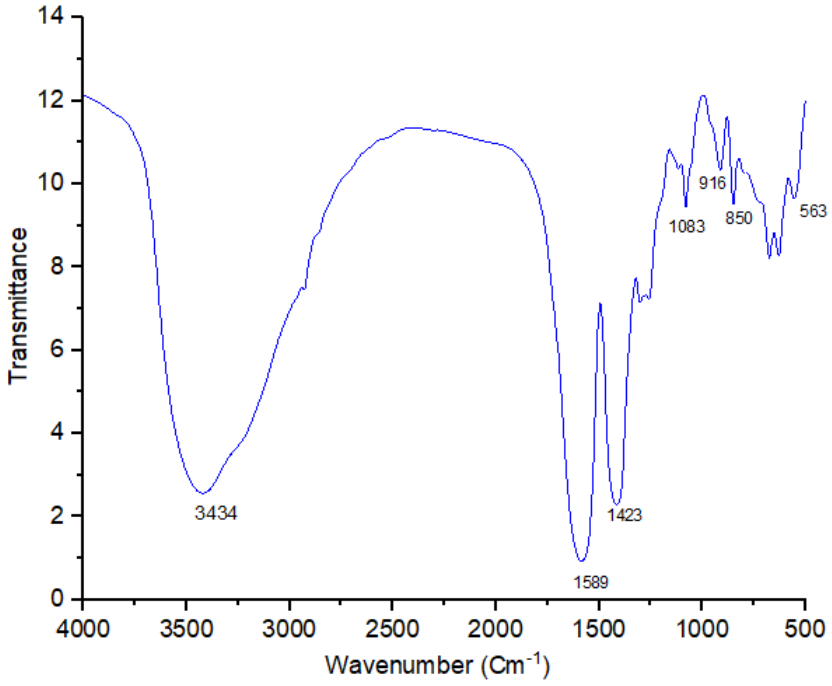

Figure 3.1. FT-IR Spectra of GdF_3: Eu^{3+}

Fig. 3.1 has shown FTIR spectra of the LaF_3:Eu^{3+} nanocrystals located at different regions. The characteristic absorption peaks have been detected in the range spanning 4000cm^{-1} to 400 cm^{-1}. The prominent absorption band about 3434cm^{-1} can be ascribed to Vas water O-H stretching and bending vibrations. The peak at 1589 cm^{-1} is due to N-H bending vibrations, while the absorption peak at 1428 cm^{-1} corresponds to the symmetric stretching vibration of the carboxyl group. The vibrations at 1083 cm^{-1} are ascribed to C-F stretching in a fluoro compound from Ammonium Fluoride. The characteristic IR peaks located at 850cm^{-1} could be assigned to C-F stretching and sharp peak at 563cm^{-1} can be attributed to C-Cl stretching [23].

Fluorescence spectroscopy

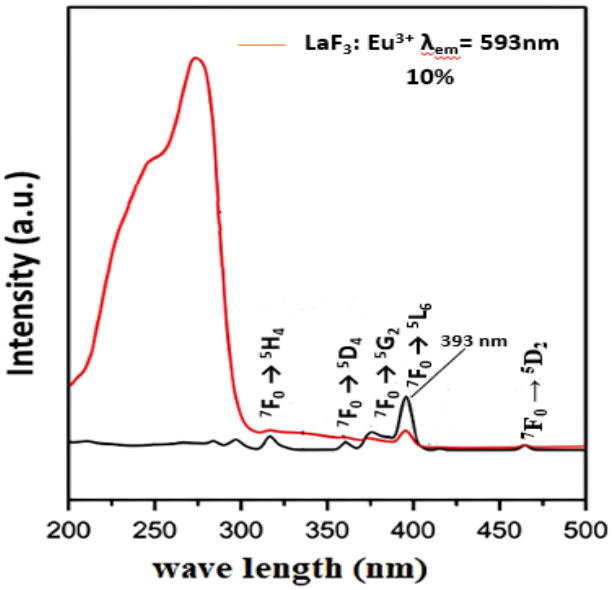

Figure 3.2. Fluorescence spectra of Lanthanum Fluoride doped with Europium compound

The excitation and emission spectra of the $LaF_3:Eu^{3+}$ sample are depicted in the provided **Fig. 3.2.** The excitation spectrum (depicted by the black line) displays distinctive excitation lines attributed to Eu^{3+}, arising from its $^7F_0$ configuration. These lines are identified as follows: 317 nm ($^7F_0 \rightarrow {}^5H_4$), 363 nm ($^7F_0 \rightarrow {}^5D_4$), 379 nm ($^7F_0 \rightarrow {}^5G_2$), and 393 nm ($^7F_0 \rightarrow {}^5L_6$). When excited at 379 nm, the resulting emission spectrum exhibits emission lines at 593 nm ($^5D_0 \rightarrow {}^7F_1$), 615 nm ($^5D_0 \rightarrow {}^7F_2$), 650 nm ($^5D_0 \rightarrow {}^7F_3$), and 695 nm ($^5D_0 \rightarrow {}^7F_4$). Research on the photophysical properties of Eu^{3+} ions suggests that the 593 nm emission, corresponding to the $^5D_0 \rightarrow {}^7F_1$ transition, is predominantly magnetic dipole in nature. Transitions to the $^7F_0$ levels are typically weak in the emission spectrum, being forbidden in both magnetic and electric dipole schemes. The emission spectrum of Eu^{3+} is significantly impacted by the symmetry of its surroundings. Electric dipole transitions are prohibited in crystal sites with inversion symmetry, with the $^5D_0 \rightarrow {}^7F_1$ transition frequently being the most prominent [6,24]. Conversely, in environments lacking inversion symmetry, electric dipole transitions exhibit higher intensity. It's worth mentioning that the significant variation in quenching observed between different types of nanoparticles is not

anticipated to apply when radio excitation is involved. In this scenario, each nanoparticle composition is anticipated to exhibit similar excitation and scintillation outputs, regardless of nanoparticle size.

XRD

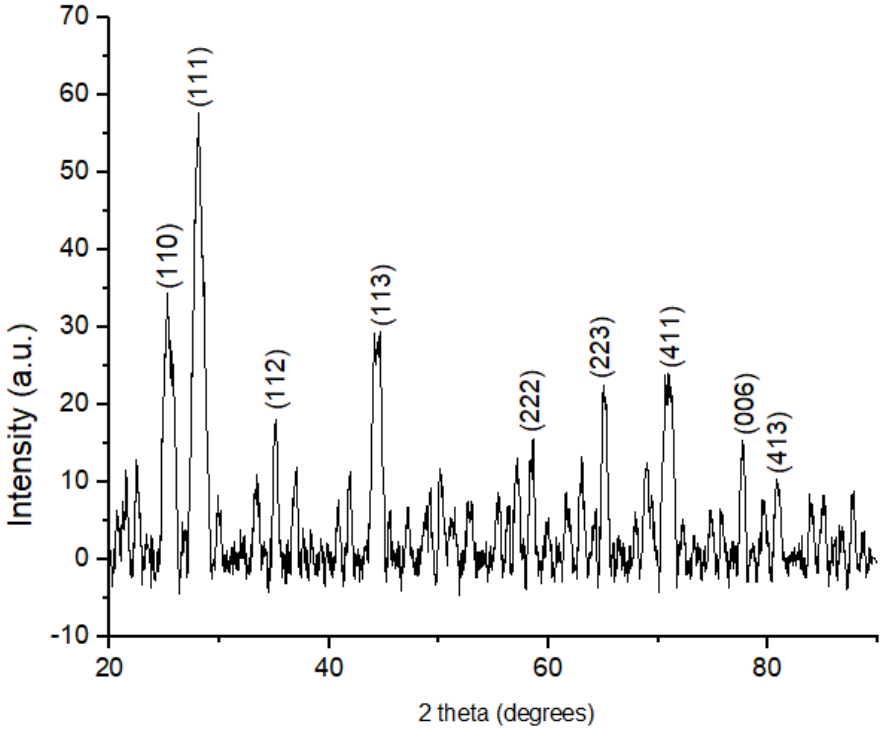

Figure 3.3. XRD pattern of $LaF_3:Eu^{3+}$ obtained by Solvothermal method

Fig. 3.3. represents the XRD pattern of $LaF_3:Eu^{3+}$ nanoparticles acquired with the aid of Powder X-Ray Diffractometer (Model: ULTIMAIV, Rigaku, Japan). From the figure, almost all reflection planes have pure crystalline hexagonal $LaF_3:Eu^{3+}$ structure (Space group number: 165, Space group: Pnma P-3c1, with lattice constants a = 7.1871; b = 7.1871, c = 7.3501, which is consistent with standard data (Reference code from JCPDS: 00-032-0483).The hexagonal phase of $LaF_3:Eu^{3+}$ with high purity can be catalogued for diffraction plane (110) (111) (112) (113) (222) (223) (411) (006) (423). It was found that there are very few spherical and nearly spherical nanoparticles among the vast bulk of the nanoparticles, which are elongated nanoparticles. The $LaF_3:Eu^{3+}$ nanoparticles are chemically stable in the water/ethanol solution, and the

solvothermal process does not reduce their quality. The elongated nanoparticles had an average length of approximately 100 nm and a width of about 50 nm [25,26]. The typical diameters of spherical and nearly spherical nanoparticles were observed to be around 10 to 20nm using Scherrer equation:

$$D\ (Å) = \frac{K\lambda}{\beta\ Cos\ \theta}$$

XPS

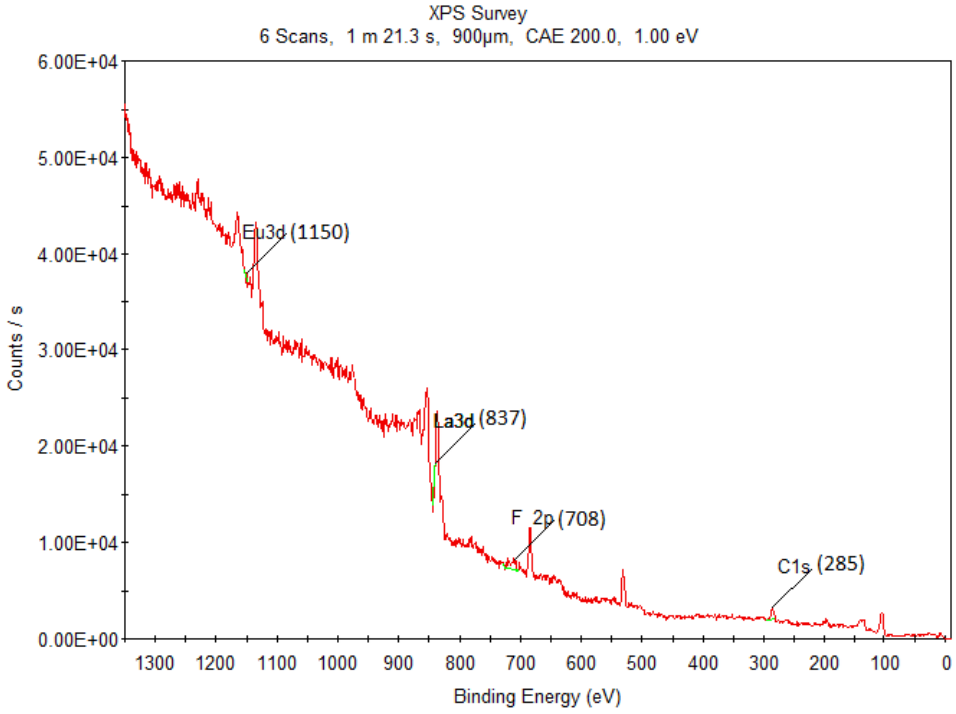

Figure 3.4. XPS Survey of LaF_3 doped with Eu^{3+}

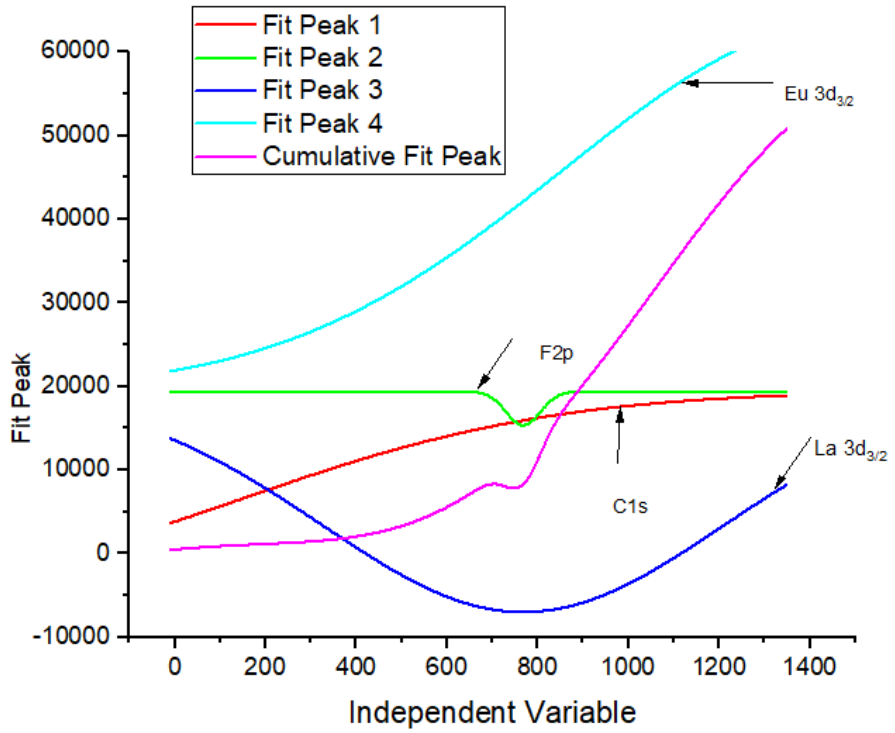

Figure 3.5. Independent Variable of different elements present in $LaF_3:Eu^{3+}$ Compound

Comparative XPS survey spectra of $LaF_3:Eu^{3+}$samples synthesized are presented in **Fig. 3.4.** The spectra show photoelectron peaks that correspond to emissions from La, Eu, and F. The emission peak positions were adjusted using the C1s peak position at 285.5 eV as a reference. The surface composition of the samples was determined based on their high resolution XPS spectra. In **Fig. 3.4,** despite maintaining a constant nominal concentration of Eu in the sample, only around 1.87 atom % of Eu was incorporated into the particles when they were synthesised at ambient temperature, resulting in the observation of the peak position of Eu3d3/2 at 1150eV. The concentration of the integrated Eu grew as the action temperature rose. The peak position and atom % of F atom was observed at 708.8eV (6.68%), whereas for La3d3/2 was found at 837eV. Additionally, the striking similarity in the distribution patterns of La, F, and Eu indicates a shared chemical origin for these elements, highlighting the efficient and uniform dispersion of Eu^{3+} ions within the host matrix. **Fig. 3.5.** shows the fit peak of La, Eu and F elements present at independent variable [27,28].

SEM

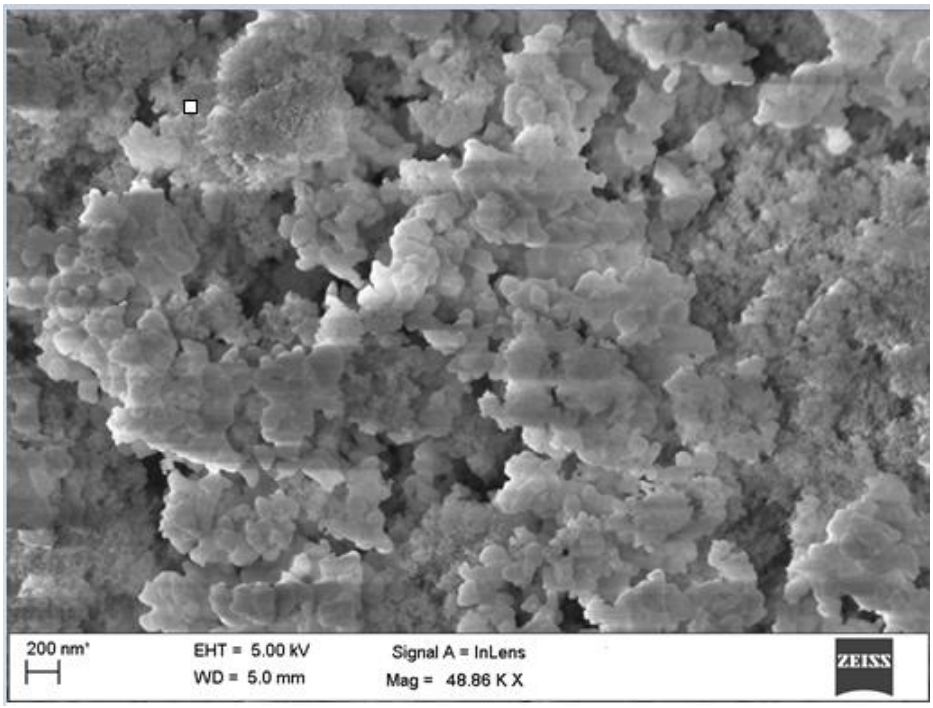

(a)

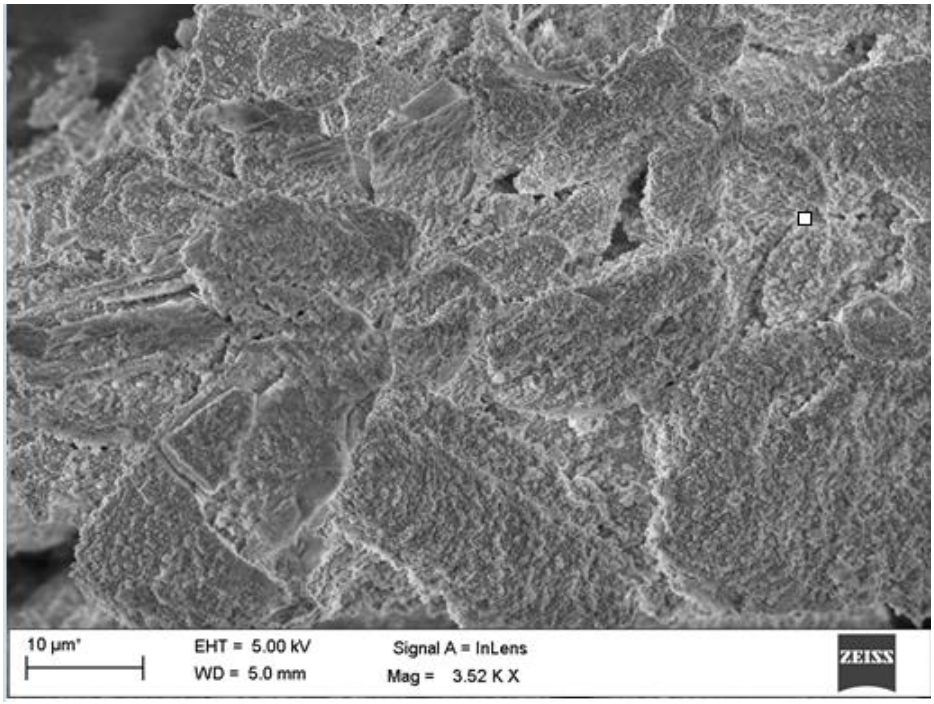

(b)

Figure 3.6. SEM image of $LaF_3:Eu^{3+}$ at (a) 200nm and (b) 10 micrometer

S.No.	1/2r (nm^{-1})	1/r(nm^{-1})	r(nm)	d-spacing(Å)	(hkl)
1	6.957	3.4785	0.287480236	2.874802357	(112)
2	9.421	4.7105	0.212291689	2.122916888	(113)
3	12.391	6.1955	0.161407473	1.614074732	(222)
4	16.522	8.261	0.12105072	1.210507203	(006)
5	19.522	9.761	0.10244852	1.024485196	(413)

Table 3.1. SAED calculations of d-spacing to compare with hkl values

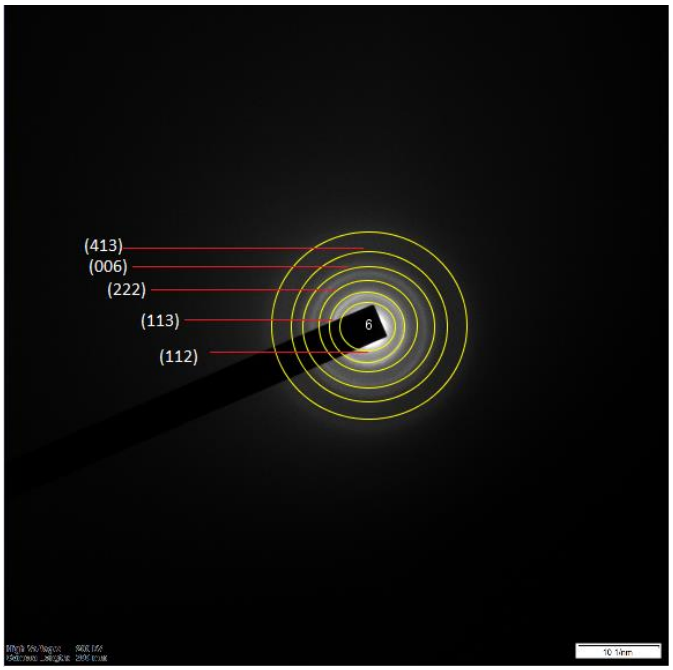

Figure 3.7. SAED pattern of $LaF_3:Eu^{3+}$ with different hkl values

From the above **Fig. 3.7.** The SAED patterns of $LaF_3:Eu^{3+}$ indicate that these nanoparticles possess a high degree of crystallinity. Nanoparticles of lanthanum fluorides grow via a sequence of chemical changes influenced by a surfactant. Citric acid can aggressively adhere to metal and mineral surfaces, causing major changes in their characteristics and mineral development patterns. The SAED image displays regular diffraction spots, indicating single crystallinity and facet dominance in the $LaF_3:Eu^{3+}$ Nano disks. Rise of the d-h k l reflections spots was noted in X-ray diffraction patterns as the atomic number of lanthanides increased. The d-h k l gap distances calculated from SAED analysis in **Table. 3.1** were readily aligned with those derived from Rietveld analysis. The finding verifies the existence of a hexagonal local

structure in both sizes and shapes of $LaF_3:Eu^{3+}$ nanoparticles, as supported by the corresponding XRD patterns [29,30].

TEM

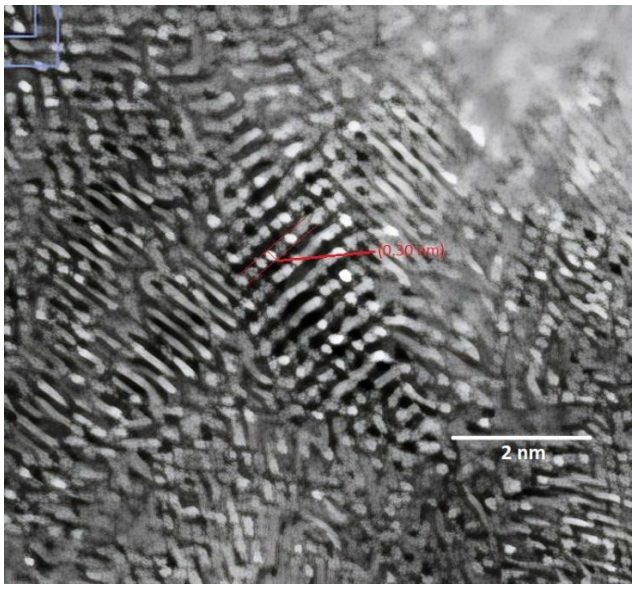

Figure 3.8. HR-TEM images of Lanthanum Fluoride doped with Europium

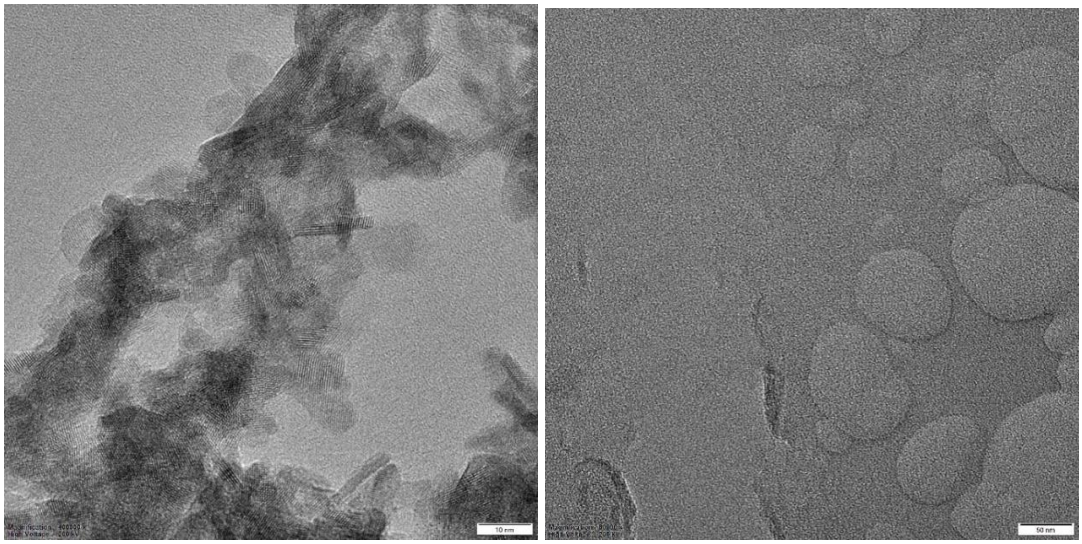

(a) (b)

Figure 3.9. TEM image of $LaF_3:Eu^{3+}$ observed at (a) 10nm and (b) 50nm

Utilising SEM, TEM, HRTEM, and SAED techniques, the microstructure and morphology of the synthetic sample were investigated. SEM images at low magnification **(Fig. 3.6 a and b)** depict the $LaF_3:Eu^{3+}$ product as uniformly sized disks with a round shape. At higher magnification, the SEM image reveals an average disk diameter of approximately 50 to100 nm, consistent with TEM observations **(Fig. 3.9 a and b)**. The thickness of the disks, observed perpendicular to the substrate, is about 10 to 20 nm. Additionally, the $LaF_3:Eu^{3+}$ nano disks exhibit smooth surfaces. The well-resolved lattice fringes are distinctly observable in the HRTEM images **(Fig. 3.8)**. The distance between neighbouring lattice fringes is simply the interplanar distance of (111) planes for $LaF_3:Eu^{3+}$, which is consistent with the d-spacing data in the literature where it was found to be 0.30 nm. Additionally, the hexagonal phase of $LaF_3:Eu^{3+}$ is revealed by the lattice fringes that correlate to the interplanar distance [31,32]. These findings point to the fact that the 83% product yield during synthesis produces $LaF_3:Eu^{3+}$nanodisks of consistent size and shape. The quick and unpredictable precipitation of lanthanum fluoride is usually caused by its poor solubility product constant. But the way it's outlined makes it possible to manipulate size and shape with pinpoint accuracy. Microscopic examination of $LaF_3:Eu^{3+}$ samples produced under the same conditions employing NH_4F as fluoride sources reveals the presence of agglomerated, irregular nanoparticles. SAED testing has shown that these samples contain polycrystallinity.

4.4. Conclusion

In this study, refined and highly crystalline Lanthanum Fluoride doped with Europium nanoparticles was successfully synthesized from the solvothermal process using probe Sonicator to mix the solution thoroughly. Recent developments in surface characterization methods and their implications for understanding surface properties and the interaction mode for the formation of $LaF_3:Eu^{3+}$ NPs are discussed. IR spectroscopy depicts the bonding interaction between Lanthanide and fluoride, while luminescence spectroscopy predicts the excitation and emission energy transfer. FTIR, SEM, TEM, and XRD are some of the structural characterisation techniques that was utilized to evaluate the shape, size, and crystalline structure of $LaF_3:Eu^{3+}$ NPs. The mean particle size of the doped compound was observed to be around 10 to 20nm. The

elemental makeup and chemical states of $LaF_3:Eu^{3+}$ NPs was analyzed using XPS. The synthesized compound was confirmed to be hexagonal in shape. The d-h k l spacing distances was derived from the SAED analysis and HRTEM depicted an individual atom within a crystal lattice having a distance of 0.30nm. The insights, gained from above characterization techniques have profound implications for optimizing synthesis methods, tailoring properties, and enhancing the performance of $LaF_3:Eu^{3+}$ NPs in various applications. These papers could convey pertinent information emphasizing the need for continued advancements in characterization techniques to meet the evolving demands of nanomaterials research and applications.

Acknowledgement

The authors would like to acknowledge the department of Chemistry and Physics, Nagaland University; Lumami for providing the laboratory facilities. The authors are also grateful to Chemical Engineering Group, CSIR-NEIST; Jorhat for allowing us to do the characterizations. The authors are grateful to UGC NON-NET fellowship for the financial support.

Declaration of interests

The authors declare that they have no known competing financial interests or personal relationships that could have appeared to influence the work reported in this paper.

References:

[1] Ahmad, T., Wani, I. A., Lone, I. H., Ganguly, A., Manzoor, N., Ahmad, A., ... & Al-Shihri, A. S. (2013). Antifungal activity of gold nanoparticles prepared by solvothermal method. *Materials Research Bulletin*, *48*(1), 12-20.

[2] Lee, J., & Jun, Y. W. (2020). Recent Advances in Lanthanide-Doped Nanoparticles for Bioimaging Applications. Molecules, 25(7), 1535.

[3] Cai, W., & Wang, J. (2012). Lanthanide-doped upconversion nanoparticles as new fluorescent reporters in the detection of DNA. The Analyst, 137(23), 5485-5489.

[4] Zhu, L., Meng, J., & Cao, X. (2007). Facile synthesis and photoluminescence of europium ion doped LaF3 nanodisks.

[5] Secco, H. D. L., Ferreira, F. F., & Peres, L. O. (2018). Simple preparation of fluorescent composite films based on cerium and europium doped LaF3 nanoparticles. *Journal of Solid State Chemistry*, *259*, 43-47.

[6] Ansari, A. A., Aldalbahi, A. K., Labis, J. P., & Manthrammel, M. A. (2017). Impact of surface coating on physical properties of europium-doped gadolinium fluoride microspheres. *Journal of Fluorine Chemistry*, *199*, 7-13.

[7] Vetrone, F., & Capobianco, J. A. (2008). Lanthanide-doped fluoride nanoparticles: luminescence, upconversion, and biological applications. *International Journal of Nanotechnology*, *5*(9-12), 1306-1339.

[8] Sahoo, S., Mondal, S., & Sarma, D. (2022). Luminescent lanthanide metal organic frameworks (LnMOFs): A versatile platform towards organomolecule sensing. *Coordination Chemistry Reviews*, *470*, 214707.

[9] Shi, L., Li, N., Wang, D., Fan, M., Zhang, S., & Gong, Z. (2021). Environmental pollution analysis based on the luminescent metal organic frameworks: A review. *TrAC Trends in Analytical Chemistry*, *134*, 116131.

[10] Zhu, H., Zhang, P., & Dai, S. (2015). Recent advances of lanthanum-based perovskite oxides for catalysis. *ACS catalysis*, *5*(11), 6370-6385.

[11] Li, Y., Chen, C., Liu, F., & Liu, J. (2022). Engineered lanthanide-doped upconversion nanoparticles for biosensing and bioimaging application. *Microchimica Acta*, *189*(3), 109.

[12] Bhattacharjee, R., Kumar, L., Mukerjee, N., Anand, U., Dhasmana, A., Preetam, S., ... & Proćków, J. (2022). The emergence of metal oxide nanoparticles (NPs) as a phytomedicine: A two-facet role in plant growth, nano-toxicity and anti-phyto-microbial activity. *Biomedicine & Pharmacotherapy*, *155*, 113658.

[13] Zhang, Q., O'Brien, S., & Grimm, J. (2022). Biomedical applications of lanthanide nanomaterials, for imaging, sensing and therapy. *Nanotheranostics*, *6*(2), 184.

[14] Runowski, Marcin, and Stefan Lis. "Preparation and photophysical properties of luminescent nanoparticles based on lanthanide doped fluorides (LaF3: Ce3+, Gd3+, Eu3+), obtained in the presence of different surfactants." *Journal of alloys and compounds* 597 (2014): 63-71.

[15] Gulina, L. B., Tolstoy, V. P., Kasatkin, I. A., Kolesnikov, I. E., & Danilov, D. V. (Year of Publication). Formation of oriented LaF3 and LaF3:Eu3+ nanocrystals at the gas-solution interface. *Journal of Fluorine Chemistry*. 200(2017) 18-23

[16] Kundu, S., Kar, A., & Patra, A. (2012). Morphology dependent luminescence properties of rare-earth doped lanthanum fluoride hierarchical microstructures. *Journal of luminescence*, *132*(6), 1400-1406.

[17] Rahman, P., & Green, M. (2009). The synthesis of rare earth fluoride based nanoparticles. *Nanoscale*, *1*(2), 214-224.

[18] Grzyb, T., Szczeszak, A., Śniadecki, Z., Idzikowski, B., & Lis, S. (2016). White and red emitting LaF3 nanocrystals doped with Eu2+ and Eu3+ ions: spectroscopic and magnetic studies. *Journal of Alloys and Compounds*, *686*, 489-495.

[19] Wang, X., Zhuang, J., Peng, Q., & Li, Y. (2005). A general strategy for nanocrystal synthesis. *Nature*, *437*(7055), 121-124.

[20] Sun, Y., & Xia, Y. (2002). Shape-controlled synthesis of gold and silver nanoparticles. *science*, *298*(5601), 2176-2179.

[21] Heine, J., & Müller-Buschbaum, K. (2013). Engineering metal-based luminescence in coordination polymers and metal–organic frameworks. *Chemical Society Reviews*, *42*(24), 9232-9242.

[22] Salavati-Niasari, M., Hosseinzadeh, G., & Davar, F. (2011). Synthesis of lanthanum hydroxide and lanthanum oxide nanoparticles by sonochemical method. *Journal of Alloys and Compounds*, *509*(10), 4098-4103.

[23] Pandurangappa, C., & Lakshminarasappa, B. N. (2012). Optical studies on lanthanum-doped calcium fluoride. *Journal of Materials Science*, *47*, 892-897.

[24] Gulina, L. B., Tolstoy, V. P., Kasatkin, I. A., Kolesnikov, I. E., & Danilov, D. V. (2017). Formation of oriented LaF3 and LaF3: Eu3+ nanocrystals at the gas− solution interface. *Journal of Fluorine Chemistry*, *200*, 18-23

[25] Ladol, J., Khajuria, H., Khajuria, S., & Sheikh, H. N. (2016). Hydrothermal synthesis, characterization and luminescent properties of lanthanide-doped NaLaF 4 nanoparticles. *Bulletin of Materials Science*, *39*, 943-952.

[26] Jacobsohn, L. G., Sprinkle, K. B., Kucera, C. J., James, T. L., Roberts, S. A., Qian, H., ... & Ballato, J. (2010). Synthesis, luminescence and scintillation of rare earth doped lanthanum fluoride nanoparticles. *Optical Materials*, *33*(2), 136-140.

[27] Jadhav, A. P., Pawar, A. U., Pal, U., & Kang, Y. S. (2014). Red emitting Y 2 O 3: Eu 3+ nanophosphors with> 80% down conversion efficiency. *Journal of Materials Chemistry C*, *2*(3), 496-500.

[28] Zhang, Y., Qian, Y., Li, W., Gao, X., & Pan, B. (2019). Fluoride uptake by three lanthanum-based nanomaterials: behavior and mechanism dependent upon lanthanum species. *Science of the Total Environment*, *683*, 609-616.

[29] Romero, M., Faccio, R., Martínez, J., Pardo, H., Montenegro, B., Cid, C. C. P., ... & Mombrú, Á. W. (2015). Effect of lanthanide on the microstructure and structure of LnMn0. 5Fe0. 5O3 nanoparticles with Ln= La, Pr, Nd, Sm and Gd prepared by the polymer precursor method. *Journal of Solid State Chemistry*, *221*, 325-333.

[30] Khan, L. U., Khan, Z. U., Rodrigues, R. V., da Costa, L. S., Gidlund, M., & Brito, H. F. (2019). Synthesis and characterization of tunable color upconversion luminescence β-NaGdF 4: Yb 3+, Er 3+ nanoparticles. *Journal of Materials Science: Materials in Electronics*, *30*, 16856-16863.

[31] Yu, C., Yu, M., Li, C., Zhang, C., Yang, P., & Lin, J. (2009). Spindle-like lanthanide orthovanadate nanoparticles: facile synthesis by ultrasonic irradiation, characterization, and luminescent properties. *Crystal Growth and Design*, *9*(2), 783-791.

[32] Yu, C., Yu, M., Li, C., Liu, X., Yang, J., Yang, P., & Lin, J. (2009). Facile sonochemical synthesis and photoluminescent properties of lanthanide orthophosphate nanoparticles. *Journal of Solid State Chemistry*, *182*(2), 339-347.

CHAPTER 5

Synthesis and Characterization of $Pr(III)F_3$:GSH Nanoparticles: Study of Antimicrobial and Antioxidant properties including mammalian blood haemolysis test

Abstract

The selection of glutathione (GSH) as a reducing agent and stabiliser was based on its harmless properties and the existence of a highly reactive thiol group that can be utilised to decrease the metal salts. GSH is a tripeptide composed of glutamic acid, cysteine, and glycine. It is a widely distributed antioxidant found in both human and plant cells. In addition to the thiol group, each GSH molecule also possesses amine and carboxylate functions that offer opportunities for connecting with other molecules of biological or sensory significance through cross-linking. A compound of $Pr(III)F_3$:GSH nanoparticles were prepared by using Hydrothermal synthesis. Taking Stoichiometric ratio. The resulting nano compounds underwent comprehensive characterization using advanced analytical techniques including Fourier-transform infrared spectroscopy (FT-IR). The average crystallite size was determined using the Scherrer equation, calculated from the full width at half-maximum (FWHM) of the XRD peaks. FRAP and DPPH was used as assays for determining antioxidant activity. Ongoing research efforts continue to explore their potential applications and optimize their properties for various practical uses. The blood hemolysis assay was demonstrated to test the sample for notable anti-hemolytic properties against mammalian erythrocytes (red blood cells). Ongoing research efforts continue to explore their potential applications and optimize their properties for various practical uses.

5.1. Introduction

The lanthanides include a series of 15 elements, from atomic number 57 to 71, which have attracted wide interest in the fields of chemistry and biology due to special electrical properties and wide applications. Lanthanide chemistry, often known as the investigation of the chemistry of the rare earth elements, covers several subjects such as coordination chemistry, catalysis, luminescence, and magnetic characteristics [1]. Lanthanides have been utilised in various fields of biology, including bioimaging, protein structure determination, and drug design [2]. The scientific community has recently shown interest in the interaction between praseodymium fluoride and glutathione, as it has potential uses in different disciplines. Both compounds possess distinct characteristics that make them highly suitable for synergistic interactions, resulting in the development of innovative functions and applications [3]. Praseodymium, along with other rare earth elements, is utilised in the manufacturing of durable permanent magnets of exceptional strength. These magnets are used in electric vehicles, wind turbines, and numerous electrical gadgets because of their outstanding magnetic qualities [4]. Praseodymium-doped materials are used in lighting technologies such as fluorescent lamps and LEDs to produce light with precise wavelengths. Moreover, telecoms rely on praseodymium-based optical fibres to transmit signals because of their minimal optical losses [5].

Praseodymium fluoride (PrF_3) is a rare earth metal fluoride compound consisting of praseodymium and fluorine. The wide range of uses of rare earth metal fluorides in areas such as catalysis, optics, electronics, and health sciences has attracted considerable interest [6]. GSH is a sulphur-containing molecule comprising three amino acids: glutamate, cysteine, and glycine. It has essential functions in cellular activities such as antioxidant defence, detoxification, and modulation of cellular signalling pathways [7]. The selection of glutathione (GSH) as a reducing agent and stabiliser was based on its harmless properties and the existence of a highly reactive thiol group that can be utilised to decrease the metal salts. GHS is a tripeptide consisting of glutamic acid, cysteine, and glycine. It comprises one of the widely distributed antioxidants, not only found in the cells of human beings but also in those of plants. In addition to the thiol group, each GSH molecule also possesses amine and

carboxylate functions that offer opportunities for connecting with other molecules of biological or sensory significance through cross-linking [8]. GSH has been shown to scavenge free radicals; hence, it is considered among the prominent cell protectors against damage caused by reactive oxygen species and xenobiotics. Glutathione may protect organs such as the kidneys, liver, lung, and intestines, which are common target sites for xenobiotics. Reduced levels of GSH are linked to the process of ageing and the development of certain diseases, such as cataracts, haemolysis, alcoholic liver injury, diabetes mellitus, and cancer [9]. These metal nanoparticles are usually synthesized with capping of the metal surface in situ and hence are quite stable both in solution and in forms that are dried. Glutathione (GSH; γ-Glu-Cys-Gly) is a unique tripeptide containing two carboxyl groups (-COOH), one amino group ($-NH_2$), and one sulfhydryl group (-SH). Due to the strong attraction between noble metals and sulphur (S), the GSH molecule can serve as a highly effective capping ligand for synthesising these metals. Glutathione's carboxylate and amine functions can be used to attach nanoparticles to metal oxides like ZnO and TiO_2. This allows for the creation of composite catalysts and therapeutic medicines that can be used in cancer therapy. The use of biomolecular glutathione as a capping ligand for synthesising water-soluble nanoparticles has been widely employed [10].

Similar hazardous effects have been attributed to a number of contaminants that exist in forms of nanoparticles, including carbon nanotubes. In general, it is not unusual to have impurities that come from the synthesis process, and these contaminants can complicate the interpretation of biological reactions [11]. Enhancing synthesis procedures to minimise contaminants is crucial in the creation of biocompatible nanomaterials in order to achieve pure nanoparticles. Several methods have been developed to minimize or even eliminate the adverse impacts created by impurities present within nanomaterial suspensions. These methods include applying an additional layer, exchanging surface ligands, removing metal components through chelation, subjecting the suspensions to high-temperature thermal treatments, using chromatography, field flow fractionation, electrophoresis, dialysis, and diafiltration [12]. Although there is data indicating the necessity of removing contaminants from nanoparticle suspensions to prevent undesired toxicity, these approaches are not

commonly used in many laboratories due to the relatively high cost and time needed for sample preparation [13]. Lanthanide ions (Ln^{3+}) can be doped to enhance their luminophore properties, allowing them to produce strong visible emission across a wide spectrum of colours when excited by UV or IR light (up-conversion) [14].

Previously in one of our reports, we discussed the potential toxicity from various nanoparticles (NPs) coated with glutathione. GSH is attached to the surface of the NPs via the thiol group which is part of its structure as a tripeptide. Although there is potential toxicity due to the poisonous core quantum dots (QDs), our conclusion is that the existence of NP does not cause a high elevation of cellular death. This is because the surface of the NP is completely covered by GSH. Additionally, we have documented the effectiveness of GSH capping, which shows that the GSH molecule maintains its capacity to bind to biological entities and possesses the ability to form specific connections [15].

Haemolysis refers to the rupturing of red blood cells. The ability of bacterial colonies to cause haemolysis when grown on blood agar is one of the features used in classifying certain bacteria. Haemolysis can be attributed to haemolytic anaemia, liver illness, or transfusion response. An important biochemical characteristic of red blood cells in primaquine sensitivity is the quick decrease in levels of reduced Glutathione when exposed to acetyl phenyl hydrazine in a laboratory setting. This discovery has been utilised as a test to determine sensitivity to medications that cause haemolysis. Reactive species are harmful to the cell components. Glutathione (GSH) serves the purpose of repairing cells that have been subjected to oxidative stress. GSH is produced in red blood cells, while Glutathione sulphide (GSSG) is exported from the cells to uphold a high GSH/GSSG ratio [16]. Glutathione performs a crucial function by protecting haemoglobin, enzymes of red blood cells, and biological cell membranes from oxidative damage. This happens through the augmentation of reduced Glutathione as a result of glycolysis. GSH deficiency or a decrease in the GSH/GSSG ratio mainly causes an increased susceptibility to oxidative stress and is considered to be involved in the pathogenesis of cancer and neurodegenerative disorders like Parkinson's and Alzheimer's diseases. GSH is an omnipresent, redox-active compound that is essential for the well-being of cells and organisms. Several studies have shown

the impact of environmental factors, including as nutrition and lifestyle, on the level of GSH in RBC [17].

5.2. Experimental

Materials

Praseodymium trinitrate hexahydrate ($Pr(NO_3)_3 \cdot 6H_2O$, purity 99.99%) was purchased from Merck and used as obtained. L-Glutathione reduced ($C_{10}H_{17}N_3O_6S$, ≥98.0%), NH_4F (99.99%, HiMedia), Ethanol (99.9%, Merck) were used as a starting material without any further purification. The powder XRD analysis was carried out using a "Rigaku Ultima IV X-ray diffractometer" with Cu K α radiation at λ = 1.540 Å from range 10° to 80° (2θ) at room temperature. Nutrient agar and streptomycin were purchased from HiMedia while DPPH and Trolox from Merck, India. All the aqueous solutions were prepared in deionized water.

Methods

Synthesis of Praseodymium Flouride doped with Glutathione

A compound of $Pr(III)F_3$:GSH nanoparticles were prepared by using Hydrothermal synthesis. Taking Stoichiometric ratio, a solution of $Pr(NO_3)_3$ with 1.1083gm, Glutathione of about 2.1511gm were mixed and heated in 40ml DI (Deionized) water using magnetic stirring. On the other hand, a solution of 0.2844gm Ammonium fluoride (NH_4F) was prepared in 24ml DI water. Next, the prepared NH_4F solution were added slowly into the heating $Pr(NO_3)_3$:GSH solution. Further Sonicator instrument "Probe Sonicator; Rivotek, Version 12.01 (5.3), CSIR-NEIST" was used to mix the solution thoroughly and thus to reduce the size of particles suspended in a liquid medium. This is particularly useful in nanoparticle synthesis, where precise control over particle size is essential for achieving desired properties and functionalities. After mixing the dissolved solution, it was transferred into a Teflon bottle which were confined in stainless steel autoclave, the solution is then secured and maintained at exact 150 °C for 24 hrs. The obtained compound at the bottom was segregated and cleaned by centrifugation process. After cleaning with DI water, it was

followed with ethanol solvent for 3 times and then the compound was dried in oven for about 18 hrs.

Characterization

The (PerkinElmer Spectrum Two FT-IR Spectrometer) spectrophotometer was used to record FTIR spectra using the KBr pellet technique.

5.3. Results and Discussion

FTIR

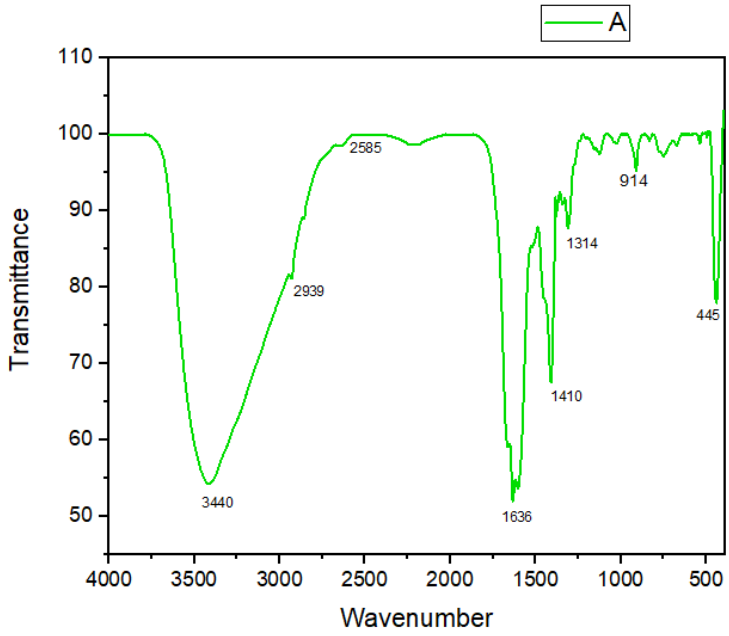

Figure 4.1. Spectra from FTIR for PrF_3 doped Glutathione

FTIR Spectroscopy

The IR analysis was conducted to examine the complexation process between praseodymium fluoride and glutathione (GSH). FTIR analysis provides insights into the chemical composition and environment of the resulting complex. The IR spectra for both free glutathione and the PrF_3 complex are shown in the **Fig. 4.1**. These spectra reveal multiple vibrations for GSH and the Pr(III)–GSH complex. The presence or absence of certain bands in the lanthanide complex, compared to free GSH, offers clues about the bonding mechanism and the binding mode within the formed complex.

A broad band around 3440 cm^{-1} likely indicates the presence of water molecules. Key vibrations in the FTIR spectra of free glutathione appear at 2585 cm^{-1} and 1636 cm^{-1}, corresponding to the sulphydryl (–SH) group and the carbonyl (C=O) group of carboxylic acid, respectively. The band at 1410 cm^{-1} is associated with S=O stretching in sulfonyl chloride, while a peak at 1314 cm^{-1} represents C-F stretching, characteristic of the fluoro compound. These bands highlight the functional groups of GSH doped with PrF_3 [15,16].

XRD (X-ray Diffraction Spectroscopy)

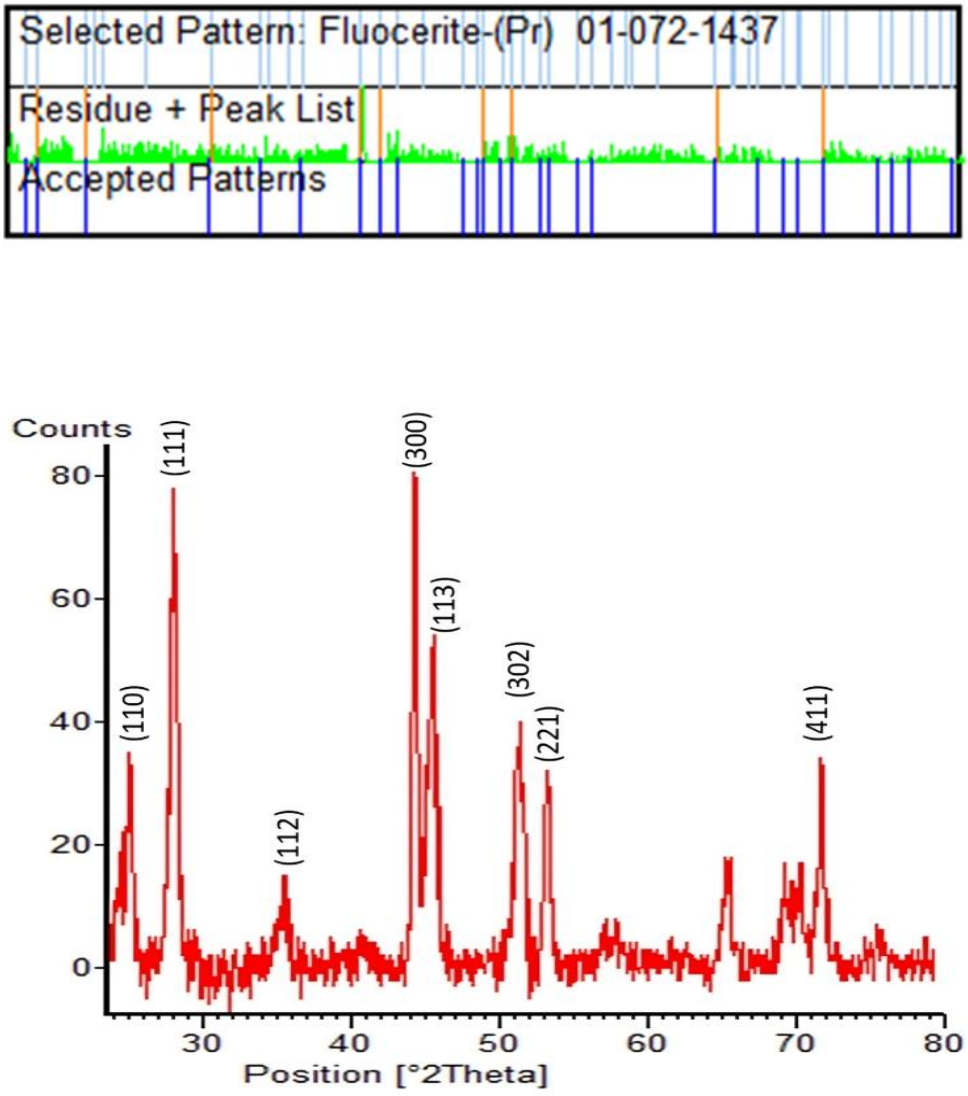

Figure 4.2. XRD pattern of PrF_3 doped Glutathione

Fig. 4.2. exhibits the XRD pattern of PrF_3:GSH nanoparticles which were collected using a Powder X-Ray Diffractometer (Model: ULTIMA IV, Rigaku, Japan). From the figure, almost all reflection planes have pure crystalline PrF_3:GSH structure (Space group number: 165, Space group: Pnma P-3c1, with lattice constants a = 7.0795; b = 7.0795, c = 7.2380, which is consistent with standard data (Reference code from JCPDS: 00-046-1167). The hexagonal phase of PrF_3:GSH of high purity can be indexed for the diffraction plane (110) (111) (112) (300) (113) (302) (221) (411). As a result, a hexagonal crystal system has been suggested for the praseodymium Fluoride complex with GSH [17]. The size of the crystallites was determined by the use of Scherrer's formula with the full width at half maximum (FWHM) for the most intense peak.

$$\text{“ D(Å)} = \frac{K\lambda}{\beta cos\theta}\text{”}$$

where k represents the Scherer constant (~0.9), λ signifies the X-ray wavelength of Cu kα radiation, β indicates the FWHM of the diffraction peak and θ represents the Braggs' angle. The PrF_3–GSH complex's average crystallite size was found to be 12 nm, suggesting the phase of the system to be nanocrystalline.

Antioxidant

Antioxidant Activity

The two most used tests for determining antioxidant activity are FRAP and DPPH. They are reasonably basic, provide quick analysis, and are easily standardisable. DPPH is a stable N-centered free radical with an odd electron that remains stable at ambient temperature. In methanol solutions, it exhibits a significant absorption at 517 nm and a purple colour. When a radical scavenger is present, the DPPH purple colour pairs with its odd electron by giving away an alkyl or hydrogen radical, turning it from purple to yellow.

DPPH Assay

The DPPH radical's free-radical scavenging effects of the sample and Trolox at several dilutions of 20, 40, 60, 80, and 100 μg/mL are illustrated in the graph of % scavenging against concentration. The IC_{50} values for the complicated sample and standard Trolox

are shown in **Table 4.1.** The half-maximal inhibitory concentration, or IC_{50}, was used to express the antioxidant activity, which was measured using the calibration curve in relation to the percentage of antioxidant activity. The concentration of a material that yields 50% of the maximum effect is known as its IC_{50}. Here, it refers to the sample concentration that is capable of either blocking 50% of the DPPH radical or lowering 50% of absorbance to the DPPH radical. The sample's antioxidant activity is higher the lower its IC_{50} value is. Compared to ordinary Trolox, which has an IC_{50} of 86, the complex displayed an IC_{50} of 64. Consequently, the PrF_3-GSH complex sample's DPPH scavenging activity was greater than that of the regular Trolox.

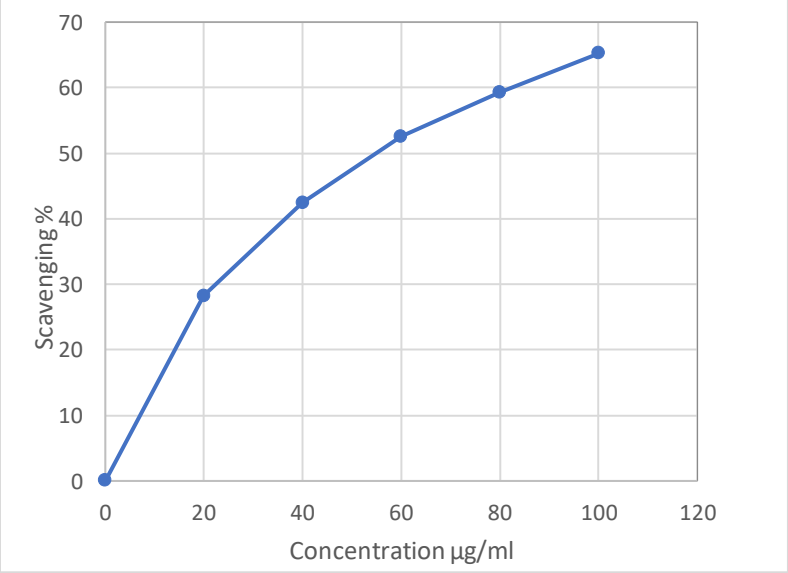

Figure 4.2. a: Assessment of DPPH free-radical scavenging activity in the presence of various concentrations of Trolox.

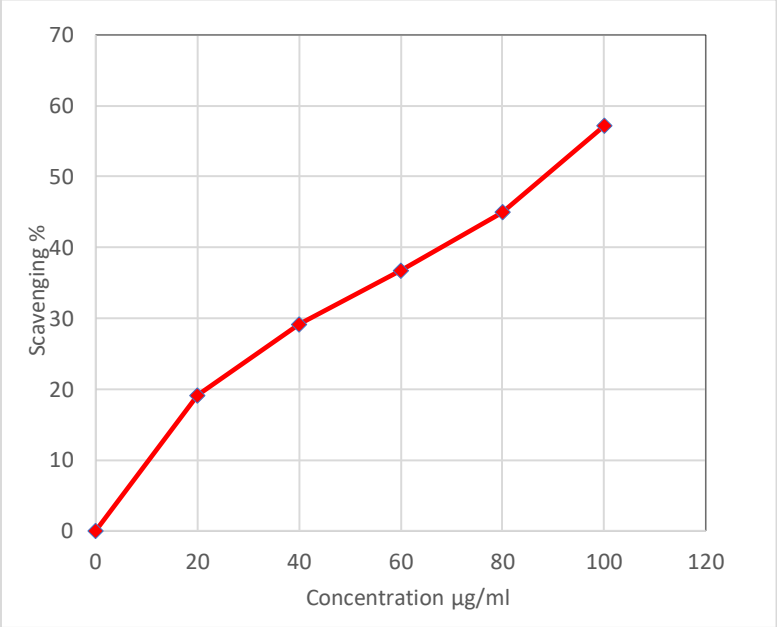

Figure 4.2 b: Assessment of DPPH free-radical scavenging activity in the presence of various concentrations of sample.

Table 4.1. DPPH radical scavenging activity and IC_{50} values of the standard Trolox and Sample.

Concentration (µg/ml) %	Trolox		Sample	
	% Inhibition	IC_{50} (µg/ml)	% Inhibition	IC_{50} (µg/ml)
20	19.1	86	28.21	64
40	29.18		42.43	
60	36.74		52.26	
80	44.95		59.26	
100	57.15		65.23	

FRAP Assay

The FRAP assay results are displayed in **Fig. 4.2 c.** It features a concentration vs sample and Trolox absorbance graph. Plotting the absorbance readings at 700 nm against the relevant concentrations (µg/ml) was done. The sample's absorbance values were less than those of Trolox, the reference chemical, suggesting that its antioxidant action had been diminished. The FRAP assay adhered to the same general pattern as the DPPH assay. The sample's reducing power showed a growing trend as

concentration increased **(Fig. 4.2 c).** The findings of this study demonstrate that the complex possesses antioxidant activity. [18-21]

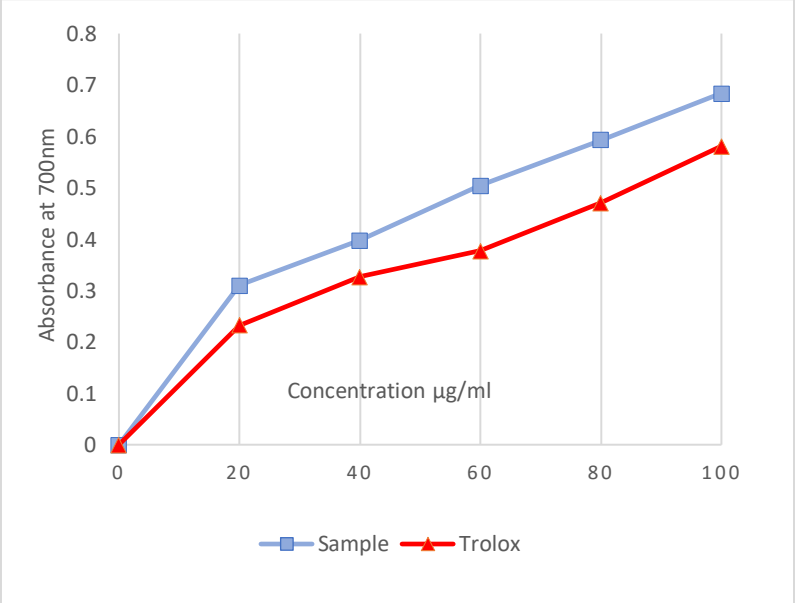

Figure 4.2 c: Antioxidant activity of standard (Trolox) and the sample using FRAP assay.

Blood Hemolysis assay (Antimicrobial Activity)

Hemolysis is one of the most important sources of error in the pre-analytic phase. Amelioration of criteria for detection, measurement, management of the parameters affected by the interference, and differentiation between in vitro and in vivo hemolysis would favor a personalized approach to the management of this artifact with higher patient safety. It is possible that, when hemolysis levels are very high, several described mechanisms happen simultaneously [22]. The interference degree caused by hemolysis is not only important in spectrophotometric biochemical tests, but also in gasometric, hematocytometric, coagulometric and immunoassay tests [23].

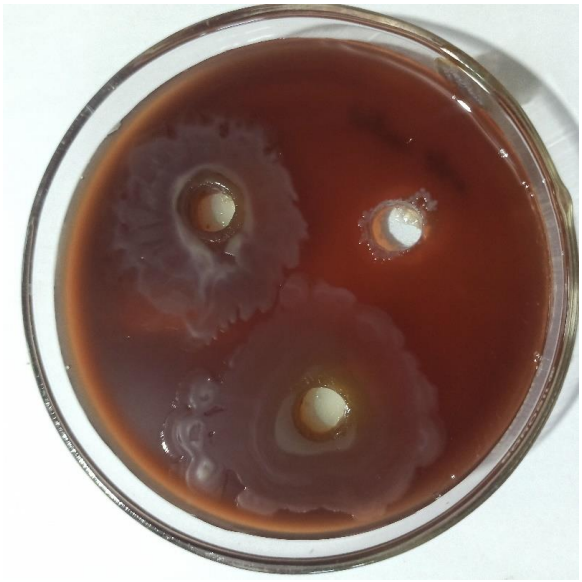

Figure 4.3. Blood Hemolysis of PrF3:GSH

Hemolytic activity of PrF_3:GSH was determined on nutrient blood agar plates supplemented with 2% (v/v) mammalian blood (goat). Fresh mammalian blood was collected in sterile tubes containing anti-coagulants (sodium citrate). The nutrient agar media was made by dissolving 28 g of nutrient agar powder in 1000 ml distilled water and then sterilizing it by autoclaving at 121˚ for 15 minutes. Next, the media was supplemented with 2% mammalian blood (v/v) and put into sterilised petri plates to allow it to solidify. Using a sterile cork borer, wells measuring 6.0 mm in diameter was carefully made on each blood agar plate under aseptic conditions. A 200 µl aliquot of the aqueous sample was added into the wells by means of a micropipette, and the plates were incubated at 37°C for 48 hours with distilled water serving as the negative control [24,25].

The results of the blood hemolysis assay demonstrate that the test sample exhibited notable anti-hemolytic properties against mammalian erythrocytes (red blood cells) as there was no clear zone seen around the wells containing the sample in the blood agar media. This finding indicates that PrF_3:GSH do not exert any negative effects on the red blood cells during the test underlining its benign nature. Hence, it may play a key role in the protection of hemoglobin and red cells' enzymes against oxidative damage by increasing the level of reduced Glutathione in the process of glycolysis.

5.4. Conclusion

The IR analysis was used to study the mode of complexation between praseodymium fluoride and GSH. FTIR analysis helped in elucidating the chemical composition and environment of the complex formed. From XRD, a hexagonal crystal system has been suggested for the praseodymium fluoride complex with GSH. The FRAP assay followed a trend almost similar to that obtained in the DPPH assay. There was an increase in the reducing power of the sample with an increase in concentration. The results of the study on the complex showed the latter to have antioxidant activity. The results of the blood hemolysis assay revealed that the test sample had remarkable anti-hemolytic properties against mammalian erythrocytes since no clear zone was seen around the wells containing the sample in the blood agar media. This finding indicates that PrF_3:GSH do not exert any negative effects on the red blood cells during the test underlining its benign nature.

Acknowledgement

The authors would like to acknowledge the department of Chemistry and Physics, Nagaland University; Lumami for providing the laboratory facilities. The authors are also grateful to Chemical Engineering Group, CSIR-NEIST; Jorhat for allowing us to do the characterizations. The authors are grateful to UGC NON-NET fellowship for the financial support.

Declaration of interests

The authors declare that they have no known competing financial interests or personal relationships that could have appeared to influence the work reported in this paper.

References:

[1] Guillou, O., Daiguebonne, C., Calvez, G., & Bernot, K. (2016). A long journey in lanthanide chemistry: From fundamental crystallogenesis studies to commercial anticounterfeiting taggants. *Accounts of chemical research*, *49*(5), 844-856.

[2] Kauffman, G. B. (2005). Book Review of Comprehensive Coordination Chemistry II: From Biology to Nanotechnology. *Journal of Coordination Chemistry*, *58*(7), 643-645.

[3] ZiekhrÃ¼, M., Imchen, P., Phucho, T., & Devi, M. I. (2023). Synthesis, characterization, antioxidant and antibacterial studies of praseodymium complex with glutathione. *Current Science*, 554-561.

[4] Stegen, K. S. (2015). Heavy rare earths, permanent magnets, and renewable energies: An imminent crisis. *Energy Policy*, *79*, 1-8.

[5] Chiodini, N., Vedda, A., & Veronese, I. (2014). Rare earth doped silica optical fibre sensors for dosimetry in medical and technical applications. *Advances in Optics, 2014*.

[6] Lu, S. C. (2013). Glutathione synthesis. *Biochimica et Biophysica Acta (BBA)-General Subjects*, *1830*(5), 3143-3153.

[7] Balavandy, S. K., Shameli, K., Biak, D. R. B. A., & Abidin, Z. Z. (2014). Stirring time effect of silver nanoparticles prepared in glutathione mediated by green method. *Chemistry Central Journal*, *8*, 1-10.

[8] Koo, S. H., Lee, J. S., Kim, G. H., & Lee, H. G. (2011). Preparation, characteristics, and stability of glutathione-loaded nanoparticles. *Journal of agricultural and food chemistry*, *59*(20), 11264-11269.

[9] Sachil, S., Bit, K., & Dongil, L. (2012). Water-Soluble Pd Nanoparticles Capped with Glutathione: Synthesis, Characterization, and Magnetic Properties.

[10] Sapsford, K.E.; Tyner, K.M.; Dair, B.J.; Deschamps, J.R.; Medintz, I.L. Analyzing nanomaterial bioconjugates: A review of current and emerging purification and characterization techniques.Anal. Chem. 2011, 83, 4453–4488.

[11] Guo, L.; Morris, D.G.; Liu, X.; Vaslet, C.; Hurt, R.H.; Kane, A.B. Iron bioavailability and redox activity in diverse carbon nanotube samples. Chem. Mater. 2007, 19, 3472–3478.

[12] Harper, S.L.; Carriere, J.L.; Miller, J.M.; Hutchison, J.E.; Maddux, B.L.S.; Tanguay, R.L. Systematic Evaluation of Nanomaterial Toxicity: Utility of Standardized Materials and Rapid Assays. ACS Nano 2011, 5, 4688–4697.

[13] Runowski, M., & Lis, S. (2016). Nanocrystalline rare earth fluorides doped with Pr3+ ions. *Journal of rare earths*, *34*(8), 802-807.

[14] Beato-López, J. J., Domínguez, M., Ramírez-del-Solar, M., & Litrán, R. (2020). Glutathione-magnetite nanoparticles: Synthesis and physical characterization for application as MRI contrast agent. *SN Applied Sciences*, *2*, 1-14.

[15] Han, G. C., & Liu, Y. N. (2010). Synthesis, characterization and fluorescent properties of cerium (III) glutathione complex. *Luminescence*, *25*(5), 389-393.

[16] Ziekhrü, M., Thakro, Z., Imsong, C., Sanchu, J., & Devi, M. I. (2021). Computation of energy interaction and intensity parameters for the complexation of Pr (III) with glutathione at different pH in the presence/absence of Mg2+: 4f-4f transition spectra as a probe. *Polyhedron*, *200*, 115099.

[17] Pérez-Herráez, I., Ferrera-González, J., Zaballos-García, E., González-Béjar, M., & Pérez-Prieto, J. (2024). Raspberry-like Nanoheterostructures Comprising Glutathione-Capped Gold Nanoclusters Grown on the Lanthanide Nanoparticle Surface. *Chemistry of Materials*.

[18] Pisoschi, A. M. and Pop, A., The role of antioxidants in the chemistry of oxidative stress: a review. Eur. J. Med. Chem., 2015, 97, 55–74.

[19] Nimse, S. B. and Pal, D., Free radicals, natural antioxidants, and their reaction mechanisms. RSC Adv., 2015, 5, 27986–28006.

[20] Cai, Y., Sun, M. and Corke, H., Antioxidant activity of betalains from plants of the amaranthaceae. J. Agric. Food Chem., 2003, 51, 2288–2294.

[21] Benzie, I. F. F. and Strain, J. J., The ferric reducing ability of plasma (FRAP) as a measure of 'antioxidant power': the FRAP assay. Anal. Biochem., 1996, 239, 70–76.

[22] Marques-Garcia F. Methods for Hemolysis Interference Study in Laboratory Medicine - A Critical Review. EJIFCC. 2020 Mar 20;31(1):85-97. PMID: 32256292; PMCID: PMC7109502.

[23] Farrell, C. J. L., & Carter, A. C. (2016). Serum indices: managing assay interference. *Annals of clinical biochemistry*, *53*(5), 527-538.

[24] Mulligan, C. N., Cooper, D. G., & NEUFELD, R. J. (1984). Selection of microbes producing biosurfactants in media without hydrocarbons. *Journal of fermentation technology*, *62*(4), 311-314.

[25] Youssef, N. H., Duncan, K. E., Nagle, D. P., Savage, K. N., Knapp, R. M., & McInerney, M. J. (2004). Comparison of methods to detect biosurfactant production by diverse microorganisms. *Journal of microbiological methods*, *56*(3), 339-347.

CHAPTER 6

Summary and conclusion

Metal binding to a specific donor site of biomolecules is determined by a variety of factors such as donor capability, structure, conformation, orientation, physiological pH, the presence of similar types of metal ions and their relative abundance. Thus, it is deemed important to research the simultaneous coordination of two or three distinct metal ions with a multidentate biological molecule. We chose glutathione reduced (GSH), a tripeptide containing active carboxylate groups, a sulphydryl group, and peptide groups. GSH was chosen because it is easily available in its pure form, is biologically significant and is an excellent ligand for simultaneous complexation by hard and soft metal ions. It has eight potential donor binding sites for complexation with endogenous metal ions and serves as an excellent multidentate ligand for metal ions. The coordination chemistry of glutathione is important for understanding a wide range of biological processes, as well as serving as an indicator for the chemistry of thiol-sulphide interchange interactions and the toxicology of numerous metals. Pr(III): Isonicotinic acid nanocrystal was fruitfully manufactured and then it was further analyzed with different scientific methods. These complexes were found to be non-hygroscopic solid and soluble in water and most of the organic solvents. Based on the *in vitro* antimicrobial study, the synthesized complex was found to be biologically active and possess remarkable antimicrobial properties. Thus, such finding indicate that the synthesized nanocrystal could have potential photochemical and therapeutic applications.

The present study represents a significant contribution to this field, where, *via* a facile solvothermal approach, uniform and well-crystallized GdF_3:Eu^{3+} nanoparticles were successfully synthesized. The orthorhombic crystal structure and nanoparticle size were also authenticated using a comprehensive suite of analytical techniques that included XRD, SEM, TEM and EDX. The well-resolved lattice fringes are clearly shown by HRTEM images and SAED image displays regular diffraction spots, indicating single crystallinity and facet dominance in the GdF_3:Eu^{3+}. This facilitated a thorough characterization of Eu^{3+} ion integration into the GdF_3 crystal lattice. The insights gleaned from this investigation serve to propel

forward the realm of lanthanide fluoride chemistry, while concurrently bestowing invaluable comprehension regarding the development and formation mechanisms of nanomaterial crystals.

The insights gleaned from this investigation serve to propel forward the realm of lanthanide fluoride chemistry, while concurrently bestowing invaluable comprehension regarding the development and formation mechanisms of nanomaterial crystals. Investigating the intricate mechanisms governing the production of varied morphologies in LnF_3 nanocrystals, infrared spectroscopy delineated the formation of chemical bonds between lanthanide and fluoride moieties

Analytical data indicates that praseodymium(III):Isonicotinic acid nanomaterial was formed with a metal-ligand stoichiometry of 1:3 and it possess good keeping qualities. The nano crystal is low water solubility solid and is soluble in methanol, ethanol, MeCN, DMF etc. Analytical values of the complex were found to be in conformation with their formation. Haemolysis is one of the major sources of error at the pre-analytical phase. Enhancing patient safety through improvements in haemolysis detection, measurement, management of the parameters interfered with, and differentiation between haemolysis in vivo and in vitro will promote patient-based haemolysis treatment. It is possible that several mechanisms above mentioned are operating simultaneously at very high levels of haemolysis.

The results of the blood hemolysis assay demonstrate that the test sample exhibited notable anti-hemolytic properties against mammalian erythrocytes (red blood cells) as there was no clear zone seen around the wells containing the sample in the blood agar media. This finding indicates that PrF_3:GSH do not exert any negative effects on the red blood cells during the test underlining its benign nature. Hence it may play an important role in protecting hemoglobin, red cells enzymes against oxidative damage by increasing the level of reduced Glutathione in the process of glycolysis.

NAGALAND UNIVERSITY

(संसद द्वारा पाररत अविवनयम 1989, क्रमांक 35 केअंतगगत स्थावपत केंद्रीय विश्वविद्यालय)

(A Central University established by an Act of Parliament No.35 of 1989)

मुख्यालय : लुमामी, विला : िुन्हेबोटो (नागालैण्ड), वपनकोड – 798627

Hqrs: Lumami, Dist. Zunheboto (Nagaland), Pin Code – 798627

िेबसाइट / Website : www.nagalanduniversity.ac.in

Ph.D. Thesis Certificate on Plagiarism Check

Name of Research Scholar	PUNAZUNGBA IMSONG
Ph.D. Registration Number	Ph.D./CHE/00057
Title of Ph.D. thesis	*Synthesis of Lanthanide Nanoparticles: Its' Characterization through crystallography and spectral techniques along with their applications*
Name & Institutional Address of the Supervisor	Prof. M. Indira Devi, Department of Chemistry, Nagaland University
Name of the Department and School	Department of Chemistry, School of Science
Date of submission	27-08-2024
Date of plagiarism check	27-08-2024
Percentage of similarity detected by the iThenticate software	7 %

I hereby declare/ certify that the Ph.D. Thesis/ M. Phil. Dissertation submitted by me is complete in all respect, as per the guidelines of Nagaland University (NU) for this purpose. I also certify that the Thesis/ Dissertation (soft copy) has been checked for plagiarism using **iThenticate** similarity check software. It is also certified that the contents of the electronic version of the thesis/dissertation are the same as the final hardcopy of the thesis /dissertation. Copy of the Report generated by the **iThenticate** software is also enclosed.

Date: (Punazungba Imsong)

Place: (Name & Signature of the Scholar)

(**Prof. M. Indira Devi**)

Name & Signature of the Supervisor

iThenticate

Similarity Report ID: oid:3117:375368812

PAPER NAME

Punazungba Imsong.pdf

WORD COUNT	CHARACTER COUNT
16969 Words	**99238 Characters**
PAGE COUNT	FILE SIZE
67 Pages	**2.8MB**
SUBMISSION DATE	REPORT DATE
Aug 23, 2024 9:40 PM GMT+5:30	**Aug 23, 2024 9:41 PM GMT+5:30**

7% Overall Similarity

The combined total of all matches, including overlapping sources, for each database.

- 2% Internet database
- 7% Publications database
- Crossref database
- Crossref Posted Content database
- 0% Submitted Works database

Excluded from Similarity Report

- Bibliographic material
- Quoted material
- Cited material
- Abstract
- Methods and Materials

List of Presentations and Workshops

1. **Paper presented** at the *National e-Seminar on Chemistry in emerging trends of Interdisciplinary Research (NeSCETIR)*, Department of Chemistry, Nagaland University, Lumami, 18-20 November 2020.
2. **Paper presented** at the *2nd Convention of NEAST and International Conference on Recent Advances on Science & Technology (ISRAST)*, organized by NEAST, Mizoram University, Aizawl, 16-18 November, 2020.
3. Participant at *National Seminar on Chemistry in Interdisciplinary Research*, Department of Chemistry, Nagaland University, Lumami, 9-10 November, 2018.
4. Participant of workshop on "*Advanced Techniques in Nano Science and Technology*", Institute of Nano Science and Technology, Mohali on 13-16 December 2017.
5. Participant of National workshop on "*Newer Frontiers in Bioinformatics and Research Methodology"* organized by Bioinformatics Infrastructure Facility(BIF) Centre, Nagaland University, Lumami, sponsored by Department of Biotechnology, Ministry of Science and Technology, Government of India, New Delhi, From 13th to 19th November 2018.
6. Participant of national conference on "*Advanced Techniques in Nano Science and Technology*", Institute of Nano Science and Technology, Mohali on 19-21 December 2017.
7. Participant of Hands on training on "*NanoDCAL & RESCU Software*" organized by IMPULSE TECHNOLOGY on 14th March 2024, Gurugram, Haryana – 122018.
8. Participant of National Workshop on " *Flourescence Spectroscopy and techniques* " organized by Department of Physics, Nagaland University, Lumami on 4th April 2022.

List of Publications

1. **Punazungba Imsong**, Juliana Sanchu,Sentienla Imsong, Mhasiriekho Ziekhrü and M.Indira Devi* , Quantitative Analysis of the Co-ordination Nature of the Synthesized Praseodymium(III) Isonicotinic acid Nanomaterial: Characterizationand Study of Antimicrobial Properties, Journal of Applicable Chemistry 2024, 13 (2): 59-72
2. Sentienla Imsong, **Punazungba Imsong**, Swapnali Hazarika* and M. Indira Devi*, Facile synthesis of lanthanum carbonate octahydrate and lanthanum oxide nanoparticles by sonochemical method: systematic characterizations, https://doi.org/10.1515/zpch-2023-0396

Available online at **www.joac.info**

ISSN: 2278-1862

Journal of Applicable Chemistry

2024, 13 (2): 59-72

(International Peer Reviewed Journal)

Quantitative Analysis of the Co-ordination Nature of the Synthesized Praseodymium(III) Isonicotinic acid Nanomaterial: Characterization and Study of Antimicrobial Properties

PunazungbaImsong, Juliana Sanchu,Sentienla Imsong, Mhasiriekho Ziekhrü and M.Indira Devi*

Department of Chemistry, Nagaland University, Lumami, Nagaland - 798627

Email: cam_indira@yahoo.co.in

Accepted on 10th March, 2024

ABSTRACT

Praseodymium (III): isonicotinic acid nano crystal was successfully synthesized through a simple technique and characterized by elemental analysis, molar conductance, FT-IR, X-ray powder diffraction, fluorescence, UV-Vis spectroscopy and the rmogravimetric studies. The evaluated Energy interaction and Judd Ofelt Intensity parameters from the UV-Vis spectra of the synthesized nano crystal could suggest the mode of co-ordination of Pr(III) with isonicotinic acid. Further, therein vitro antimicrobial properties were also studied. The isonicotinic acid ligand is composed of carbonyl oxygen atom and nitrogen atom of the pyridine ring as potential donor sites. Deprotonation of the ligand sites enabled metal-ligand coordination, and as a result, isonicotinic acid behaves as a bidentate ligand. A coordination number of nine was assigned to the praseodymium (III) ion in this nano crystal with monoclinic structure. The nanomaterial was found to be thermally stable and shows good photochemical and antimicrobial properties.

Graphical Abstract:

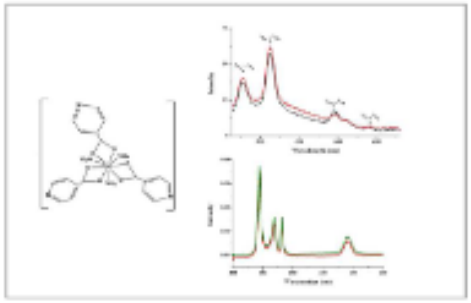

Synthesis, Characterization, and Functional Properties of Praseodymium(III) Isonicotinic Acid Nano Crystal with Enhanced Antimicrobial and Photochemical Attributes

Keywords: Pyridine, Praseodymium(III) nitrate hexahydrate, Antimicrobial activity.

Sentienla Imsong, Punazungba Imsong, Swapnali Hazarika* and M. Indira Devi*

Facile synthesis of lanthanum carbonate octahydrate and lanthanum oxide nanoparticles by sonochemical method: systematic characterizations

https://doi.org/10.1515/zpch-2023-0396
Received October 25, 2023; accepted February 23, 2024; published online March 19, 2024

Abstract: This study could present the size and morphology of two synthesized nanoparticles (NPs) by observing their smallest possible dimensions. Lanthanum carbonate nanoparticles were synthesized by sonochemical method through the interaction of lanthanum acetate hydrate and sodium carbonate in an aqueous medium with a probe sonicator. After rigorous washing followed by drying, the $La_2(CO_3)_3{\cdot}8H_2O$(S1) NPs were calcined at a temperature of 600 °C to obtain lanthanum oxide nanoparticles (S2). Both NPs were characterised through various instrumental techniques. PXRD study showed orthorhombic with space group of *Pccn* (56) and hexagonal phases with space group of $P\bar{3}m1$(164) for S1 and S2 respectively whose morphology and elemental analysis were studied through FESEM and EDX. High resolution TEM image of $La_2(CO_3)_3{\cdot}8H_2O$ and La_2O_3 showed spherical shapes of the nanoparticles. Further study of XPS and FTIR conveyed detailed information of both nanoparticles whose TGA-DSC showed three step decomposition curves. The size and morphology of the synthesized nanoparticles have been found to have a distinct morphology and are found comparatively smaller in size than those observed in the earlier reported works (Table 1).

Keywords: sonochemical; rare earths; calcination; lanthanide nanoparticles

***Corresponding authors: Swapnali Hazarika**, Chemical Engineering Group and Centre for Petroleum Research, CSIR-North East Institute of Science and Technology, Jorhat 785006 Assam, India, E-mail: shrrljt@yahoo.com; and **M. Indira Devi**, Department of Chemistry, Nagaland University, Lumami-798626, Zunheboto, India, E-mail: cam_indira@yahoo.co.in
Sentienla Imsong and Punazungba Imsong, Department of Chemistry, Nagaland University, Lumami-798626, Zunheboto, India

(12) PATENT APPLICATION PUBLICATION
(19) INDIA
(22) Date of filing of Application :05/04/2024
(21) Application No.202431028201 A
(43) Publication Date : 19/04/2024

(54) Title of the invention : A NOVEL PROCESS OF MAKING LANTHANUM NANOPARTICLES

(51) International classification :A61K0033244000, C02F0001280000, C01F0017247000, A61P0043000000, H01M0010052500
(86) International Application No :NA
Filing Date :NA
(87) International Publication No : NA
(61) Patent of Addition to Application Number :NA
Filing Date :NA
(62) Divisional to Application Number :NA
Filing Date :NA

(71)**Name of Applicant :**
1)Nagaland University
Address of Applicant :Nagaland University, Lumami Headquarters, Zunheboto district-798627, Nagaland, India Zunheboto ---------- ----------
Name of Applicant : NA
Address of Applicant : NA
(72)**Name of Inventor :**
1)Punazungba
Address of Applicant :Nagaland University, Lumami Headquarters, Zunheboto district Zunheboto ---------- ----------
2)Sentienla Imsong
Address of Applicant :Nagaland University, Lumami Headquarters, Zunheboto district, Nagaland India Zunheboto ---------- ----------
3)M. Indira Devi
Address of Applicant :Nagaland University, Lumami Headquarters, Zunheboto district, Nagaland India Zunheboto ---------- ----------
4)Swapnali Hazarika
Address of Applicant :CSIR-NEIST, Jorhat, 785006, India, Jorhat assam Phagwara ---------- ----------

(57) Abstract :
The smallest possible dimensions of two synthesized nanoparticles (NPs) may be used to present the size and morphology of the particles in this study. By using a probe sonicator to interact with sodium carbonate and lanthanum acetate hydrate in an aqueous medium, lanthanum carbonate nanoparticles are created using a sonochemical technique. Lanthanum oxide nanoparticles (S2) are obtained by calcining the La2(CO3)3.8H2O(S1) NPs at 600-700 ˚C following a thorough ishing and drying process. The two NPs are described using a range of instrumental methods. PXRD analysis revealed hexagonal phases with space group P-3m1(164) for S2 and orthorhombic phases with space group Pccn(56) for S1, respectively. FESEM and EDX are used to analyze the morphology and elemental analysis of these phases. La2(CO3)3.8H2O and La2O3 high resolution TEM images revealed spherical nanoparticle shapes.

No. of Pages : 27 No. of Claims : 3

(12) PATENT APPLICATION PUBLICATION
(19) INDIA
(22) Date of filing of Application :05/04/2024

(21) Application No.202431028202 A
(43) Publication Date : 19/04/2024

(54) Title of the invention : NOVEL CATALYST FOR ORGANIC REACTIONS AND PROCESS THEREOF

(51) International classification :A61B0005000000, C09K0011770000, B82Y0030000000, C30B0029600000, C08G0083000000
(86) International Application No :NA
Filing Date :NA
(87) International Publication No : NA
(61) Patent of Addition to Application Number :NA
Filing Date :NA
(62) Divisional to Application Number :NA
Filing Date :NA

(71)**Name of Applicant :**
1)Nagaland University
Address of Applicant :Nagaland University, Lumami Headquarters, Zunheboto district, Nagaland, India Zunheboto ---------- ----------
Name of Applicant : NA
Address of Applicant : NA
(72)**Name of Inventor :**
1)Punazungba
Address of Applicant :Nagaland University, Lumami Headquarters, Zunheboto district, Nagaland India Zunheboto ---------- ----------
2)Wangkhem
Address of Applicant :Nagaland University, Lumami Headquarters, Zunheboto district, Nagaland India Zunheboto ---------- ----------
3)Sentienla Imsong
Address of Applicant :Nagaland University, Lumami Headquarters, Zunheboto district, Nagaland India Zunheboto ---------- ----------
4)M. Indira Devi
Address of Applicant :Nagaland University, Lumami Headquarters, Zunheboto district, Nagaland, India Zunheboto ---------- ----------
5)Swapnali Hazarika
Address of Applicant :CSIR-NEIST, Jorhat, 785006, India, Jorhat India Jorhat ---------- ----------

(57) Abstract :
The field of lanthanide-doped nanomaterials is a major driver of the current state of materials science. They represent a revolutionary era in material engineering, with applications ranging from the production of advanced optical devices to solar cells, phosphors, lasers, and biomedical technologies. The current work is a noteworthy contribution to this field since it successfully synthesized uniform and well-crystallized GdF3:Eu3+ nanoparticles using a simple solvothermal method. While luminescence spectroscopy clarified the dynamics of excitation and emission energy transfer, infrared spectroscopy explored the complex mechanisms underlying the formation of diverse morphologies in LnF3 nanocrystals. It also identified the formation of chemical bonds between lanthanide and fluoride moieties. A wide range of analytical methods, such as X-ray, were also used to confirm the orthorhombic crystal structure and nanoparticle size.

No. of Pages : 19 No. of Claims : 2

Bio-data of Research Scholars

Name : **Mr. Punazungba Imsong**

Designation : Research scholar, Department of Chemistry

Department/Institute/University: Nagaland University

Date of Birth: 26-08-1992 Sex (M/F): M SC/ST: ST

A. Education (Post-Graduation onwards & Professional Career):

S. No.	Institution Place	Degree Awarded	Year	Field of Study
1.	Nagaland University, Lumami	M. Sc	2014-2016	Chemistry
2.	Nagaland University, Lumami	Ph. D	2017-2024	Physical Chemistry

Work experience: Hands on guidance and mentored M.Sc. students through their physical chemistry practicals for two consecutive semesters**.**

Publications (Numbers only):

Research Papers & Patent: **4**

Papers presented in symposia: **2**

Publications in chronological order):

1.) **Punazungba Imsong**, Juliana Sanchu, Sentienla Imsong, Mhasiriekho Ziekhrü and M.Indira Devi* , Quantitative Analysis of the Co-ordination Nature of the Synthesized Praseodymium(III) Isonicotinic acid Nanomaterial: Characterizationand Study of Antimicrobial Properties, Journal of Applicable Chemistry 2024, 13 (2): 59-72

2.) Sentienla Imsong, **Punazungba Imsong**, Swapnali Hazarika* and M. Indira Devi*, Facile synthesis of lanthanum carbonate octahydrate and

lanthanum oxide nanoparticles by sonochemical method: systematic characterizations, https://doi.org/10.1515/zpch-2023-0396

3.) **Punazungba Imsong**, Sentienla Imsong, Swapnali Hazarika* and M. Indira Devi*, Novel Catalyst for Organic Reactions and Process Thereof. The Patent office Journal No. 16/2024 Dated 19/04/2024-37554

4.) **Punazungba Imsong**, Sentienla Imsong, Swapnali Hazarika* and M. Indira Devi*, A Novel Process of making Lanthanum Nanoparticles. The Patent office Journal No. 16/2024 Dated 19/04/2024-37553